OAK RIDGE
NATIONAL LABORATORY
MANAGED BY UT-BATTELLE
FOR THE DEPARTMENT OF ENERGY

ORNL/SUB/99-XSZ175V-5

Neutronic Benchmarks for the Utilization of Mixed-Oxide Fuel: Joint U.S./Russian Progress Report for Fiscal Year 1997

Volume 4, Part 6—ESADA Plutonium Program Critical Experiments: Power Distribution Measurements

Hatice Akkurt
Naeem M. Abdurrahman
R. T. Primm III
J. M. Barnes
M. W. Yambert

UT-BATTELLE
ORNL-27 (4-00)

Fissile Materials Disposition Program

ORNL/SUB/99XSZ175V-5

NEUTRONIC BENCHMARKS FOR THE UTILIZATION OF MIXED-OXIDE FUEL: JOINT U.S./RUSSIAN PROGRESS REPORT FOR FISCAL YEAR 1997

VOLUME 4, PART 6—ESADA PLUTONIUM PROGRAM CRITICAL EXPERIMENTS: POWER DISTRIBUTION MEASUREMENTS

Hatice Akkurt
Naeem M. Abdurrahman
University of Texas

R. T. Primm III
John M. Barnes
M. W. Yambert
Oak Ridge National Laboratory

Manuscript Completed: February 1999
Date Published: May 2001

Report prepared by
LOCKHEED MARTIN ENERGY RESEARCH CORP.
P.O. Box 2008
Oak Ridge, Tennessee 37831-6363
under
Subcontract Number 99XSZ175V

Funded by
Office of Fissile Materials Disposition
U.S. Department of Energy

Prepared for
Computational Physics and Engineering Division
OAK RIDGE NATIONAL LABORATORY
Oak Ridge, Tennessee 37831
managed by
UT-BATTELLE, LLC
for the
U.S. DEPARTMENT OF ENERGY
under contract DE-AC05-00OR22725

FINAL REPORT

ESADA PLUTONIUM PROGRAM CRITICAL EXPERIMENTS: POWER DISTRIBUTION MEASUREMENTS

Hatice Akkurt and Naeem M. Abdurrahman

College of Engineering
Department of Mechanical Engineering
University of Texas
Austin, TX 78712

February 1999

CONTENTS

Page

LIST OF FIGURES

LIST OF TABLES

NEUTRONIC BENCHMARKS FOR THE UTILIZATION OF MIXED-OXIDE FUEL: JOINT U.S./RUSSIAN PROGRESS REPORT FOR FISCAL YEAR 1997

VOLUME 4, PART 6—ESADA PLUTONIUM PROGRAM CRITICAL EXPERIMENTS: POWER DISTRIBUTION MEASUREMENTS*

Hatice Akkurt
Naeem M. Abdurrahman
University of Texas

1. POWER DISTRIBUTION MEASUREMENTS

1.1 OVERVIEW OF EXPERIMENTS

In 1967, a series of critical experiments were conducted at the Westinghouse Reactor Evaluation Center (WREC) using mixed-oxide (MOX) PuO_2-UO_2 and/or UO_2 fuels in various lattices and configurations.[1] These experiments were performed under the joint sponsorship of Empire State Atomic Development Associates (ESADA) plutonium program and Westinghouse.[2] The purpose of these experiments was to develop experimental data useful in validating analytical methods used in the design of plutonium-bearing replacement fuel for water reactors.

Three different fuel types were used during the experimental program: two MOX fuels and a low-enriched UO_2 fuel. The MOX fuels were distinguished by their ^{240}Pu content: 8 wt % ^{240}Pu and 24 wt % ^{240}Pu. Both MOX fuels contained 2.0 wt % PuO_2 in natural UO_2. The UO_2 fuel with 2.72 wt % enrichment was used for comparison with the plutonium data and for use in multiregion experiments.

1.2 DESCRIPTION OF EXPERIMENTAL CONFIGURATION

A total of 88 different critical core configurations were constructed for the experimental program. Both single and multiregion core configurations were used in the ESADA experiments. These core configurations were constructed by changing the lattice pitch, fuel configuration, and fuel isotopic composition. All experiments were performed in an ~112-cm-diam pool. Criticality was achieved by adjusting the height of the light-water moderator in the pool.

---

*__IDENTIFICATION NUMBERS:__ The following designations are applied in the International Handbook of Evaluated Criticality Safety Benchmark Experiments Project:

All rods are 8 wt % ^{240}Pu in plutonium, no boron in moderator—MIX-COMP-THERM-006
All rods are 8 wt % ^{240}Pu in plutonium, boron in moderator—MIX-COMP-THERM-007
All rods are 24 wt % ^{240}Pu in plutonium, no boron in moderator—MIX-COMP-THERM-008
All rods are 2.72 wt % ^{235}U in uranium, no boron in moderator—MIX-COMP-THERM-009
Two types of rods, 2.72 wt % ^{235}U in uranium and 8 wt % ^{240}Pu in plutonium, no boron in moderator—MIX-COMP-THERM-010
Two types of rods, 2.72 wt % ^{235}U in uranium and 8 wt % ^{240}Pu in plutonium, boron in moderator—MIX-COMP-THERM-011

Of these experiments, 53 were performed for single-region core configurations. Buckling, reactivity worth, and power distribution measurements were performed for single-region core configurations. The description and criticality benchmark calculation results for single-region ESADA experiments are provided in Ref. 3.

Thirty-five of these experiments were performed for multiregion core configurations. Reactivity worth and power distribution measurements were performed using multiregion core configurations. The multiregion core configurations were constructed in three ways: concentric-region core configurations, salt-and-pepper core configurations, and a third configuration that can be generally described as two rectangular slabs loaded with UO_2, sandwiching a center region loaded with MOX fuel. The description and criticality benchmark calculation results for multiregion ESADA experiments are provided in Ref. 4.

Power distribution measurements were performed for 28 different core configurations; however, the power data for only 26 of these configurations were reported in Ref. 1. For this reason, the two cases without power data are excluded from the evaluation.

Power distribution measurements were carried out for both single and multiregion cores. The measurements can be arranged in four categories: single-region uniform cores, multiregion slab cores, concentric-region cores, and salt-and-pepper cores.

The installation of MOX fuel in a single-region core configuration is shown in Fig. 1. The fuel rods were supported by three layers of aluminum plates. The thickness of the bottom and midcore plates was 0.635 cm, and the thickness of the top plate was 1.27 cm. The fuel rods rested on a 5.24-cm-thick aluminum plate.

The installation of MOX and UO_2 fuel rods in a salt-and-pepper core configuration is illustrated in Fig. 2. The UO_2 fuel rods rested on a 5.24-cm aluminum plate. The height of the UO_2 and MOX fuels were different. The MOX fuel rested on an aluminum plate with thickness of 1.9050 cm, and there was a 0.635-cm space available between these two aluminum plates. Both fuel rods were supported by three layers of aluminum plates. The thickness of the bottom and central aluminum plates was 0.635-cm, and the thickness of the top aluminum plate was 1.27 cm. For the installation of salt-and-pepper core configurations composed of 8% and 24% ^{240}Pu fuels, a single-lattice pitch is used.

The installation of MOX and UO_2 fuel rods in a multiregion slab core configuration is shown in Fig. 3.

1.3 POWER DISTRIBUTION MEASUREMENT TECHNIQUE

Power distribution measurements were performed by relating the fission product gamma activity of irradiated fuel rods to the temperature rise of the clad surface. The temperature rise of the clad surface is proportional to the rod power. Low background fuel rods were placed in the core and irradiated; the resulting fission product activity was counted with a well-collimated gamma scintillation counter. For this purpose, two identical gamma detector-scaler systems were used. One system or channel counted a fixed point on a monitor rod, which had the same irradiation history as the data rods. The other channel determined the count rate at various axial positions on the data rods. The monitor rod was placed in a shielded location and remained there during the entire scan, while the data rod was mounted on a traverse card that automatically moved up or down, stopping at the position to be counted. Both scalers in the counting system were started and stopped simultaneously when a preset count (usually 20000 counts at each count position) had been reached in the monitor channel. In this way, an automatic correction was made for the fission product decay, providing both monitor rod and the fuel rod being counted were of the same fuel type.[1]

However, in configurations composed of both MOX and UO_2 fuels, it was not possible to determine the correct relative power in each fuel by a gamma scan of the fuel rods because the

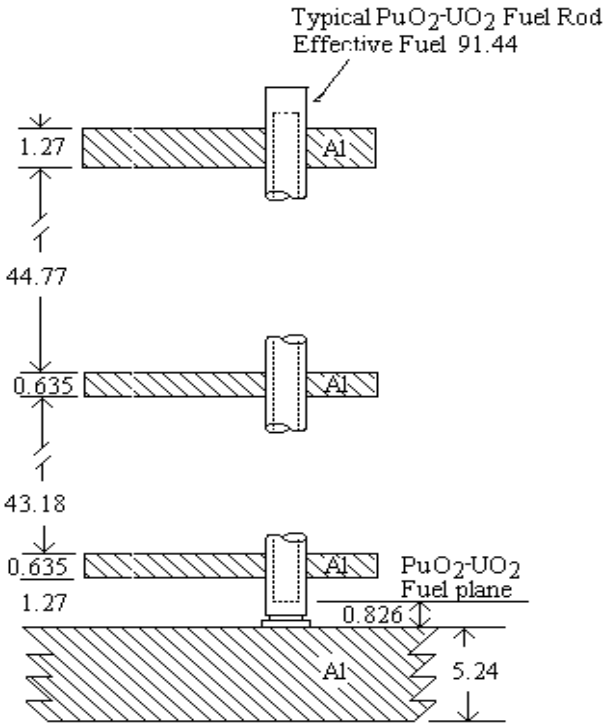

Fig. 1. The installation of MOX fuel in a uniform lattice. (Not drawn to scale; units are in centimeters except where specified otherwise.)

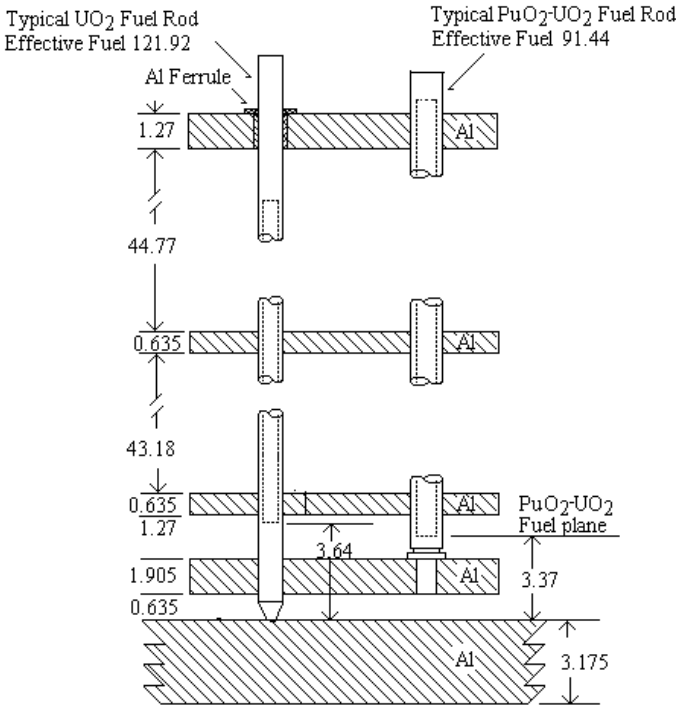

Fig. 2. The installation of a salt-and-pepper core. (Not drawn to scale; units are in centimeters except where specified otherwise.)

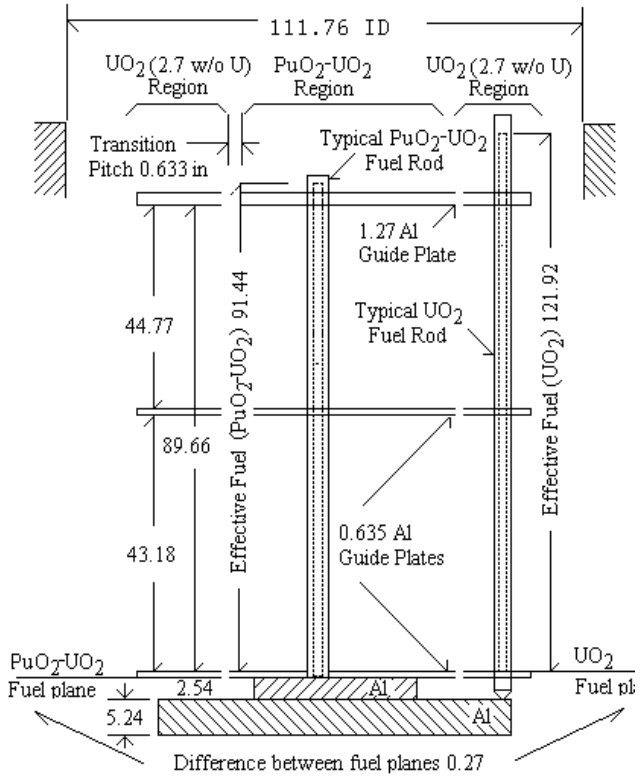

Fig. 3. The installation of a multiregion core. (Not drawn to scale; units in centimeters except where specified otherwise.)

gamma source and decay characteristics of the two fuels are different. During the Saxton Plutonium Program, temperature measurements in thermally insulated rods of both UO_2 and MOX fuel and foil irradiation experiments using foils of both fuel types were used to determine the time-dependent factors to relate the measured gamma activity to rod power[5] after shutdown. These time-dependent correction factors were determined in fuel rods with the same geometry. The MOX and UO_2 fuel rods used in ESADA experiments had different diameters, and the MOX fuels had different ^{240}Pu contents. Consequently, additional heat rate experiments were carried out to permit reevaluation of the power-to-gamma activity time-dependent factor.[1]

In the heat rate experiments, thermally insulated and instrumented fuel rods were irradiated, and the temperature rise was measured. After shutdown, these same rods were counted in the fuel rod gamma scanner. The resulting ratio of heating rate to gamma activity provides a time-dependent "calorimetric" correction factor similar to that determined in the Saxton Plutonium Program but with an improved technique. The largest error incurred previously was in the determination of the temperatures of the rods while they were being heated. For the ESADA program, a digital voltmeter was used and greatly increased the speed of the temperature measurements with a very high accuracies. This procedure permitted many more points to be obtained on the temperature vs time curves for the fuels. Three sets of measurements were taken: UO_2 vs 8% ^{240}Pu, UO_2 vs 24% ^{240}Pu, and 8% vs 24% ^{240}Pu.

The calorimetric factors were used to relate the measured relative gamma activity in the different types of fuel to a relative clad temperature rise. Because the thermal capacitance of each fuel was different, it was necessary to make an additional correction to relate the clad temperature rise to the fuel rod power.

The relation between thermal power and clad temperature rate was determined from the following relations:

$$q' = C_f \frac{dT_f}{dt} + \frac{T_f - T_c}{R_f} \quad , \tag{1}$$

$$\frac{T_f - T_c}{R_f} = C_c \frac{dT_c}{dt} + \frac{T_c - T_i}{R_c} \quad , \tag{2}$$

where

q' = linear power,
T_f = average fuel temperature,
T_c = average clad temperature,
T_i = average insulation temperature.
C_f = capacitance of fuel pellet, $C_f = \pi r_f^2 c_f \rho_f$
C_c = capacitance of clad, $C_c = \pi \left(r_{c_1}^2 - r_{c_2}^2 \right) c_c \rho_c$
r_f = radius of fuel
C_f = specific heat of fuel
p_f = density of fuel
r_{c_1} = outer radius of clad
r_{c_2} = inner radius of clad
C_c = specific heat of clad
p_c = density of clad
R_f = resistance of fuel and gap
$R_F = \frac{1}{8\pi k_f} + \frac{1}{2\pi r_f h_g}$
k_f = thermal conductivity fuel, h_g = gap or contact resistance
R_c = resistance of clad and insulation
$Rc = \frac{\mathrm{n}\left(r_i / r_c\right)}{2\pi k_i}$ (neglecting clad resistance)
ki = thermal conductivity of insulation

For a short time after the step increase in power, the clad temperature rises adiabatically, for which $\frac{T_c - T_i}{R_c} = 0$. From Ref. 1, the solution of Eqs. (1) and (2) for T_c with constant linear power, q', is

$$T_c = T_c(0) e^{\alpha t} + \frac{q'}{C_f + C_c} \quad .$$

The total constant thermal power in terms of clad temperature rate is thus

$$q = l(C_f + C_c)\frac{dT_c}{dt} \text{ (since } e^{\alpha t} = 0 \text{ after 10 s and } \alpha < -1) \ ,$$

where $q = q`l$, and l = power producing length of rod. The ratio of power in the MOX rod to power in the UO_2 rod is

$$\frac{q_{mox}}{q_u} = \frac{(C_f + C_c)_{mox}}{(C_f + C_c)_u}\frac{(dT_c / dt)_{mox}}{(dT_c / dt)_u} \ ,$$

where $l_{mox} = l_u$. For material temperatures of 75°F, Ref. 1 reports

$$\frac{(C_f + C_c)_{mox}}{(C_f + C_c)_u} = 1.41 \ .$$

The power distribution values for MOX–UO_2 cores have been corrected by the calorimetric factors. However, no correction to the data reported in Ref. 1 was made to account for the difference in thermal capacitance of the different fuel rod types. Therefore, for MOX–UO_2 cores, the relative power values, which were provided in Ref. 1, for MOX fuel rods should be multiplied by 1.41 to correct for this difference.

A reevaluation of the power ratio between LEU and MOX fuel (the value of 1.41 shown above) was made using current values of physical property data, calculated radial power distributions inside the LEU and MOX pins, and the HEATING-6 computer program. A value of 1.51 was determined. In this report, the corrected relative power data using the power ratio of 1.51 are provided.

1.4 POWER DISTRIBUTION MEASUREMENTS DATA

1.4.1 Single-Region Power Distribution Measurements

Single-region power distribution measurements were performed for six different core configurations. Five measurements were performed by using 8% ^{240}Pu MOX fuel, and one measurement was performed using 24% ^{240}Pu MOX fuel. The installation of MOX fuel rods in a uniform lattice is shown in Fig. 1.

In single-region cores, the power peaking effects near water holes and water slots were investigated. Power peaking effects of a water hole and a water slot were measured for both clean and borated cores using 8% ^{240}Pu in the 1.7526-cm (0.69-in.) lattice. Water hole peaking was determined for a clean core with an 8% ^{240}Pu fuel in the 1.9050-cm (0.75-in.) lattice and with a 24% ^{240}Pu fuel in the 2.6942-cm (1.0607-in.) lattice.

Reported data for single-region power distribution measurements with 8% ^{240}Pu and 24% ^{240}Pu fuels are listed in Table 1. The related core configurations and the measurement rods are presented in Figs. 4–9. In these figures, fuel rods are either indicated by the solid circles or by numbers that show the measurement rods. Power data from each experiment are given in Tables 2–7.

Reference 1 does not indicate which rod is taken as the reference rod for power distribution measurements.

Table 1. Reported data for single-region power distribution measurements with 8% ^{240}Pu and 24% ^{240}Pu fuels

Case No.	Power data (table)	Core diagram (figure)	Fuel type	Lattice pitch (cm)	Number of fuel rods	Boron concentration (ppm)	Critical water height (cm)	Perturbation
1	2	4	8% ^{240}Pu	1.7526	574	0	75.68	Center water hole
2	3	5	8% ^{240}Pu	1.7526	570	0	70.95	Five-rod water slot
3	4	6	8% ^{240}Pu	1.7526	728	315	77.77	Center water hole
4	5	7	8% ^{240}Pu	1.7526	724	315	75.11	Five-rod water slot
5	6	8	8% ^{240}Pu	1.9050	440	0	52.23	Center water hole
6	7	9	24% ^{240}Pu	2.6942	300	0	62.62	Center water hole

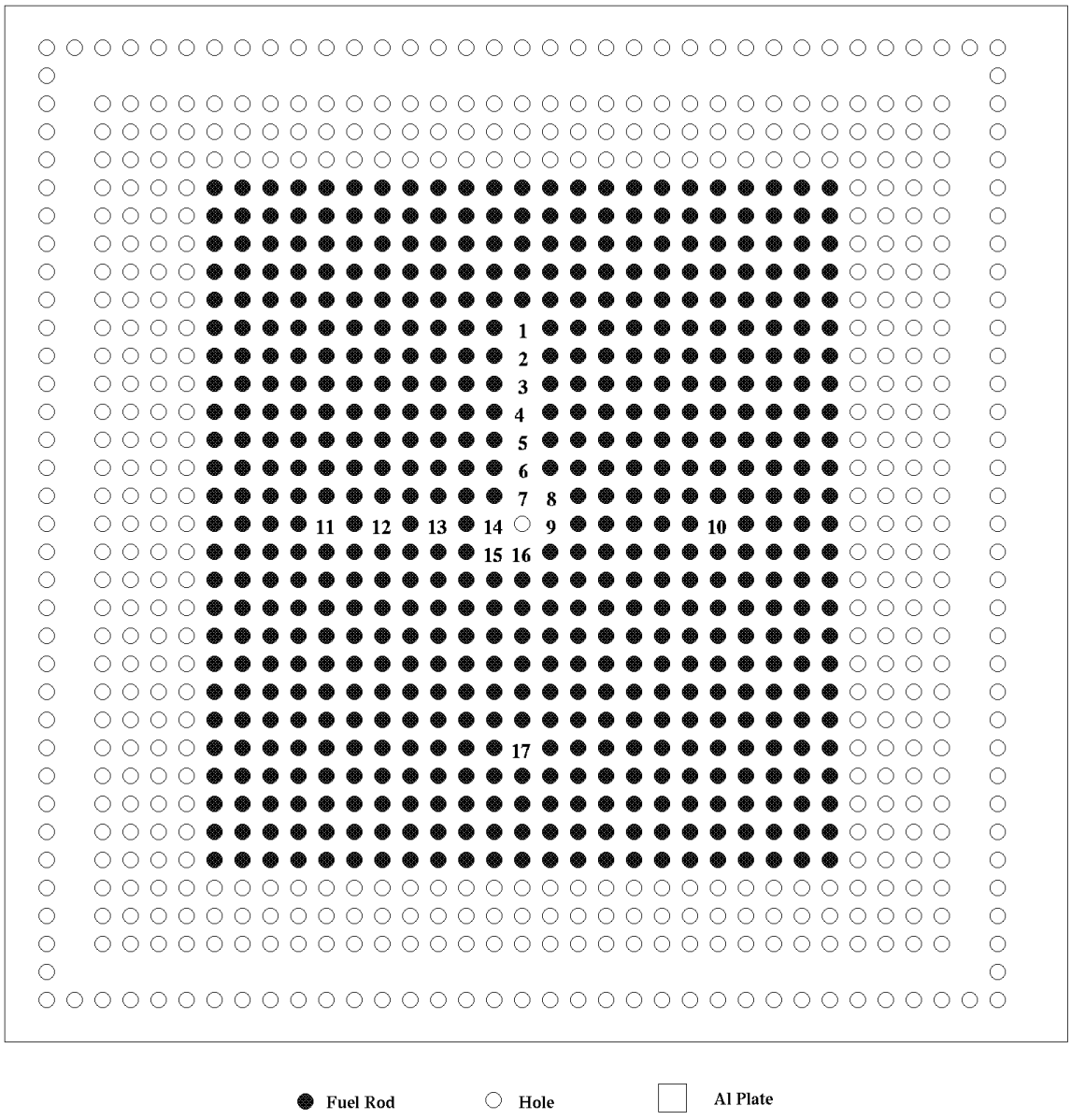

Fig. 4. A 23 × 25 rectangular core configuration with a center water hole in the 1.7526-cm lattice.

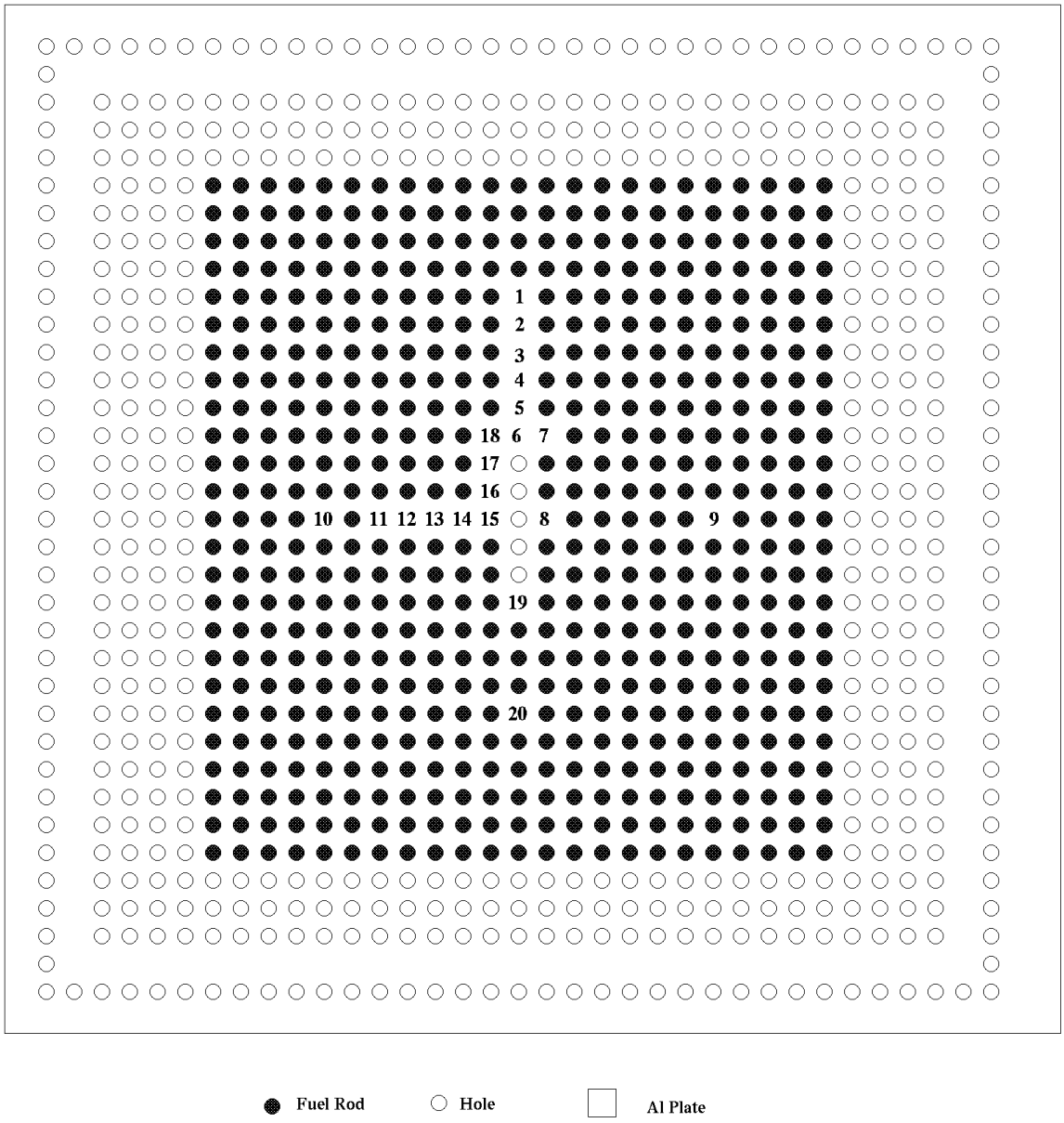

Fig. 5. A 23 × 25 rectangular core configuration with a five-rod water slot pattern in the 1.7526-cm lattice.

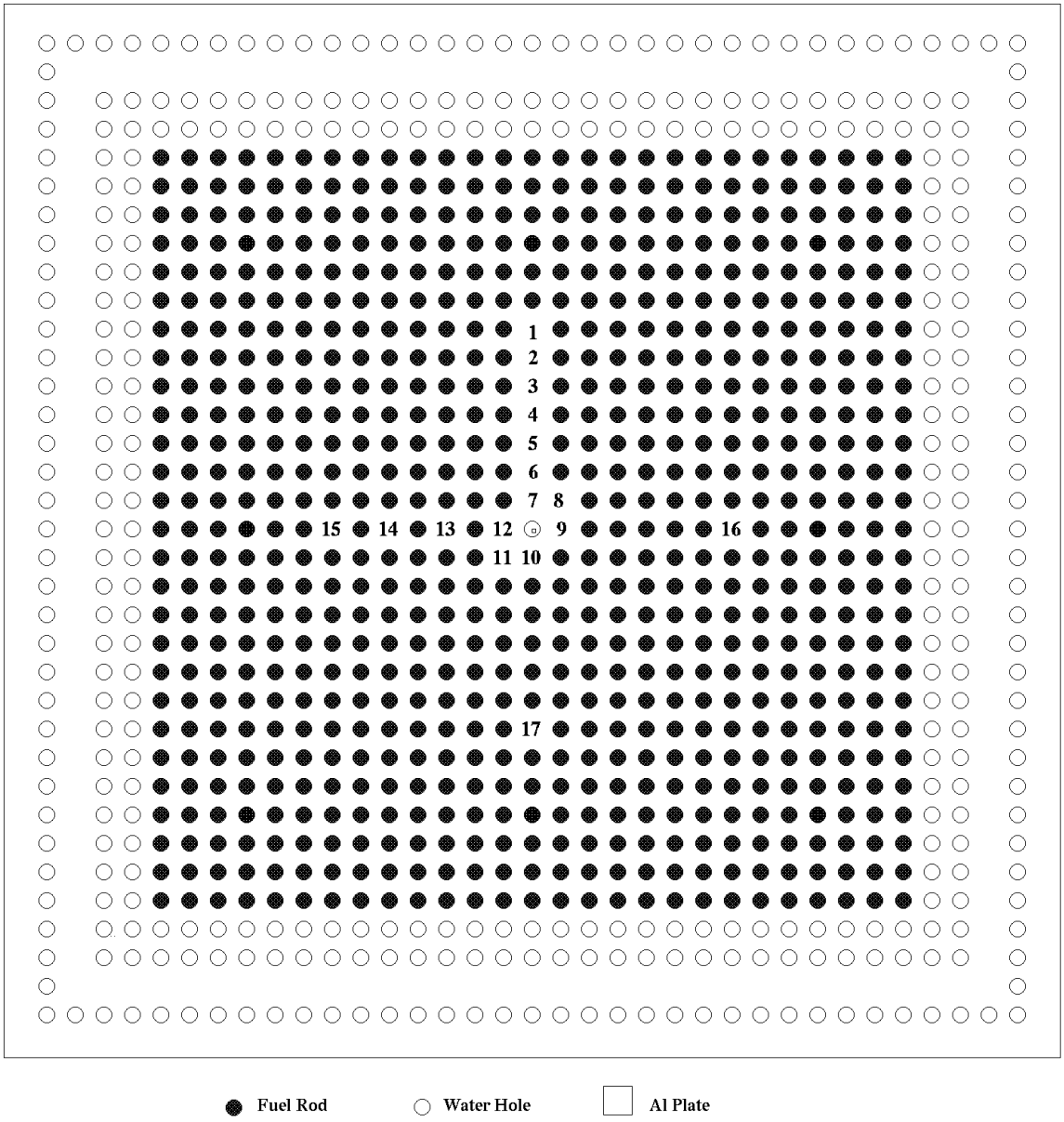

Fig. 6. A 27 × 27 rectangular core configuration with a center water hole in the 1.7526-cm lattice.

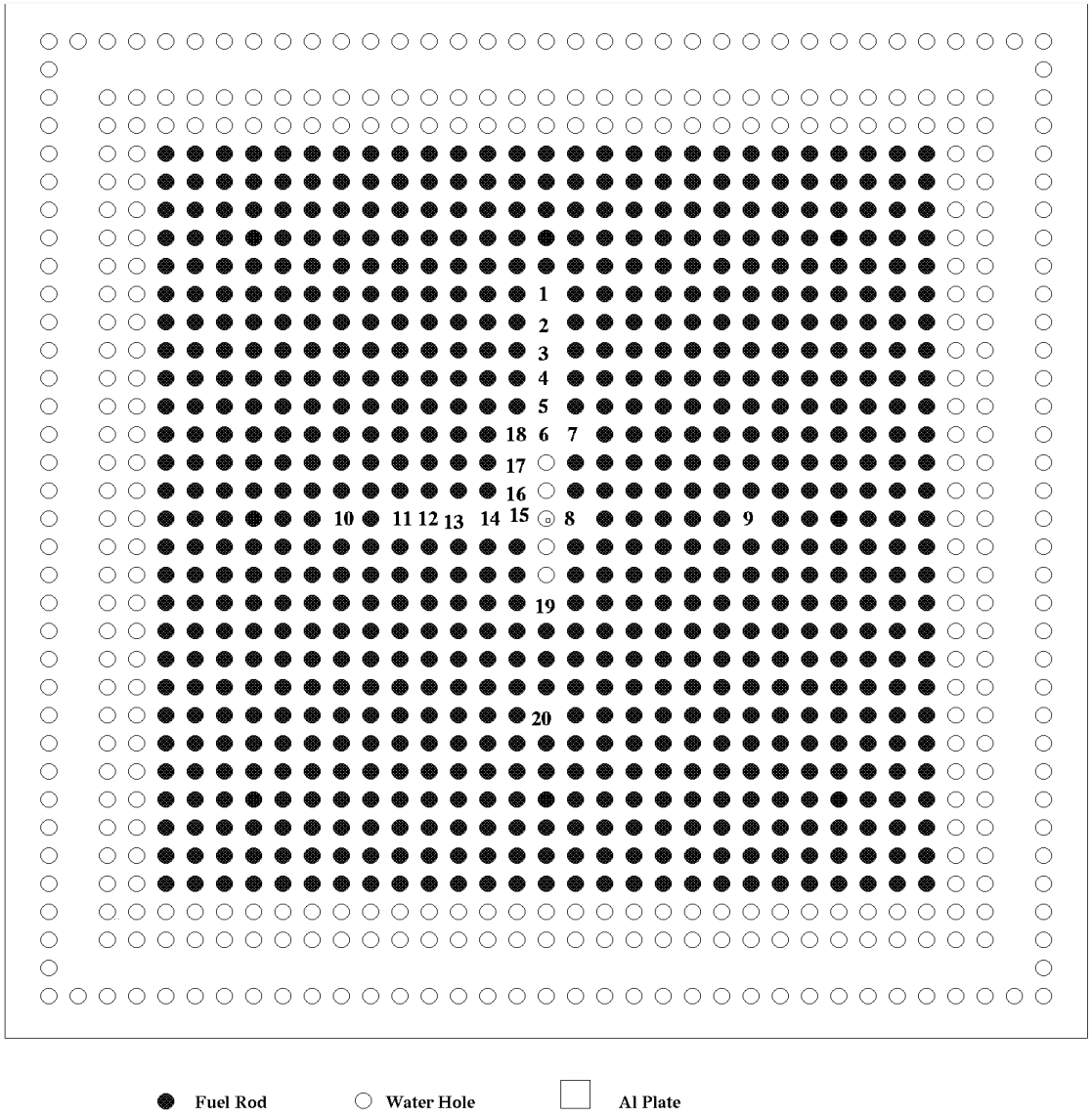

Fig. 7. A 27 × 27 rectangular core configuration with a five-rod water slot pattern in the 1.7526-cm lattice.

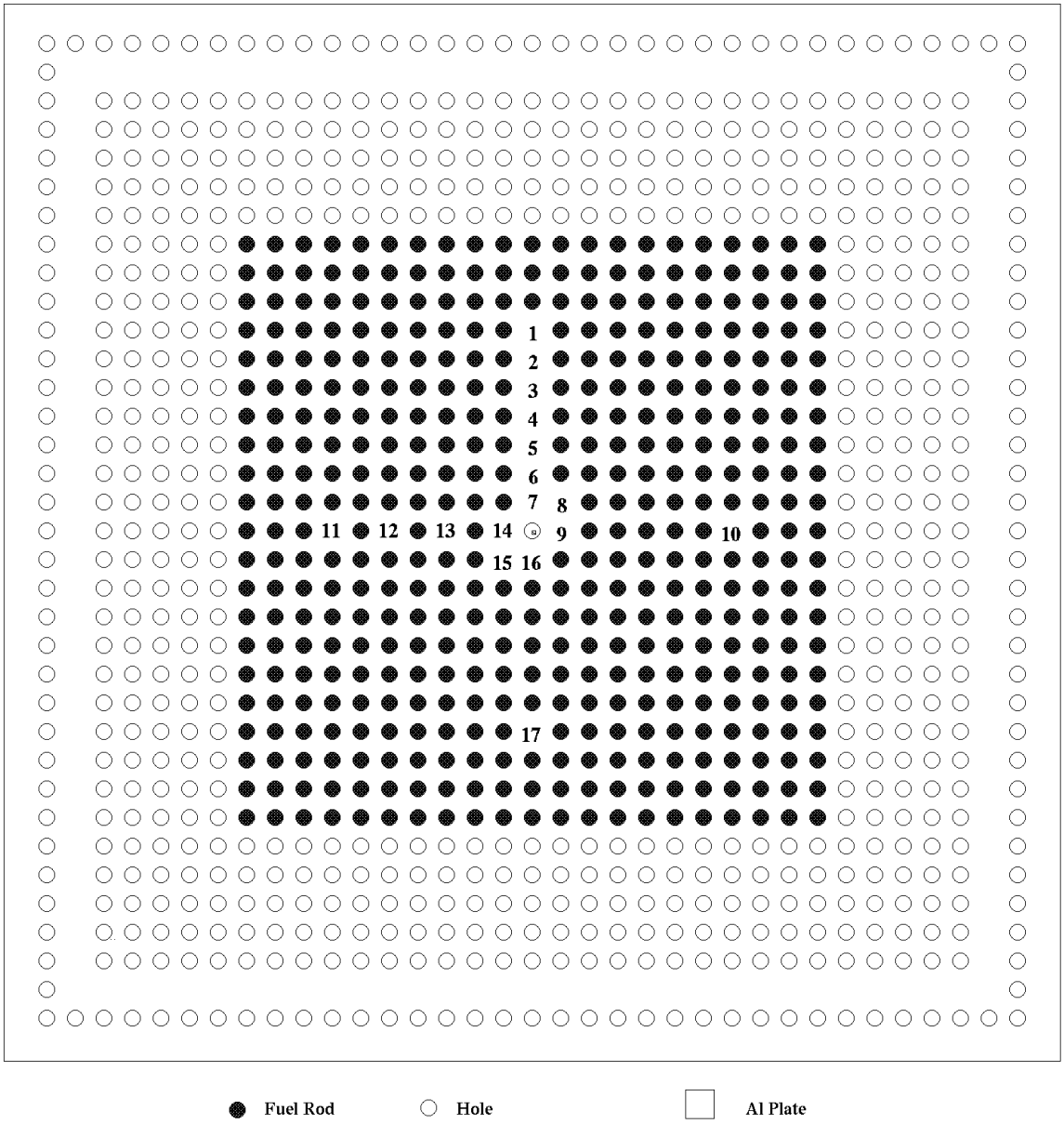

Fig. 8. A 21 × 21 rectangular core configuration with a center water hole in the 1.9050-cm lattice.

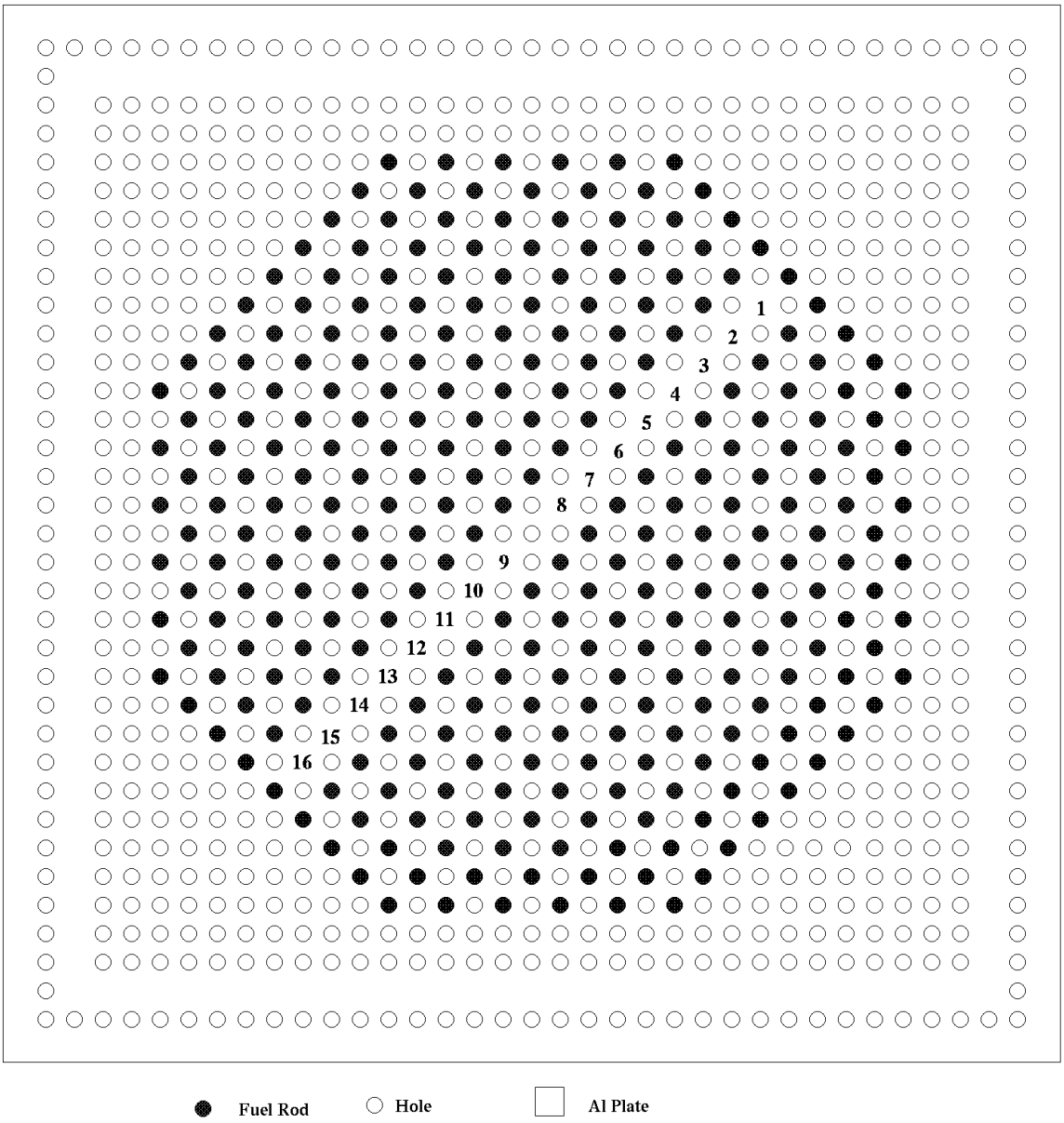

Fig. 9. A cylindrical core configuration with a center water hole in the 2.6942-cm lattice.

Table 2. Relative power data for a 23 × 25 single-region core configuration with a center water hole

Rod No.	Relative power
1	0.808
2	0.848
3	0.899
4	0.950
5	0.973
6	1.025
7	1.240
8	1.109
9	1.253
10	0.775
11	0.790
12	0.897
13	0.994
14	1.266
15	1.125
16	1.255
17	0.806

Table 3. Relative power data for 23 × 25 single-region core configuration with five-rod water slot

Rod No.	Relative power
1	0.741
2	0.811
3	0.862
4	0.925
5	1.011
6	1.299
7	1.121
8	1.709
9	0.769
10	0.784
11	0.890
12	0.952
13	1.019
14	1.181
15	1.709
16	1.556
17	1.430
18	1.146
19	1.286
20	0.809

Table 4. Relative power data for a 27 × 27 single-region core configuration with a center water hole

Rod No.	Relative power
1	0.794
2	0.838
3	0.890
4	0.933
5	0.956
6	1.024
7	1.214
8	1.091
9	1.196
10	1.211
11	1.142
12	1.230
13	0.955
14	0.900
15	0.806
16	0.806
17	0.806

Table 5. Relative power data for a borated 27 × 27 single-region core configuration with a five-rod water slot

Rod No.	Relative power
1	0.732
2	0.793
3	0.835
4	0.895
5	0.968
6	1.241
7	1.069
8	1.602
9	0.798
10	0.809
11	0.891
12	0.941
13	0.988
14	1.137
15	1.586
16	1.584
17	1.409
18	1.119
19	1.258
20	0.812

Table 6. Relative power data for a 21 × 21 single-region core configuration with a center water hole

Rod No.	Relative power
1	1.365
2	1.514
3	1.607
4	1.740
5	1.807
6	1.938
7	2.263
8	2.044
9	2.270
10	1.367
11	1.357
12	1.616
13	1.884
14	2.277
15	2.058
16	2.284
17	1.378

Table 7. Relative power data for a cylindrical core configuration with center water hole

Rod No.	Relative power
1	2.897
2	3.533
3	4.139
4	4.633
5	5.092
6	5.482
7	5.823
8	6.641
9	6.560
10	5.841
11	5.467
12	5.065
13	4.649
14	4.105
15	3.438
16	2.893

1.4.2 Multiregion Power Distribution Measurements

The multiregion power distribution measurements were performed for 20 different core configurations. The multiregion core configurations were constructed in three ways: concentric-region core configurations, salt-and-pepper core configurations, and a third configuration that can be generally described as two rectangular slabs loaded with UO_2, sandwiching a center region loaded with MOX fuel.

For the concentric-region and salt-and-pepper core configurations composed of two types of MOX fuels, the installation of MOX fuel rods in a uniform lattice (Fig. 1) is used. The installation of salt-and-pepper cores for the core configurations composed of UO_2 and MOX fuel is given in Fig. 2. The installation of MOX and UO_2 fuel rods in a multiregion slab core configuration is given in Fig. 3.

Because the UO_2 and MOX fuel rods had different diameters, the use of these two fuels within the same lattice meant there was a variation in the fuel-to-moderator ratio between regions. In the concentric-region and salt-and-pepper core configurations, which were composed of the two different MOX fuels, however, the fuel-to-moderator ratio in each region was the same. In one concentric-region cylindrical configuration, the plutonium fuel in the outer region was loaded on the diagonal, thus introducing a variation in fuel-to-moderator ratio in regions containing the two plutonium fuels as well.

As explained in Sect. 1.3, the power distribution values for MOX–UO_2 cores have been corrected by the calorimetric factors. However, no correction to the data was made to account for the difference in thermal capacitance of the different fuel rod types. Therefore, it was reported in Ref. 1 that for MOX–UO_2 cores the relative power values listed for MOX fuel rods should be multiplied by 1.41 to correct for this difference. In this report, the corrected values are also provided in the corresponding power data tables.

Reference 1 does not provide data for the reference (monitor) rods for the power distribution measurements.

1.4.2.1 Concentric-region power distribution measurements

The concentric-region core configurations were constructed by using two different fuel types in the inner and outer regions of the core. Various combinations of the available fuels were used during the construction of the core configurations. Power distribution measurements for the concentric-region core configurations were performed for seven core configurations. Measurements were performed for rectangular and cylindrical cores composed of various combinations of the available fuels. Four core configurations were constructed by using a 24 wt % ^{240}Pu fuel in the inner region and an 8% ^{240}Pu fuel in the outer region. Two of these four experiments were performed for a 1.7526-cm lattice pitch. A third experiment was performed for a 1.9050-cm lattice pitch. Because both types of MOX fuel rods had the same dimensions, the moderator-to-fuel ratio remains the same for each fuel in these core configurations. However, for one of the configurations with both MOX fuel in the inner and outer regions, the fuel of the outer region was loaded on the diagonal; thus, different moderator-to-fuel volume ratios were introduced in the same configuration for different regions. For this configuration, a 1.9050-cm lattice pitch was used in the three regions, but the outer region fuel was loaded on the diagonal; therefore, the lattice pitch for the outer region was 2.6942 cm.

In addition to core configurations with MOX fuels, three additional core configurations were constructed by using MOX and UO_2 fuels with different loading combinations. For all three of these configurations, 1.7526-cm lattice pitches were used. Two core configurations were constructed by using the 24% ^{240}Pu and UO_2 fuels with different loading patterns. Moreover,

one configuration with an 8% ^{240}Pu inner region and a UO_2 outer region was also constructed. The MOX and UO_2 fuel rods have different diameters and heights. In concentric-region core configurations, the MOX and UO_2 fuel rods were used in the same lattice pitch. Therefore, for these cases with the same lattice pitches, different moderator-to-fuel volume ratios were obtained in the same configuration.

For the concentric-region core configurations composed of two different MOX fuels, installation of the core is given in Fig. 1. For the core configurations composed of the MOX and UO_2 fuels, the installation of a salt-and-pepper core configuration is shown in Fig. 2.

A summary of the concentric-region experiments is given in Table 8. Core diagrams showing the experimental configurations and also the measured rods are presented in Figs. 10–16. Relative power data from each experiment are given in Tables 9–15.

Table 8. Reported data for concentric-region core configurations[a]

Case No.	Power data (table)	Core diagram (figure)	Inner region			Outer region			Critical water height (cm)
			Fuel	Number of fuel rods	Lattice pitch (cm)	Fuel	Number of fuel rods	Lattice pitch (cm)	
7	9	10	8% ^{240}Pu	225	1.7526	UO_2	400	1.7526	50.43
8	10	11	UO_2	225	1.7526	24% ^{240}Pu	400	1.7526	50.08
9	11	12	24% ^{240}Pu	225	1.7526	UO_2	400	1.7526	79.53
10	12	13	24% ^{240}Pu	225	1.7526	8% ^{240}Pu	492	1.7526	93.48
11	13	14	24% ^{240}Pu	221	1.7526	8% ^{240}Pu	468	1.7526	95.36
12	14	15	24% ^{240}Pu	157	1.9050	8% ^{240}Pu	264	1.9050	92.65
13	15	16	24% ^{240}Pu	89	1.9050	8% ^{240}Pu	143	2.6942	93.42

[a]These are clean core experiments containing no boron.

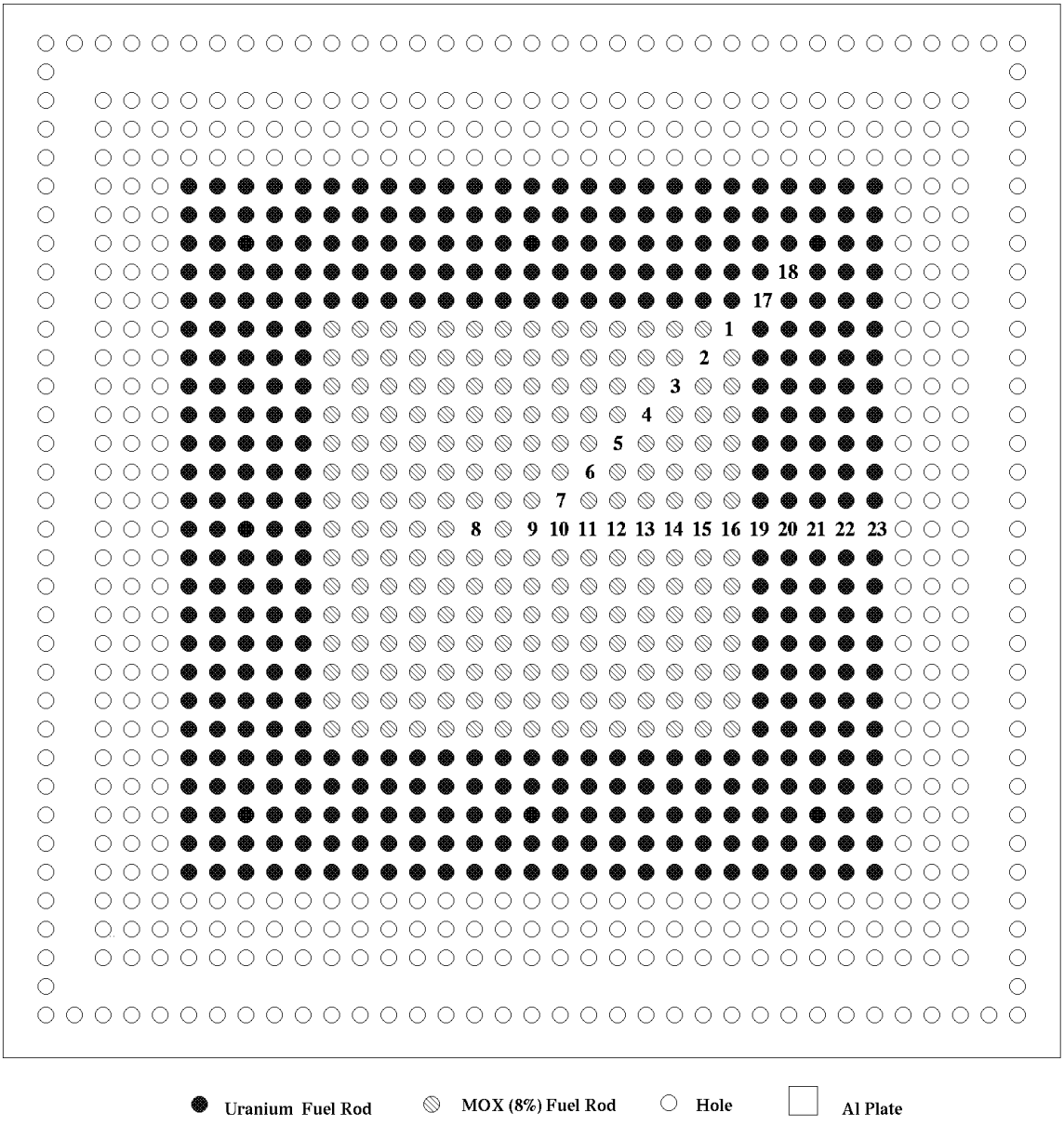

Fig. 10. A 25 × 25 concentric-region core configuration containing a 15 × 15 8 wt % ^{240}Pu inner region and a UO_2 outer region.

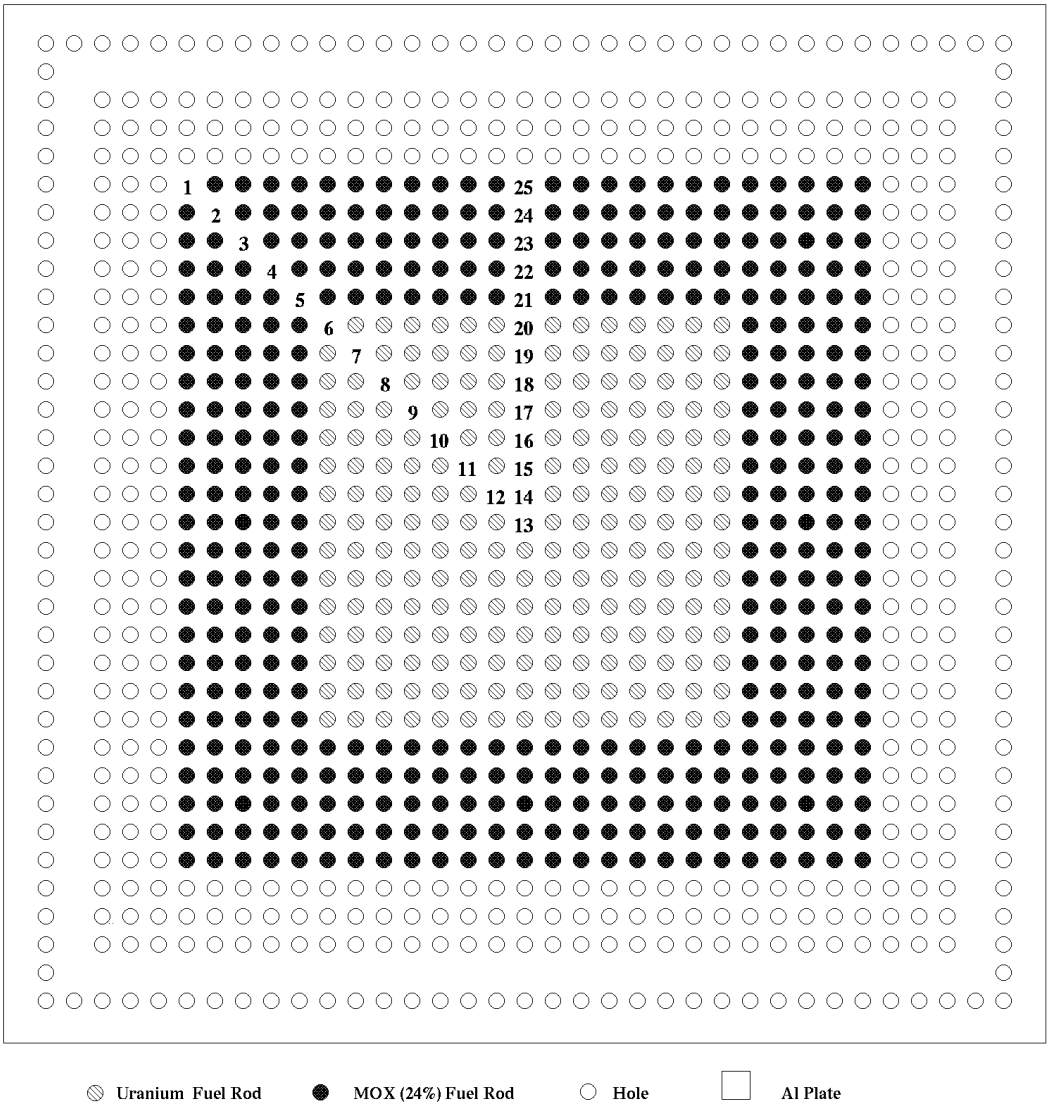

Fig. 11. A 25 × 25 concentric-region core configuration containing a 15 × 15 UO_2 inner region and a 24% ^{240}Pu outer region.

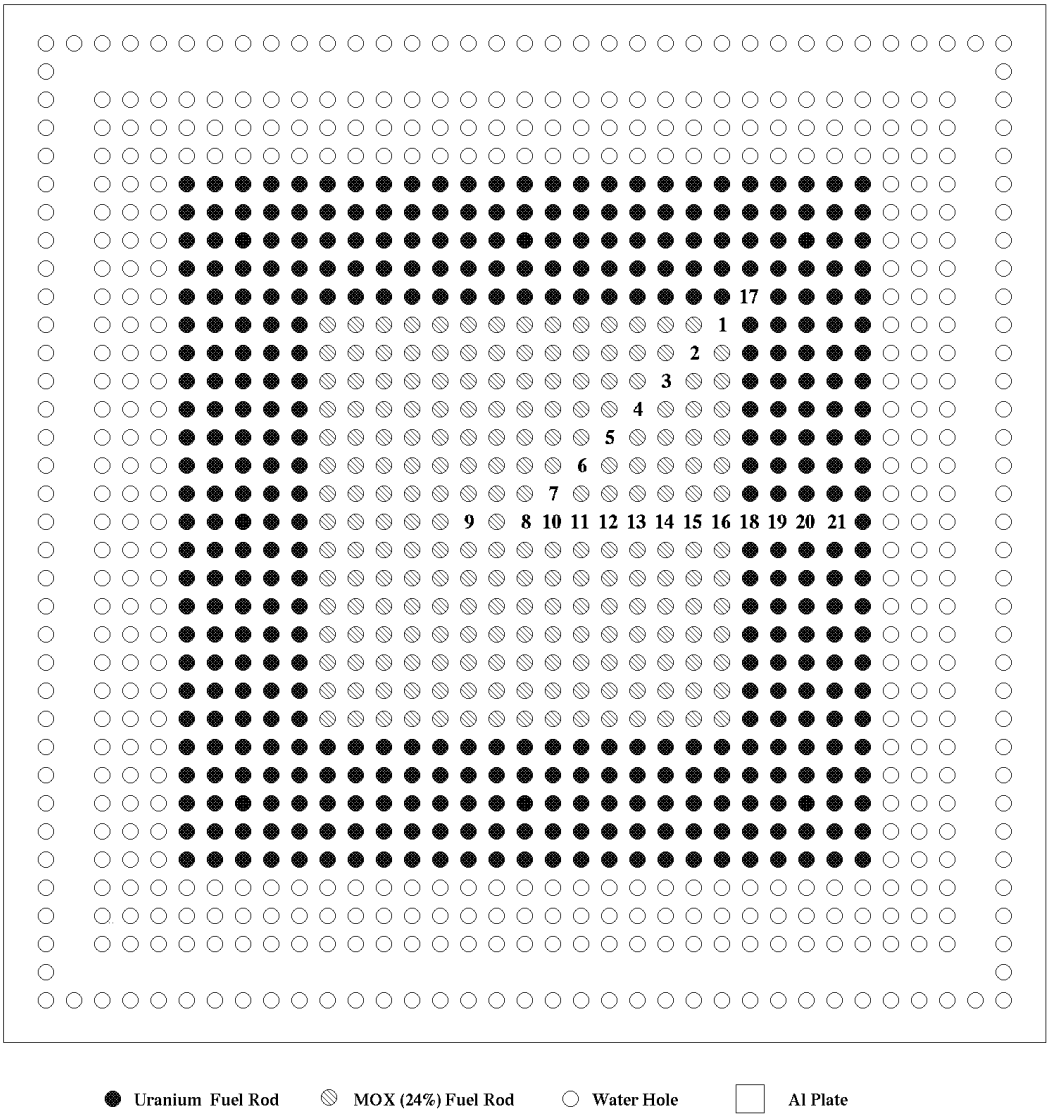

Fig. 12. A 25 × 25 concentric-region core configuration containing a 15 × 15 24% ^{240}Pu inner region and UO_2 outer region.

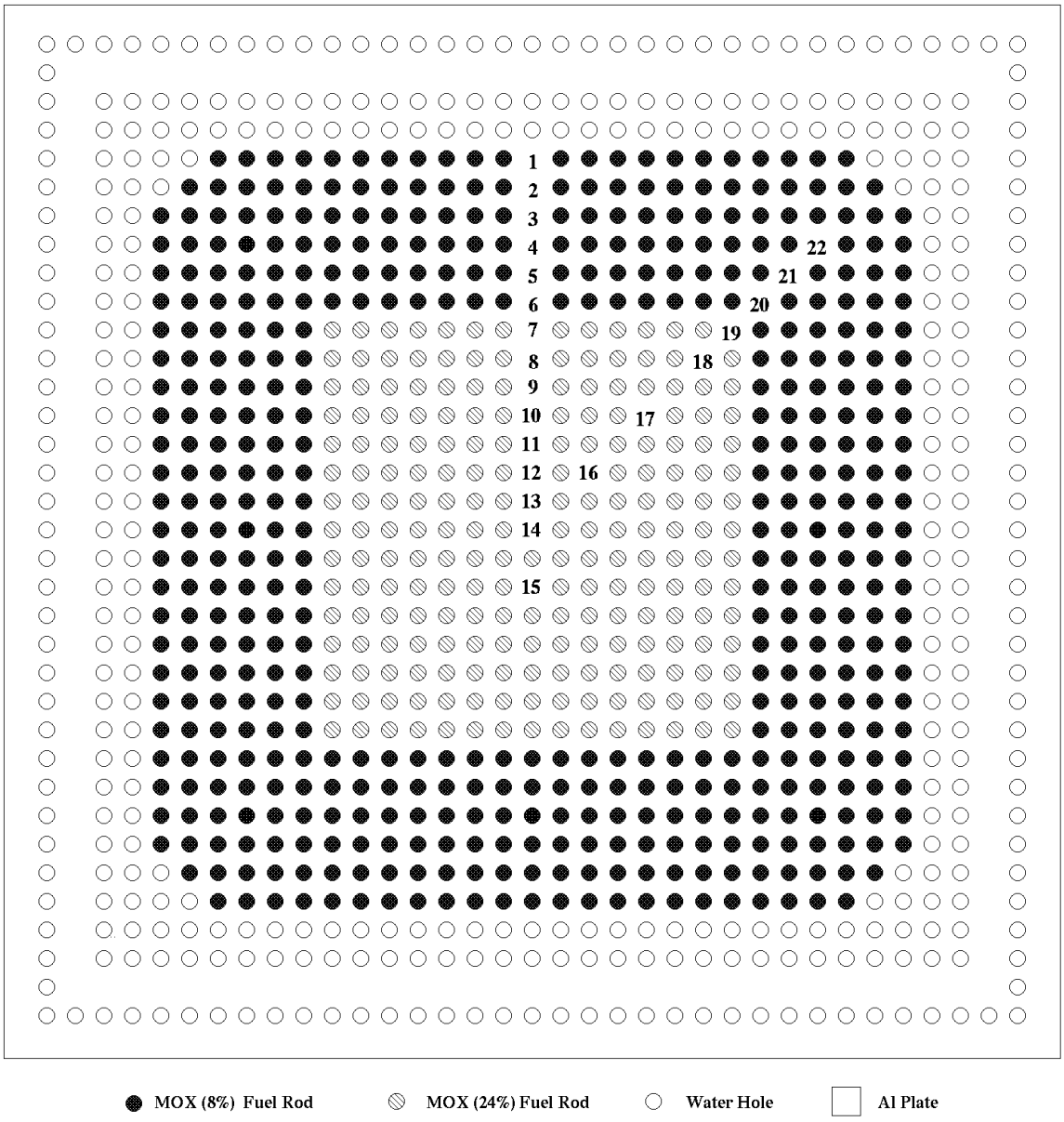

Fig. 13. A 27 × 27 concentric-region core configuration containing a 15 × 15 24% ^{240}Pu inner region and an 8% ^{240}Pu outer region.

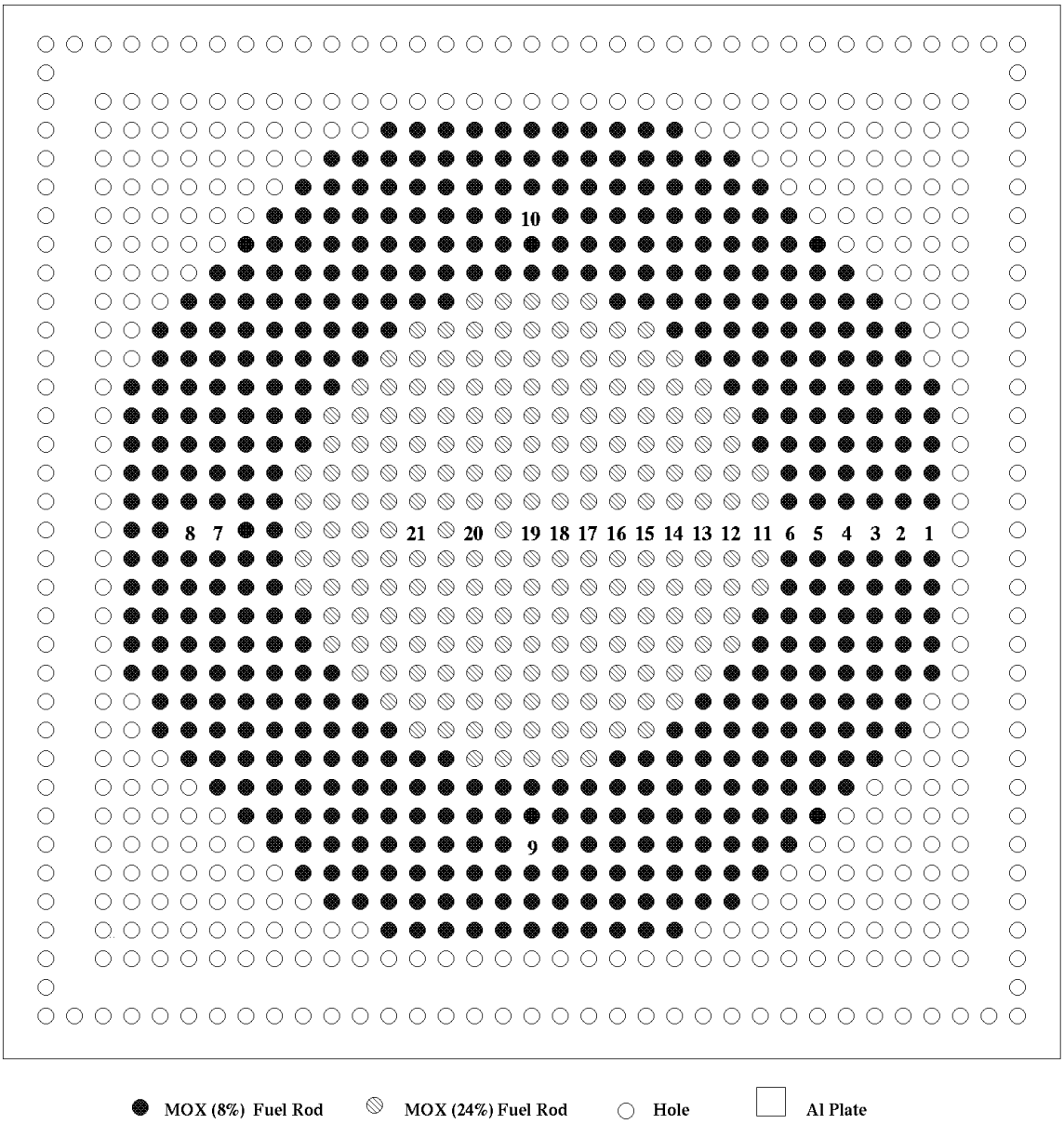

Fig. 14. A cylindrical concentric-region core configuration containing a 24% ^{240}Pu inner region and an 8% ^{240}Pu outer region.

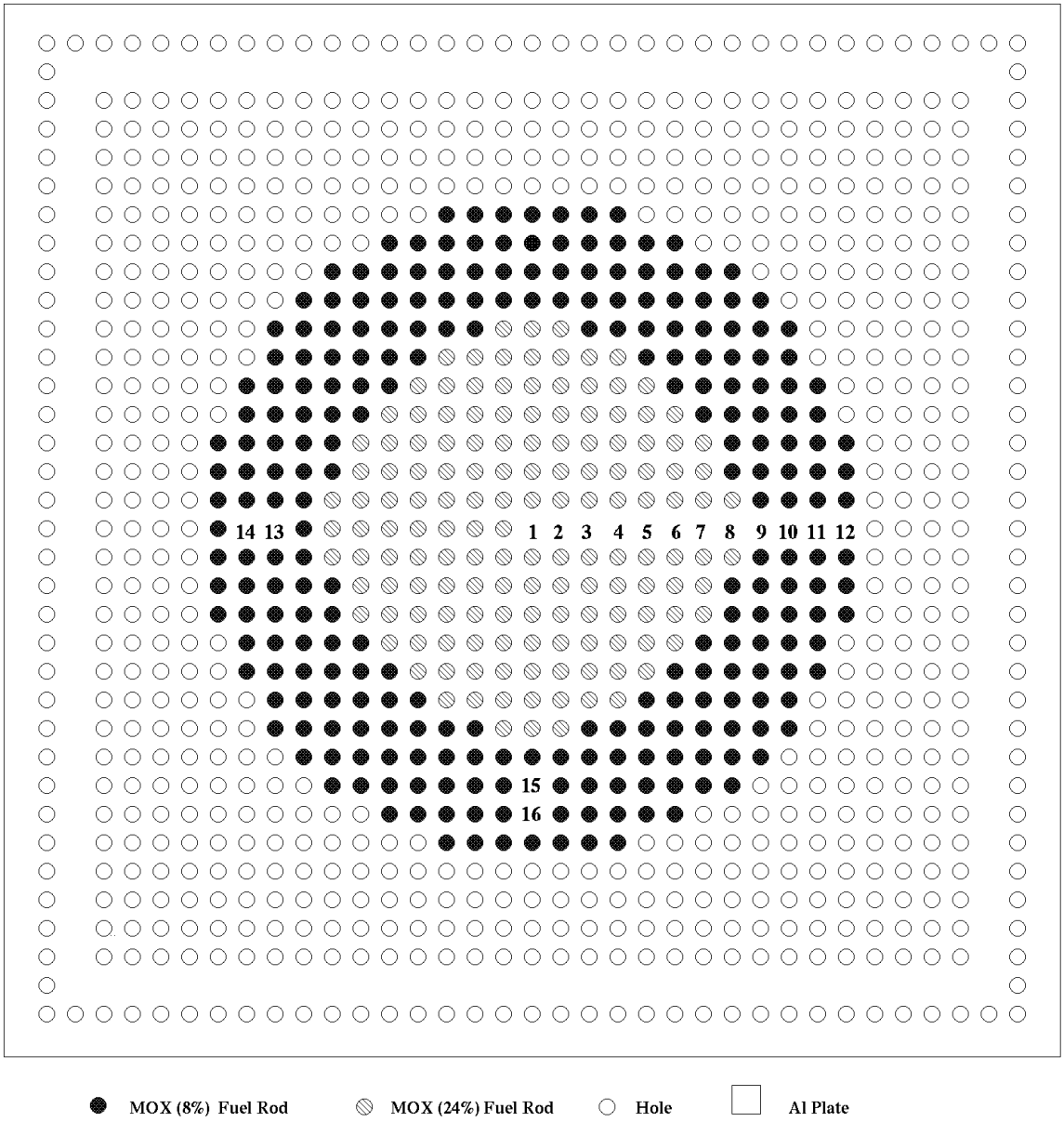

Fig. 15. A cylindrical concentric-region core configuration containing a 24% ^{240}Pu inner region and an 8% ^{240}Pu outer region.

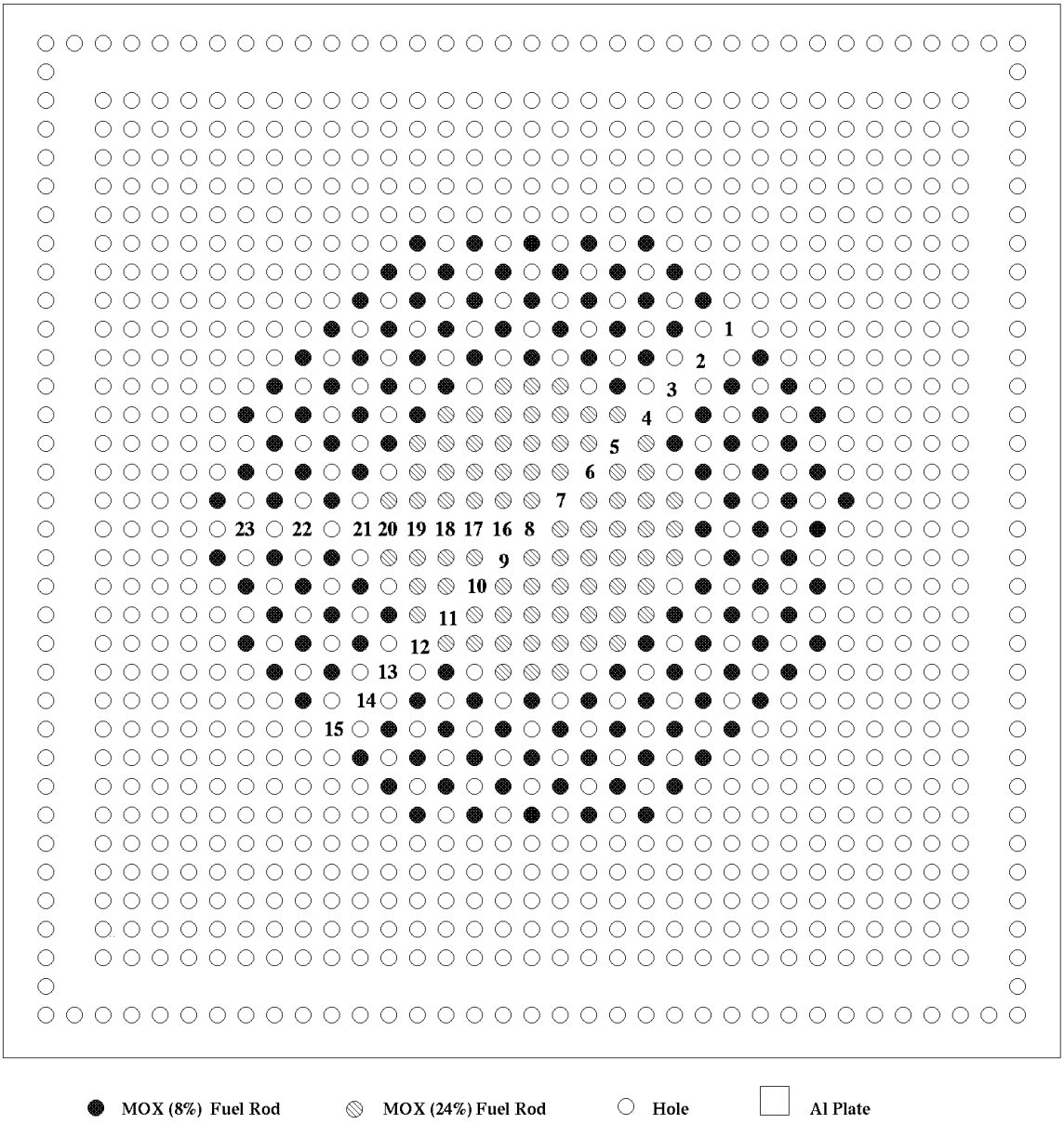

Fig. 16. A cylindrical concentric-region core configuration containing a 24% ^{240}Pu inner region and an 8% ^{240}Pu outer region with a regional variation in lattice pitch.

Table 9. Relative power data for a 25 × 25 concentric-region core configuration containing a 15 × 15 8% ^{240}Pu inner region and UO_2 outer region

Fuel type	Rod No.	Relative power	Corrected relative power[a]	Normalized corrected relative power
8% ^{240}Pu	1	1.032	1.558	1.251
8% ^{240}Pu	2	0.851	1.285	1.032
8% ^{240}Pu	3	0.830	1.253	1.006
8% ^{240}Pu	4	0.875	1.322	1.061
8% ^{240}Pu	5	0.921	1.391	1.117
8% ^{240}Pu	6	0.949	1.433	1.150
8% ^{240}Pu	7	0.980	1.480	1.188
8% ^{240}Pu	8	0.966	1.459	1.171
8% ^{240}Pu	9	0.972	1.468	1.179
8% ^{240}Pu	10	0.983	1.484	1.191
8% ^{240}Pu	11	0.987	1.491	1.197
8% ^{240}Pu	12	0.968	1.462	1.174
8% ^{240}Pu	13	0.923	1.393	1.118
8% ^{240}Pu	14	0.903	1.363	1.094
8% ^{240}Pu	15	0.912	1.377	1.105
8% ^{240}Pu	16	1.069	1.614	1.296
UO_2	17	0.890	0.890	0.715
UO_2	18	0.793	0.793	0.637
UO_2	19	0.997	0.997	0.800
UO_2	20	1.097	1.097	0.881
UO_2	21	1.063	1.063	0.853
UO_2	22	1.042	1.042	0.837
UO_2	23	1.180	1.180	0.947

[a]The relative power value for MOX fuel rods is multiplied by 1.51 to correct for the difference in thermal capacitance of MOX and UO_2 fuel rods (see Sect. 1.3).

Table 10. Relative power data for 25 × 25 concentric-region core configuration containing a 15 × 15 UO_2 inner region and 24% ^{240}Pu outer region

Fuel type	Rod No.	Relative power	Corrected relative power[a]	Normalized corrected relative power
24% ^{240}Pu	1	2.207	3.333	0.547
24% ^{240}Pu	2	1.372	2.072	0.340
24% ^{240}Pu	3	1.425	2.151	0.353
24% ^{240}Pu	4	1.723	2.601	0.427
24% ^{240}Pu	5	2.383	3.598	0.591
UO_2	6	3.403	3.403	0.559
UO_2	7	5.406	5.406	0.888
UO_2	8	6.594	6.594	1.083
UO_2	9	7.730	7.730	1.270
UO_2	10	8.203	8.203	1.347
UO_2	11	8.987	8.987	1.476
UO_2	12	9.100	9.100	1.494
UO_2	13	9.471	9.471	1.555
UO_2	14	9.194	9.194	1.510
UO_2	15	9.052	9.052	1.487
UO_2	16	8.557	8.557	1.405
UO_2	17	8.532	8.532	1.401
UO_2	18	7.886	7.886	1.295
UO_2	19	7.168	7.168	1.177
UO_2	20	5.573	5.573	0.915
24% ^{240}Pu	21	4.237	6.398	1.051
24% ^{240}Pu	22	3.039	4.589	0.754
24% ^{240}Pu	23	2.484	3.750	0.616
24% ^{240}Pu	24	2.407	3.635	0.597
24% ^{240}Pu	25	3.465	5.233	0.859

[a]The relative power value for MOX fuel rods is multiplied by 1.51 to correct for the difference in thermal capacitance of MOX and UO_2 fuel rods (see Sect. 1.3).

Table 11. Relative power data for 25 × 25 concentric-region core configuration containing a 15 × 15 24% ^{240}Pu inner region and UO_2 outer region

Fuel type	Rod No.	Relative power	Corrected relative power[a]	Normalized corrected relative power
24% ^{240}Pu	1	0.956	1.444	1.189
24% ^{240}Pu	2	0.770	1.163	0.958
24% ^{240}Pu	3	0.742	1.120	0.923
24% ^{240}Pu	4	0.775	1.171	0.965
24% ^{240}Pu	5	0.805	1.215	1.001
24% ^{240}Pu	6	0.828	1.250	1.030
24% ^{240}Pu	7	0.858	1.296	1.068
24% ^{240}Pu	8	0.856	1.227	1.011
24% ^{240}Pu	9	0.846	1.278	1.053
24% ^{240}Pu	10	0.859	1.297	1.068
24% ^{240}Pu	11	0.848	1.281	1.055
24% ^{240}Pu	12	0.815	1.230	1.013
24% ^{240}Pu	13	0.796	1.202	0.990
24% ^{240}Pu	14	0.799	1.207	0.994
24% ^{240}Pu	15	0.806	1.217	1.002
24% ^{240}Pu	16	0.953	1.439	1.185
UO_2	17	0.950	0.950	0.783
UO_2	18	1.052	1.052	0.867
UO_2	19	1.170	1.170	0.964
UO_2	20	1.147	1.147	0.945
UO_2	21	1.145	1.145	0.943

[a]The relative power value for MOX fuel rods is multiplied by 1.51 to correct for the difference in thermal capacitance of MOX and UO_2 fuel rods (see Sect. 1.3).

Table 12. Relative power data for a 27 × 27 concentric-region core configuration containing a 15 × 15 24% ^{240}Pu inner region and 8% ^{240}Pu outer region

Fuel type	Rod No.	Relative power	Normalized relative power
8% ^{240}Pu	1	1.228	1.315
8% ^{240}Pu	2	0.795	0.851
8% ^{240}Pu	3	0.652	0.698
8% ^{240}Pu	4	0.868	0.929
8% ^{240}Pu	5	0.965	1.033
8% ^{240}Pu	6	0.994	1.064
24% ^{240}Pu	7	0.929	0.995
24% ^{240}Pu	8	0.968	1.036
24% ^{240}Pu	9	1.008	1.079
24% ^{240}Pu	10	1.045	1.119
24% ^{240}Pu	11	1.070	1.146
24% ^{240}Pu	12	1.064	1.139
24% ^{240}Pu	13	1.085	1.162
24% ^{240}Pu	14	1.084	1.161
24% ^{240}Pu	15	1.080	1.156
24% ^{240}Pu	16	1.058	1.133
24% ^{240}Pu	17	0.980	1.049
24% ^{240}Pu	18	0.871	0.933
24% ^{240}Pu	19	0.784	0.839
8% ^{240}Pu	20	0.760	0.814
8% ^{240}Pu	21	0.717	0.768
8% ^{240}Pu	22	0.541	0.579

Table 13. Relative power data for a cylindrical concentric-region core configuration containing a 24% ^{240}Pu inner region and an 8% ^{240}Pu outer region

Fuel type	Rod No.	Relative power	Normalized relative power
8% ^{240}Pu	1	0.853	1.153
8% ^{240}Pu	2	0.582	0.786
8% ^{240}Pu	3	0.579	0.782
8% ^{240}Pu	4	0.625	0.845
8% ^{240}Pu	5	0.694	0.938
8% ^{240}Pu	6	0.742	1.003
8% ^{240}Pu	7	0.623	0.842
8% ^{240}Pu	8	0.576	0.778
8% ^{240}Pu	9	0.641	0.866
8% ^{240}Pu	10	0.627	0.847
24% ^{240}Pu	11	0.704	0.951
24% ^{240}Pu	12	0.741	1.001
24% ^{240}Pu	13	0.788	1.065
24% ^{240}Pu	14	0.811	1.096
24% ^{240}Pu	15	0.826	1.116
24% ^{240}Pu	16	0.832	1.124
24% ^{240}Pu	17	0.858	1.159
24% ^{240}Pu	18	0.870	1.176
24% ^{240}Pu	19	0.886	1.197
24% ^{240}Pu	20	0.856	1.157
24% ^{240}Pu	21	0.821	1.109

Table 14. Relative power data for a cylindrical concentric-region core configuration containing a 24% ^{240}Pu inner region and an 8% ^{240}Pu outer region

Fuel type	Rod No.	Relative power	Normalized relative power
24% ^{240}Pu	1	1.032	1.221
24% ^{240}Pu	2	1.037	1.227
24% ^{240}Pu	3	1.036	1.226
24% ^{240}Pu	4	0.984	1.164
24% ^{240}Pu	5	0.944	1.117
24% ^{240}Pu	6	0.897	1.062
24% ^{240}Pu	7	0.859	1.017
24% ^{240}Pu	8	0.790	0.935
8% ^{240}Pu	9	0.812	0.961
8% ^{240}Pu	10	0.726	0.859
8% ^{240}Pu	11	0.683	0.808
8% ^{240}Pu	12	0.903	1.069
8% ^{240}Pu	13	0.730	0.864
8% ^{240}Pu	14	0.686	0.812
8% ^{240}Pu	15	0.719	0.851
8% ^{240}Pu	16	0.683	0.808

Table 15. Relative power data for a cylindrical concentric-region core configuration with a 24% ^{240}Pu inner region and an 8% ^{240}Pu outer region and a regional variation in lattice pitch

Fuel type	Rod No.	Relative power
8% ^{240}Pu	1	1.559
8% ^{240}Pu	2	1.652
8% ^{240}Pu	3	1.862
8% ^{240}Pu	4	1.546
24% ^{240}Pu	5	1.047
24% ^{240}Pu	6	1.031
24% ^{240}Pu	7	1.032
24% ^{240}Pu	8	1.052
24% ^{240}Pu	9	1.044
24% ^{240}Pu	10	1.035
24% ^{240}Pu	11	1.072
8% ^{240}Pu	12	1.568
8% ^{240}Pu	13	1.873
8% ^{240}Pu	14	1.671
8% ^{240}Pu	15	1.568
24% ^{240}Pu	16	1.053
24% ^{240}Pu	17	1.024
24% ^{240}Pu	18	1.029
24% ^{240}Pu	19	1.074
24% ^{240}Pu	20	1.207
8% ^{240}Pu	21	1.802
8% ^{240}Pu	22	1.779
8% ^{240}Pu	23	1.406

1.4.2.2 Salt-and-pepper power distribution measurements

The salt-and-pepper core configurations were constructed by loading two different fuel types in checkerboard pattern. The variations included differences in core size, core geometry, and fuel type. All available fuel types were used in various combinations for salt-and-pepper core configurations. Power distribution measurements were performed for clean cores. All experiments were performed with a 1.7526-cm lattice pitch.

Power distribution measurements were performed for five configurations with several combinations of fuel types. One configuration was composed of 8% ^{240}Pu fuel and 2.72% UO_2 fuel, three configurations were composed of 24% ^{240}Pu fuel and 2.72% UO_2 fuel, and another configuration was composed of 8% ^{240}Pu fuel and 24% ^{240}Pu fuel.

The MOX and UO_2 fuel rods had different diameters. In the salt-and-pepper core configurations MOX, and UO_2 fuels were used in the same lattice pitch; therefore, with the same lattice pitches different moderator-to-fuel volume ratios were obtained in the same core configuration. Because the dimensions of both MOX fuels were the same for the core configurations composed of these fuels, the moderator-to-fuel ratios were the same.

The installation of MOX fuel is given in Fig. 1. The installation of MOX and UO_2 fuel rods for a salt-and-pepper core configuration is given in Fig. 2. A summary of the salt-and-pepper experiments is given in Table 16. Core diagrams showing the experimental configurations and the measured rods are presented in Figs. 17–21. Relative power data from each experiment are given in Tables 17–21.

Table 16. Reported data for salt-and-pepper configurations[a,b]

Case No.	Power data (table)	Core diagram (figure)	Number of fuel rods	Fuel type	Number of fuel rods	Fuel type	Critical water height (cm)
14	17	17	365	8% ^{240}Pu	364	24% ^{240}Pu	89.18
15	18	18	265	8% ^{240}Pu	264	UO_2	49.90
16	19	19	265	24% ^{240}Pu	264	UO_2	89.64
17	20	20	288	24% ^{240}Pu	288	UO_2	73.42
18	21	21	313	24% ^{240}Pu	312	UO_2	63.49

[a]These are clean experiments containing no boron.
[b]All experiments were performed in a 1.7526-cm lattice.

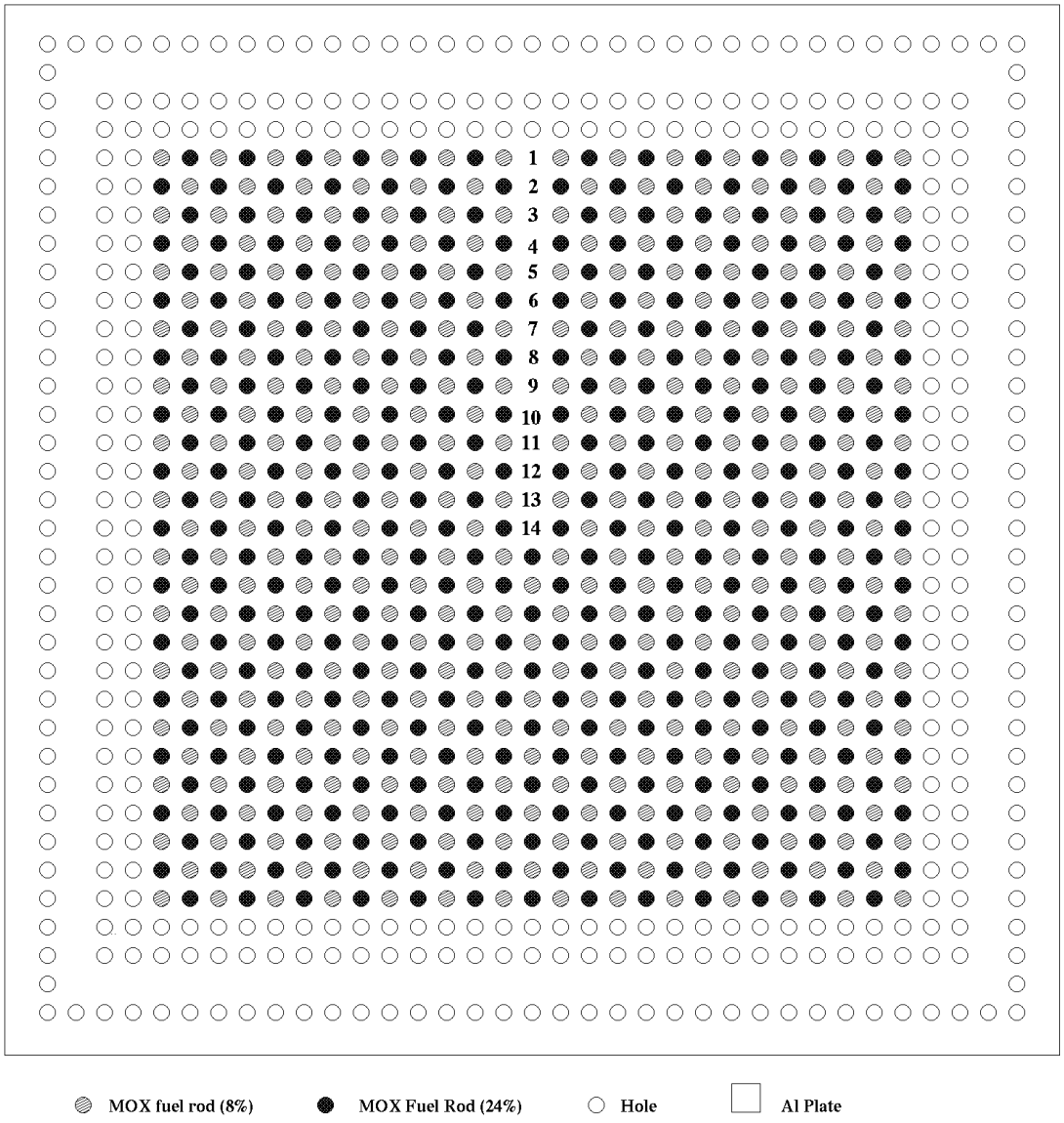

Fig. 17. A 27 × 27 salt-and-pepper core configuration composed of 8% ^{240}Pu and 24% ^{240}Pu fuels.

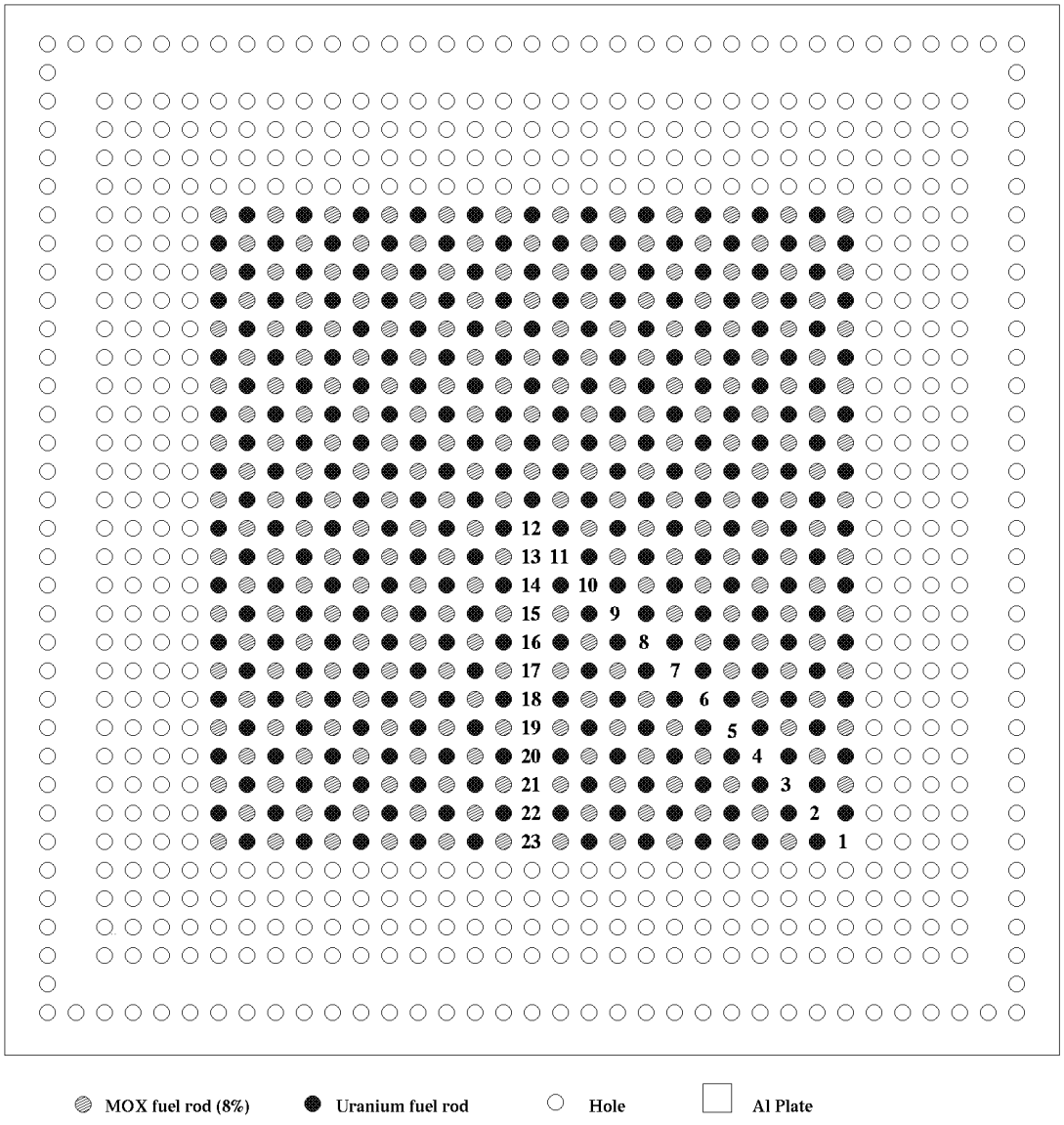

Fig. 18. A 23 × 23 salt-and-pepper core configuration composed of 8% ^{240}Pu and UO_2 fuels.

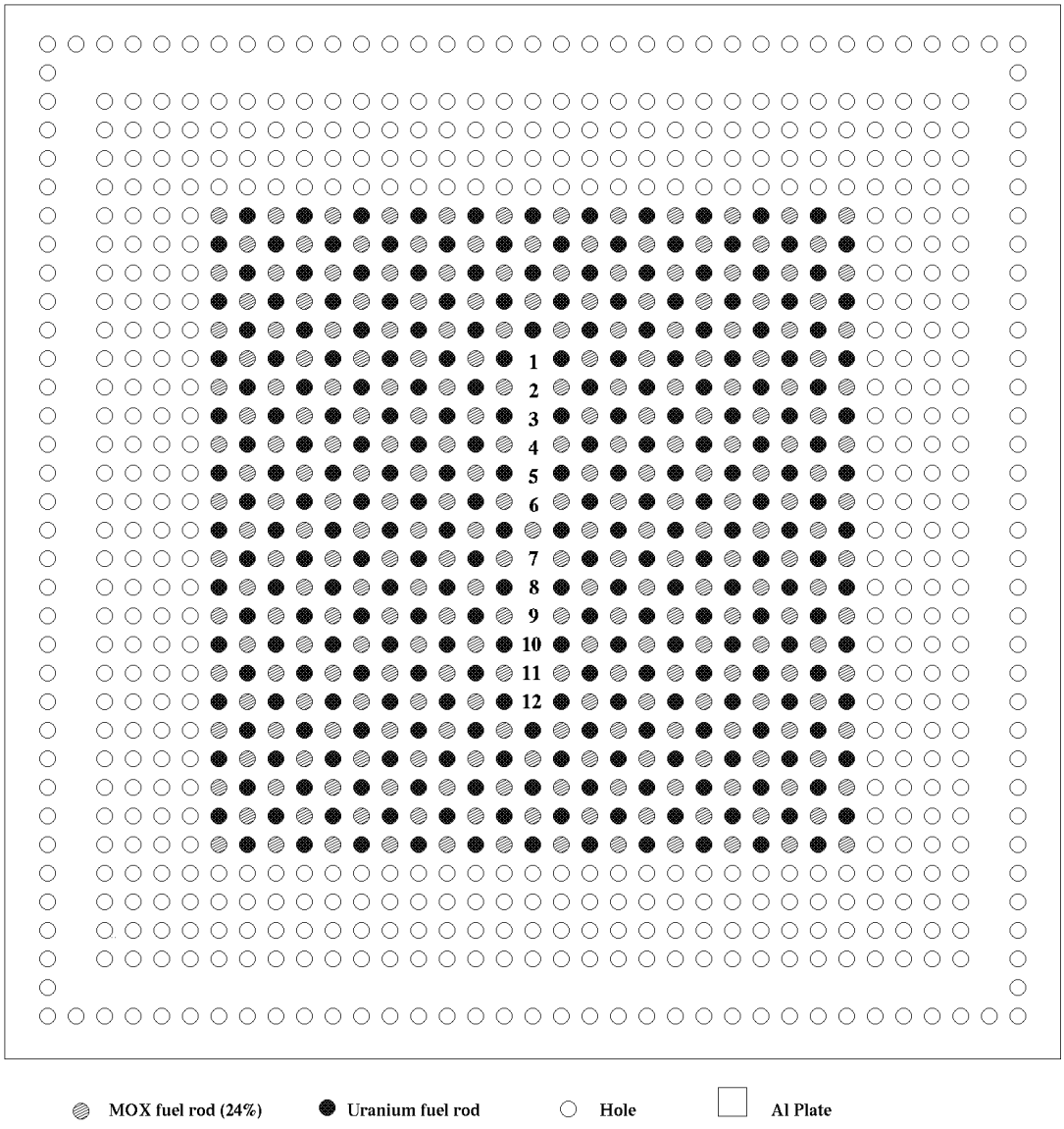

Fig. 19. A 23 × 23 salt-and-pepper core configuration composed of 24% ^{240}Pu and UO_2 fuels.

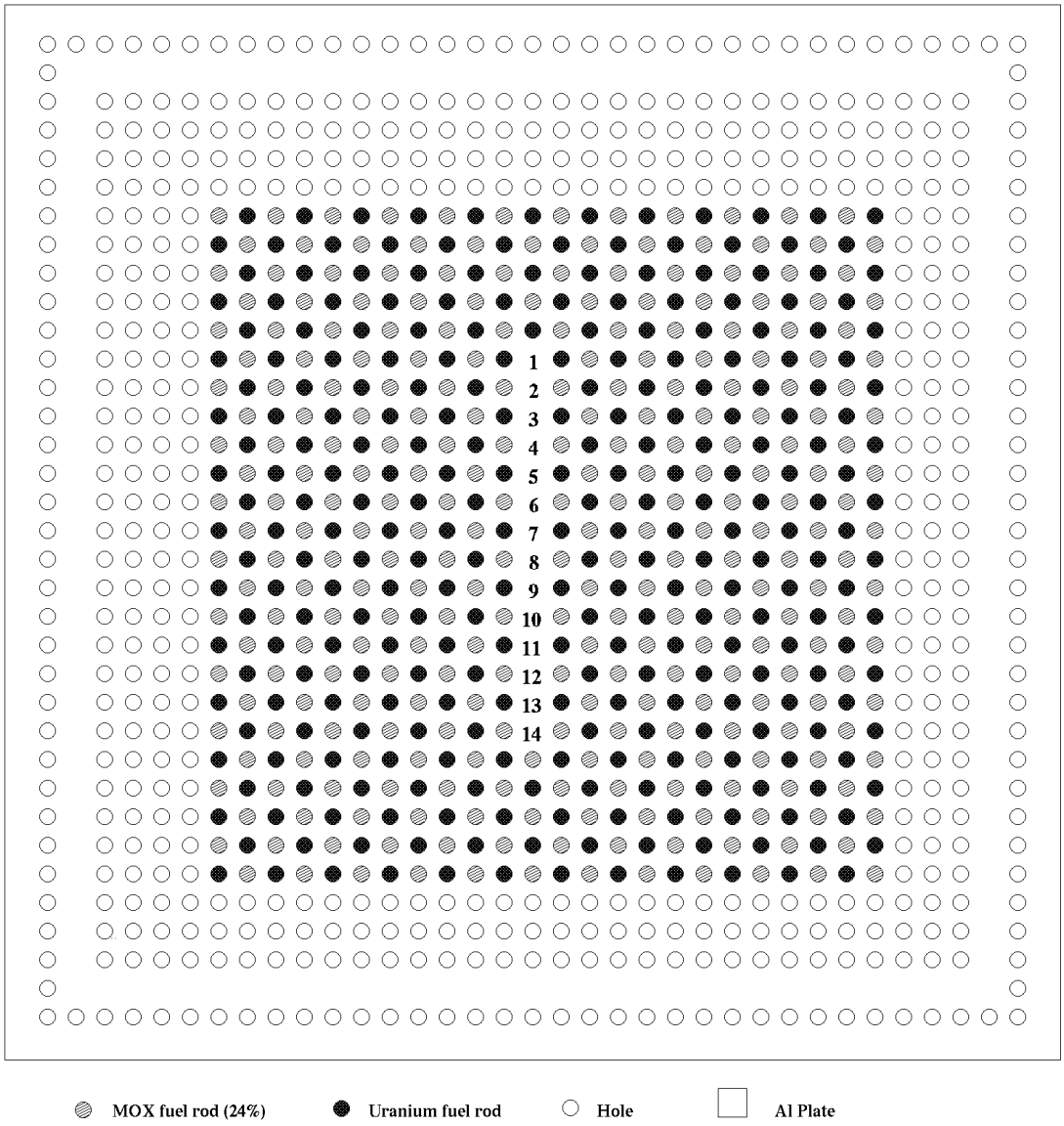

Fig. 20. A 24 × 24 salt-and-pepper core configuration composed of 24% ^{240}Pu and UO_2 fuels.

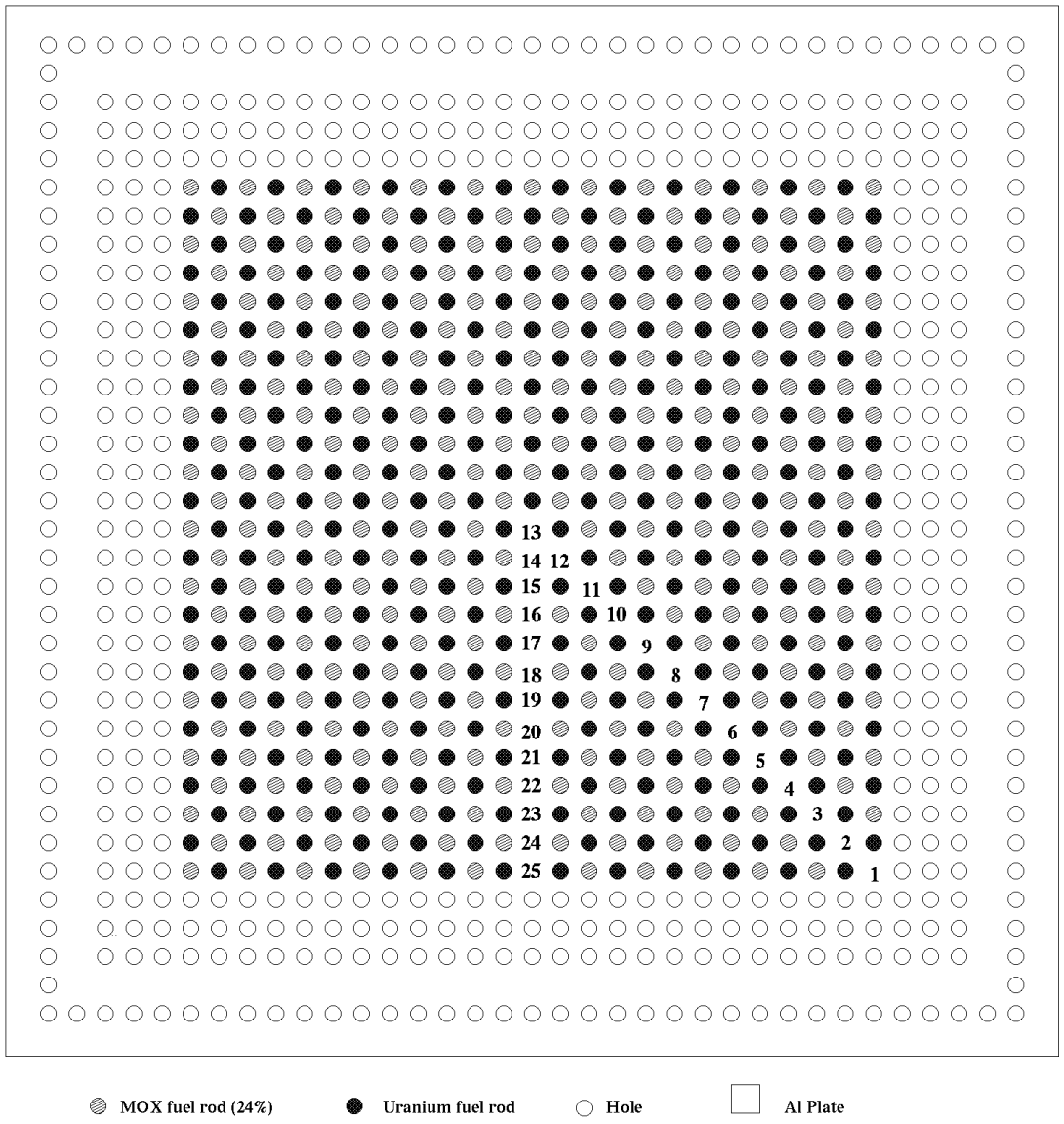

Fig. 21. A 25 × 25 salt-and-pepper core configuration composed of 24% ^{240}Pu and UO_2 fuels.

Table 17. Relative power data for 27 × 27 salt-and-pepper core configuration composed of 8% ^{240}Pu and 24% ^{240}Pu fuels

Fuel type	Rod No.	Relative power
24% ^{240}Pu	1	2.165
8% ^{240}Pu	2	1.801
24% ^{240}Pu	3	1.511
8% ^{240}Pu	4	1.922
24% ^{240}Pu	5	1.752
8% ^{240}Pu	6	2.233
24% ^{240}Pu	7	1.998
8% ^{240}Pu	8	2.577
24% ^{240}Pu	9	2.223
8% ^{240}Pu	10	2.725
24% ^{240}Pu	11	2.370
8% ^{240}Pu	12	2.881
24% ^{240}Pu	13	2.400
8% ^{240}Pu	14	2.889

Table 18. Relative power data for a 23 × 23 salt-and-pepper core configuration composed of 8% ^{240}Pu and UO_2 fuels

Fuel type	Rod No.	Relative power	Corrected, normalized, relative power[a]
8% ^{240}Pu	1	5.255	0.770
8% ^{240}Pu	2	4.032	0.591
8% ^{240}Pu	3	4.357	0.639
8% ^{240}Pu	4	5.170	0.758
8% ^{240}Pu	5	6.146	0.901
8% ^{240}Pu	6	7.026	1.030
8% ^{240}Pu	7	8.042	1.179
8% ^{240}Pu	8	9.046	1.326
8% ^{240}Pu	9	9.769	1.432
8% ^{240}Pu	10	10.144	1.487
8% ^{240}Pu	11	10.293	1.509
8% ^{240}Pu	12	10.501	1.540
UO_2	13	7.250	0.704
8% ^{240}Pu	14	10.353	1.518
UO_2	15	7.103	0.690
8% ^{240}Pu	16	9.738	1.428
UO_2	17	6.380	0.619
8% ^{240}Pu	18	8.539	1.252
UO_2	19	5.581	0.542
8% ^{240}Pu	20	7.400	1.085
UO_2	21	4.656	0.452
8% ^{240}Pu	22	6.504	0.954
UO_2	23	6.129	0.595

[a]The relative power value for MOX fuel rods is multiplied by 1.51 to correct for the difference in thermal capacitance of MOX and UO_2 fuel rods (see Sect. 1.3).

Table 19. Relative power data for a 23 × 23 salt-and-pepper core configuration composed of 24% ^{240}Pu and UO_2 fuels

Fuel type	Rod No.	Relative power	Corrected, normalized, relative power[a]
24% ^{240}Pu	1	11.213	1.151
UO_2	2	10.260	0.697
24% ^{240}Pu	3	12.391	1.272
UO_2	4	10.898	0.741
24% ^{240}Pu	5	13.224	1.357
UO_2	6	11.482	0.780
UO_2	7	11.345	0.771
24% ^{240}Pu	8	13.424	1.378
UO_2	9	11.111	0.755
24% ^{240}Pu	10	12.536	1.287
UO_2	11	10.121	0.688
24% ^{240}Pu	12	10.951	1.124

[a]The relative power value for MOX fuel rods is multiplied by 1.51 to correct for the difference in thermal capacitance of MOX and UO_2 fuel rods (see Sect. 1.3).

Table 20. Relative power data for 24 × 24 salt-and-pepper core configuration composed of 24% ^{240}Pu and UO_2 fuels

Fuel type	Rod No.	Relative power	Corrected, normalized, relative power[a]
24% ^{240}Pu	1	8.809	1.131
UO_2	2	7.420	0.631
24% ^{240}Pu	3	9.958	1.278
UO_2	4	8.486	0.721
24% ^{240}Pu	5	10.515	1.349
UO_2	6	8.834	0.751
24% ^{240}Pu	7	10.818	1.388
UO_2	8	8.814	0.749
24% ^{240}Pu	9	10.824	1.389
UO_2	10	8.861	0.753
24% ^{240}Pu	11	10.300	1.322
UO_2	12	8.265	0.702
24% ^{240}Pu	13	9.428	1.210
UO_2	14	7.357	0.625

[a]The relative power value for MOX fuel rods is multiplied by 1.51 to correct for the difference in thermal capacitance of MOX and UO_2 fuel rods (see Sect. 1.3).

Table 21. Relative power data for a 25 × 25 salt-and-pepper core configuration composed of 24% ^{240}Pu and UO_2 fuels

Fuel type	Rod No.	Relative power	Corrected, normalized, relative power[a]
24% ^{240}Pu	1	6.915	0.685
24% ^{240}Pu	2	5.295	0.525
24% ^{240}Pu	3	5.662	0.561
24% ^{240}Pu	4	6.834	0.677
24% ^{240}Pu	5	8.134	0.806
24% ^{240}Pu	6	9.682	0.960
24% ^{240}Pu	7	10.996	1.090
24% ^{240}Pu	8	12.012	1.191
24% ^{240}Pu	9	13.052	1.294
24% ^{240}Pu	10	13.931	1.381
24% ^{240}Pu	11	14.752	1.462
24% ^{240}Pu	12	15.034	1.490
24% ^{240}Pu	13	15.032	1.490
UO_2	14	12.311	0.808
24% ^{240}Pu	15	14.744	1.461
UO_2	16	12.217	0.802
24% ^{240}Pu	17	14.201	1.408
UO_2	18	11.286	0.741
24% ^{240}Pu	19	12.894	1.278
UO_2	20	10.245	0.672
24% ^{240}Pu	21	11.088	1.099
UO_2	22	8.397	0.551
24% ^{240}Pu	23	9.293	0.921
UO_2	24	7.616	0.500
24% ^{240}Pu	25	11.572	1.147

[a]The relative power value for MOX fuel rods is multiplied by 1.51 to correct for the difference in thermal capacitance of MOX and UO_2 fuel rods (see Sect. 1.3).

1.4.2.3 Multiregion slab power distribution measurements

Multiregion slab power distribution measurements were performed in a number of different configurations. Each of these cores was composed of two UO_2 slabs, sandwiching a center MOX-fueled slab. In each configuration, the length of the central region was the same with the number of plutonium fueled rods between the two surrounding UO_2 slabs fixed at 19 rods. The width of the three slabs was varied to compensate for gross reactivity changes, as in the change from a clean to borated core. The different diameters of the plutonium and uranium fuel rods required that the lattices in the UO_2-fueled region and the plutonium-fueled region have different pitch in order to preserve a constant fuel-to-moderator ratio in each region. In the UO_2 regions, a smaller lattice pitch was used compared to the MOX (central) region in order to have the same fuel-to-moderator ratio throughout the core. Two slab array core configurations were constructed using all available fuel types. One of these core configurations was constructed by using the 24%

^{240}Pu fuel in the inner region and the 8% ^{240}Pu fuel in the outer region. The other multiregion core configuration contains alternate rows of 8% and 24% ^{240}Pu fuels in the central region.

The installation of MOX and UO_2 fuel rods for multiregion slab core configurations is given in Fig. 3. The lattice pitch for UO_2 slabs was 1.4605 cm (0.575 in.), whereas the lattice pitch for MOX fuel was 1.7526 cm (0.69 in.). In this way, the fuel-to-moderator ratio was the same for both MOX and UO_2 regions. A 1.608-cm (0.633-in.) water gap was present between each slab region. This gap was between the unit cells; therefore, the distance between the centers of the MOX and UO_2 fuel rods is 3.21455 cm (1.608 cm plus one-half of the MOX and UO_2 lattice pitches). The two fuel rods had different lengths; therefore, vertical buckling measurements were made in each region in each configuration.

A summary of the multiregion slab experiments is given in Table 22. Core diagrams showing the experimental configurations and the measured rods are presented in Figs. 22–29. Power data from each experiment are given in Tables 23–30. In these figures, fuel rods are either indicated by solid circles or by numbers that show the measurement rods.

Table 22. Reported data for multiregion slab core configurations[a]

Case No.	Power data (table)	Core diagram (figure)	Number of UO_2 fuel rods	Number of MOX fuel rods	Boron concentration	Critical water height (cm)	Test configuration
19	23	22	460	361 (8% ^{240}Pu)	0	62.83	Reference core
20	24	23	460	361 (8% ^{240}Pu)	0	64.45	Aluminum void tubes (4 × 4)
21	25	24	460	361 (8% ^{240}Pu)	0	72.74	Aluminum void tubes (10 × 10)
22	26	25	810	437 (8% ^{240}Pu)	526	69.04	Reference core
23	27	26	810	437 (8% ^{240}Pu)	526	70.31	Aluminum void tubes (4 × 4)
24	28	27	810	437 (8% ^{240}Pu)	526	77.73	Aluminum void tubes (10 × 10)
25	29	28	500	228 (8% ^{240}Pu) 171 (24% ^{240}Pu)	0	75.41	—
26	30	29	500	210 (8% ^{240}Pu) 189 (24% ^{240}Pu)	0	71.05	—

[a]The lattice pitch for the UO_2 slab was 1.4605 cm and 1.7526 cm for the MOX region for all configurations.

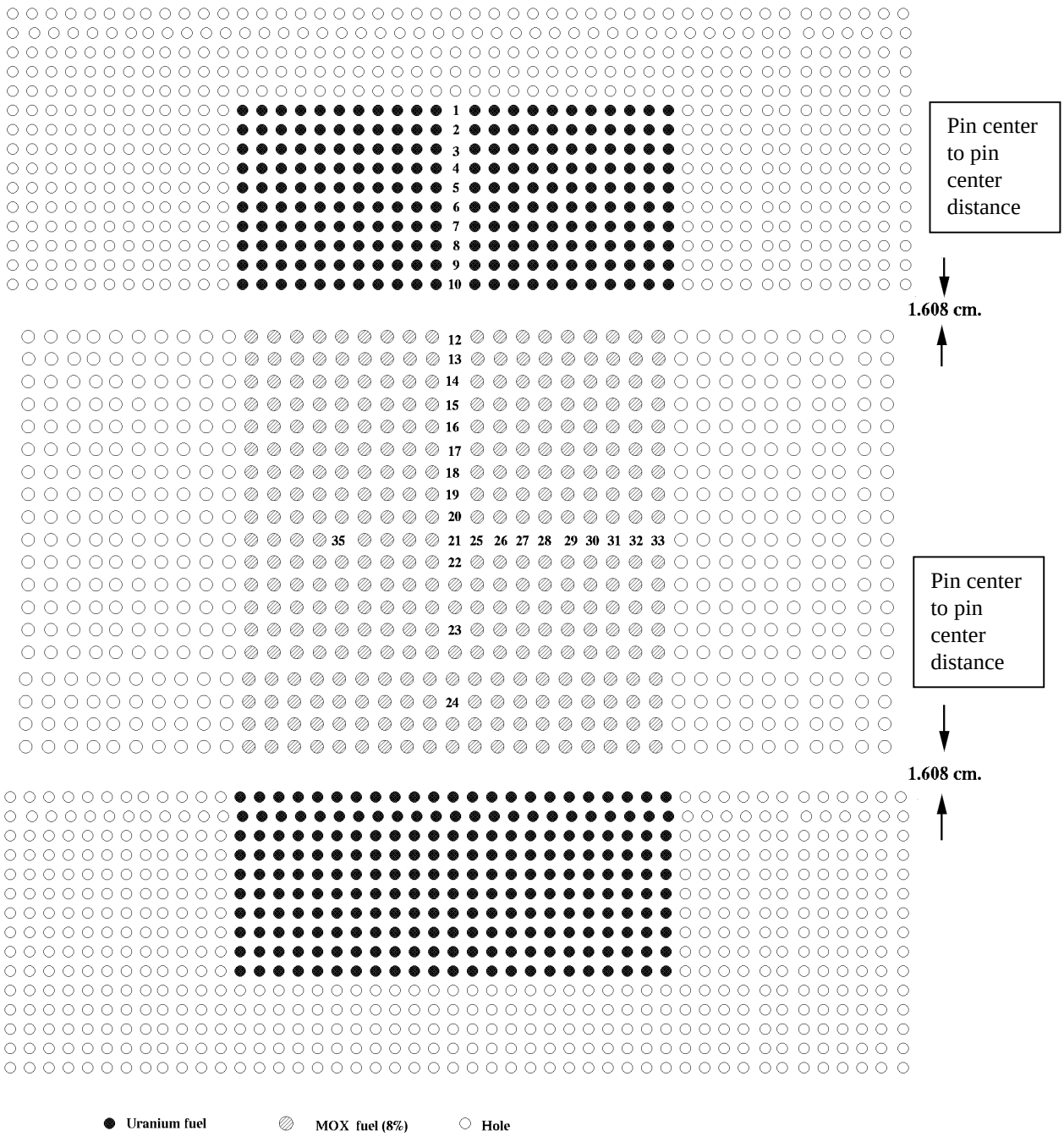

Fig. 22. A multiregion slab core configuration containing 8% ^{240}Pu central region (19 × 19) and UO_2 outer regions.

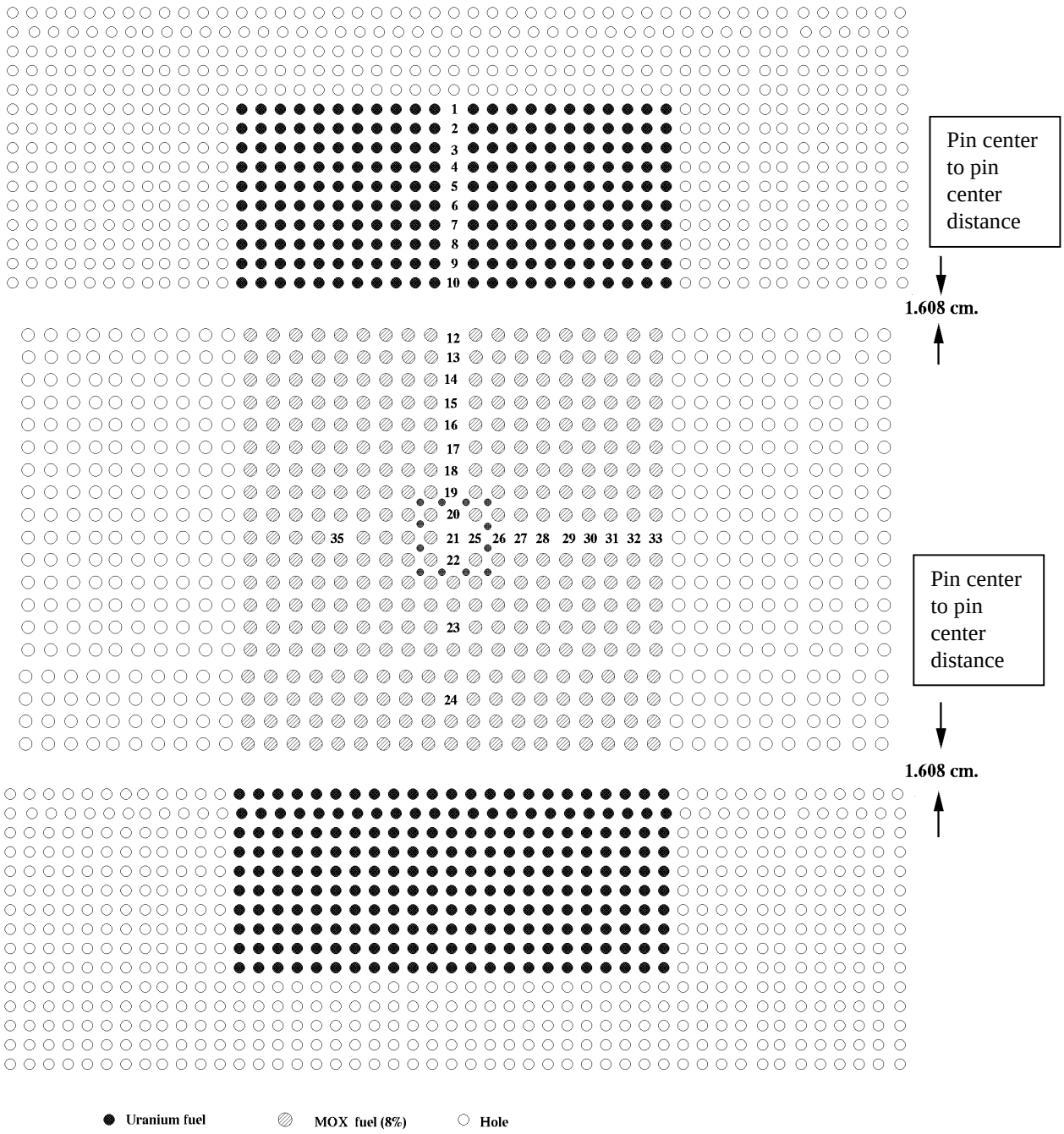

Fig. 23. A multiregion slab core configuration containing an 8% ^{240}Pu central region (19 × 19) and UO_2 outer regions (10 × 23) with a 4 × 4 central void pattern.

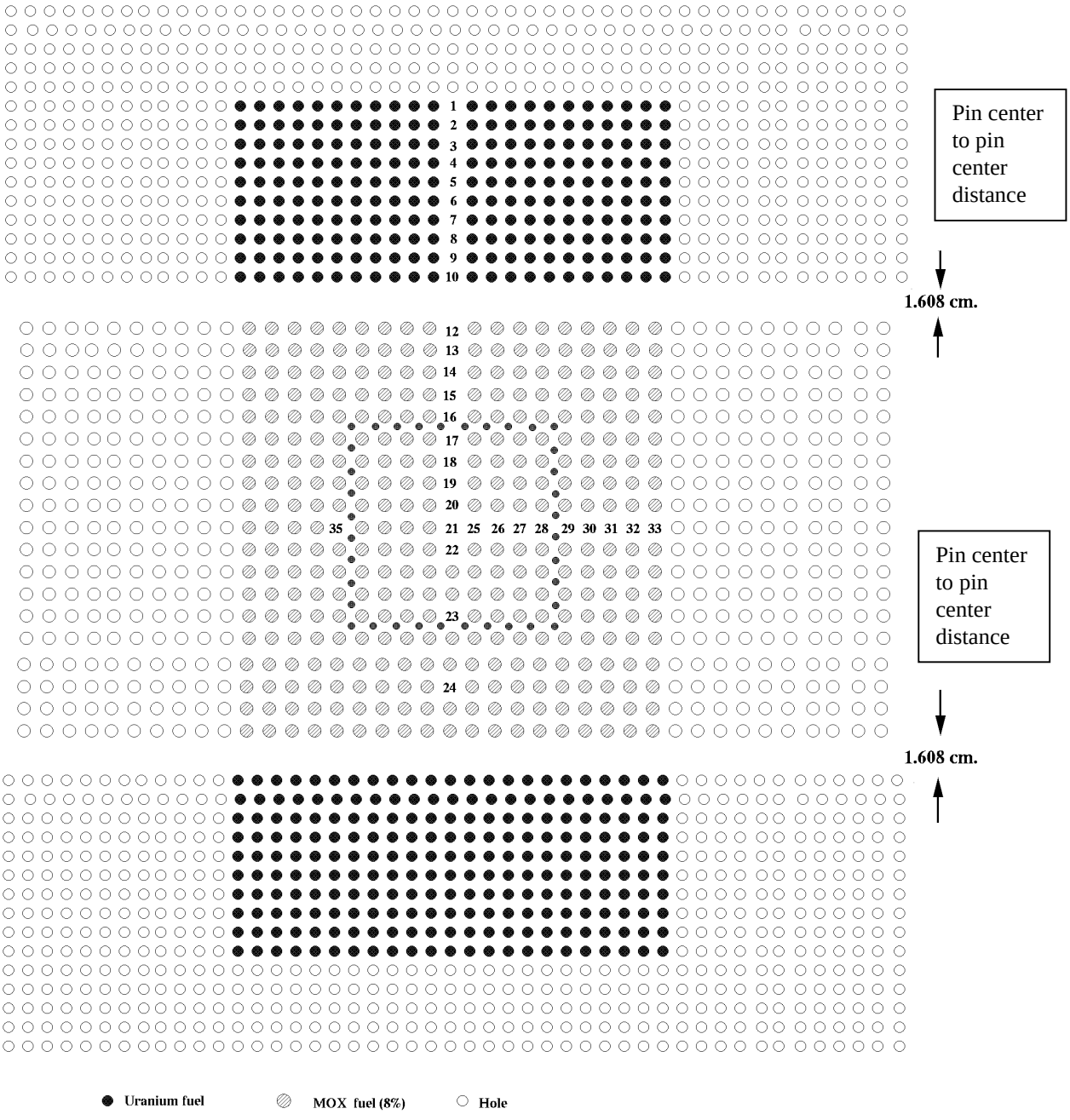

Fig. 24. A multiregion slab core configuration containing an 8% ^{240}Pu central region (19 × 19) and UO_2 outer regions (10 × 23) with a 10 × 10 central void pattern.

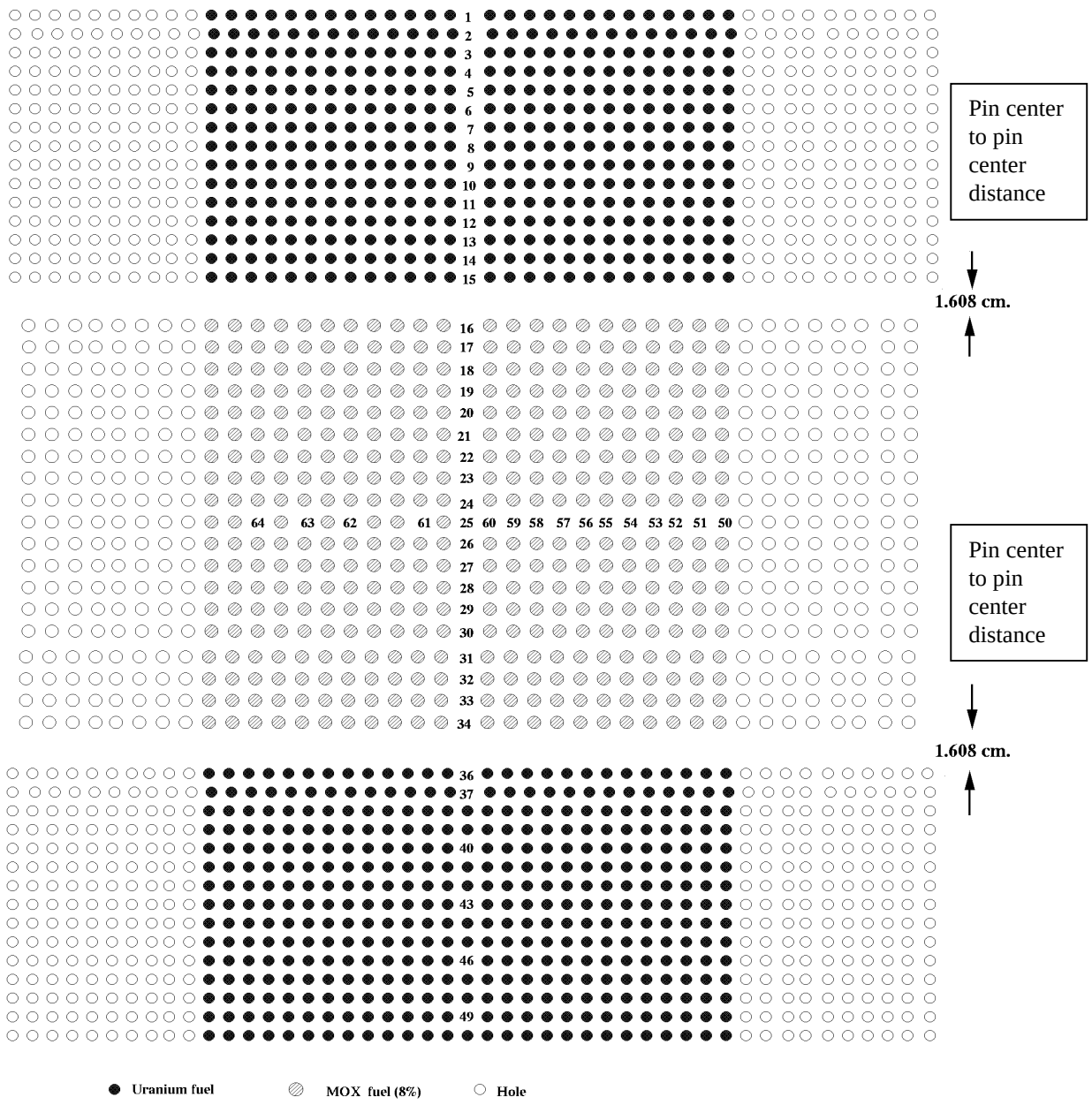

Fig. 25. A multiregion slab core configuration containing an 8% ^{240}Pu central region (19 × 23) and UO_2 outer regions (15 × 27).

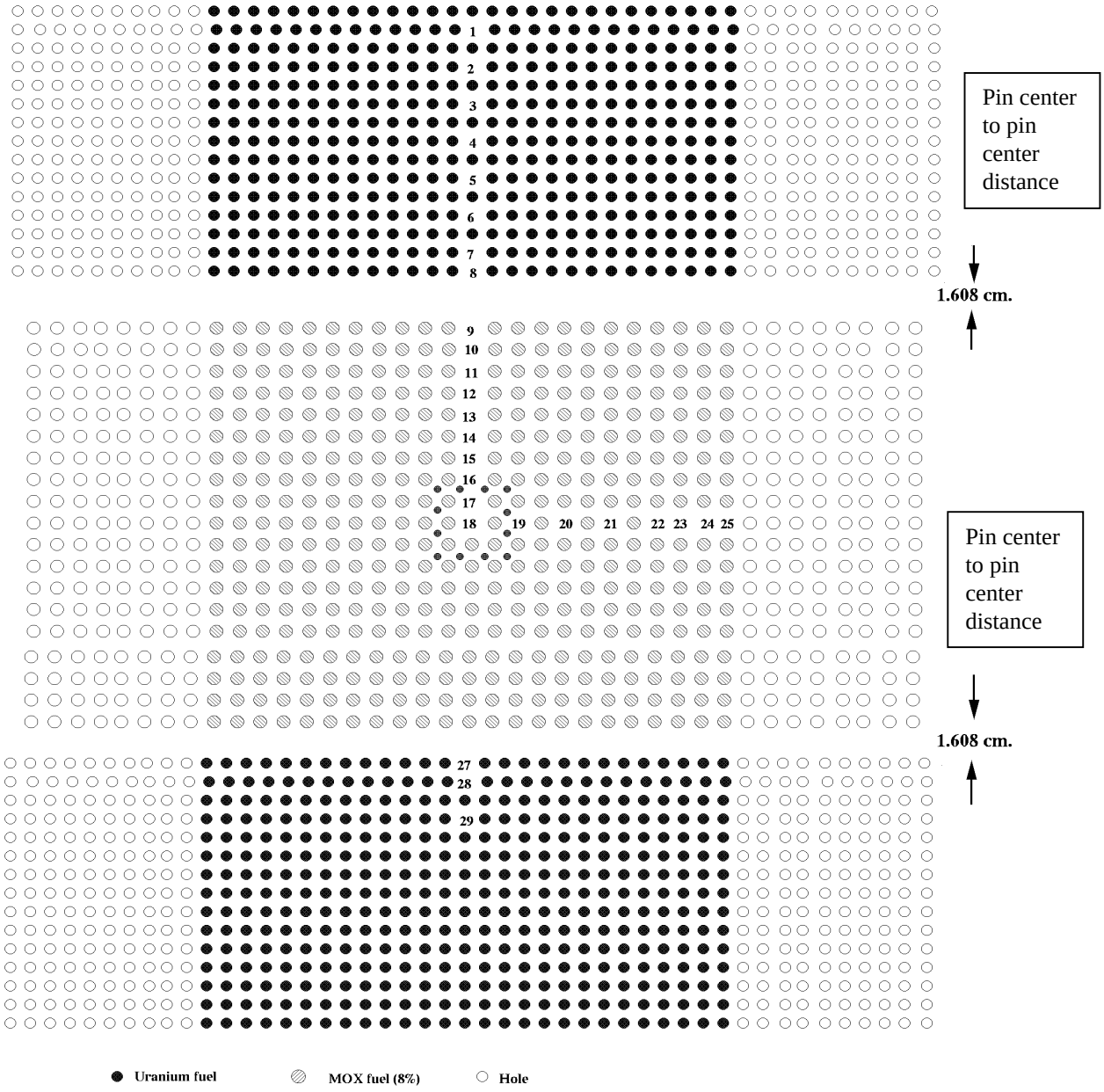

Fig. 26. A multiregion slab core configuration containing an 8% ^{240}Pu central region (19 × 23) and UO_2 outer regions (15 × 27) with a 4 × 4 central void pattern.

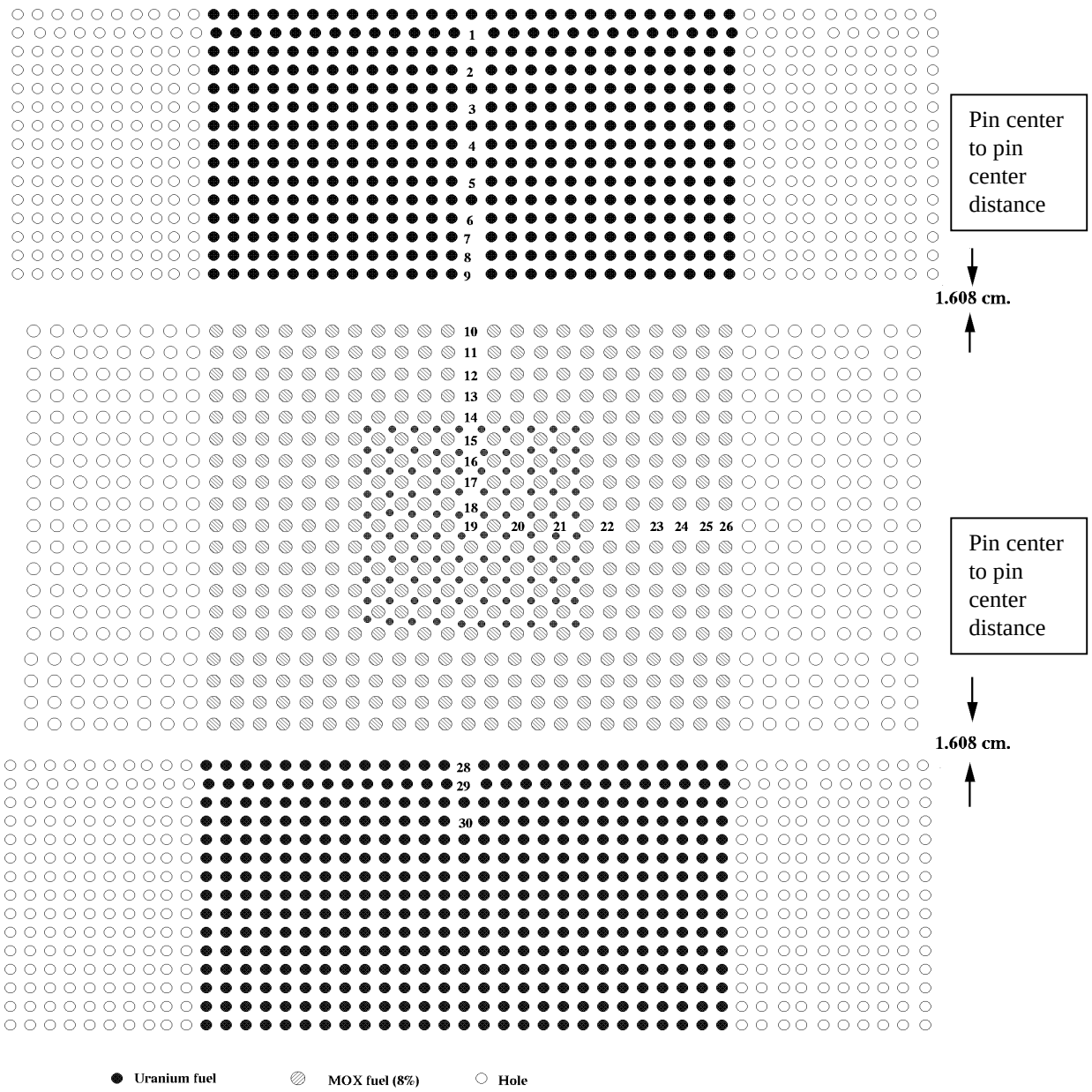

Fig. 27. A multiregion slab core configuration containing an 8% ^{240}Pu central region (19 × 23) and UO_2 outer regions (15 × 27) with a 10 × 10 central void pattern.

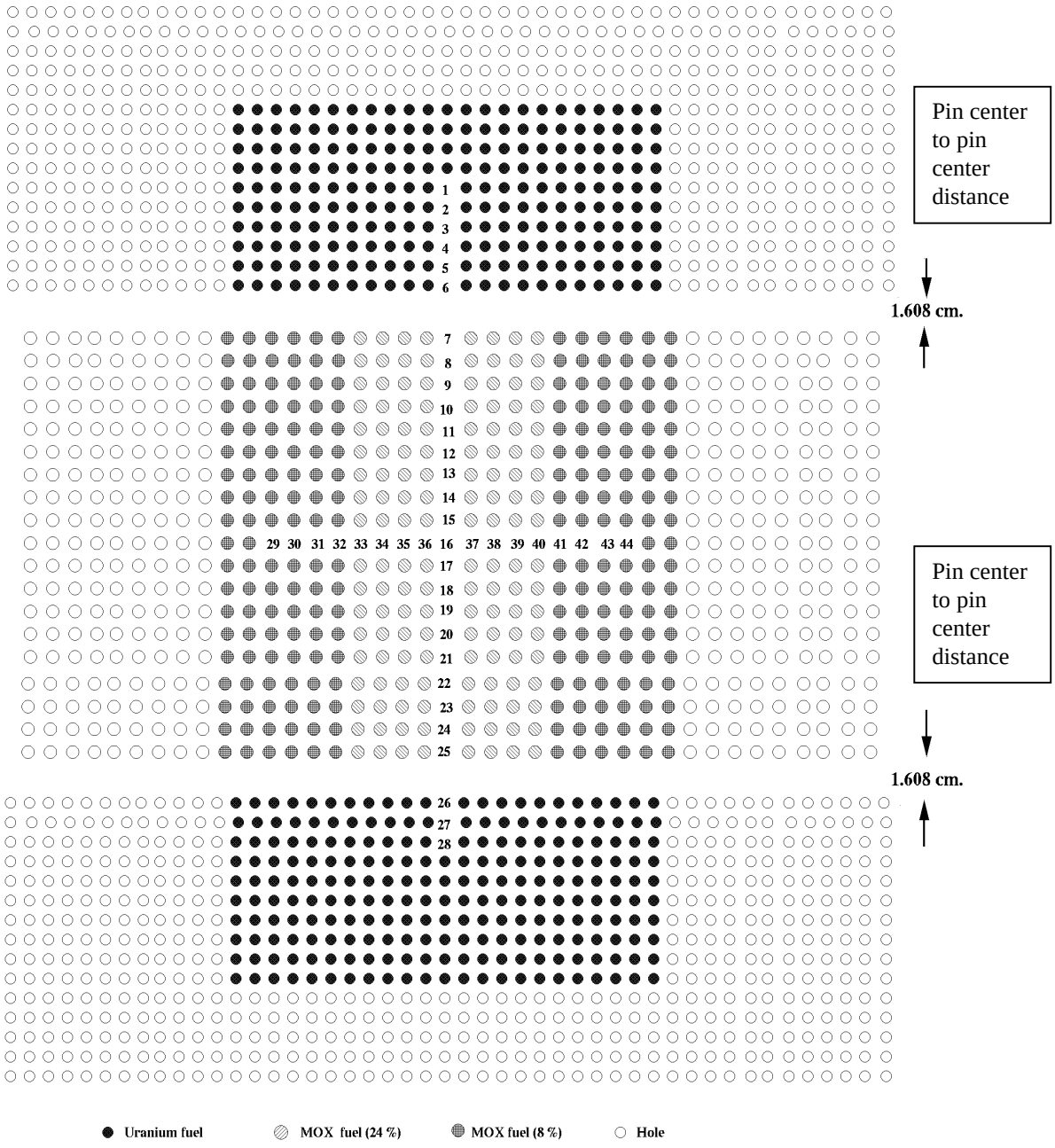

Fig. 28. A multiregion slab core configuration containing central traverse slabs of 8% ^{240}Pu and 24% ^{240}Pu in the central region (19 × 21) and UO_2 outer regions (10 × 25).

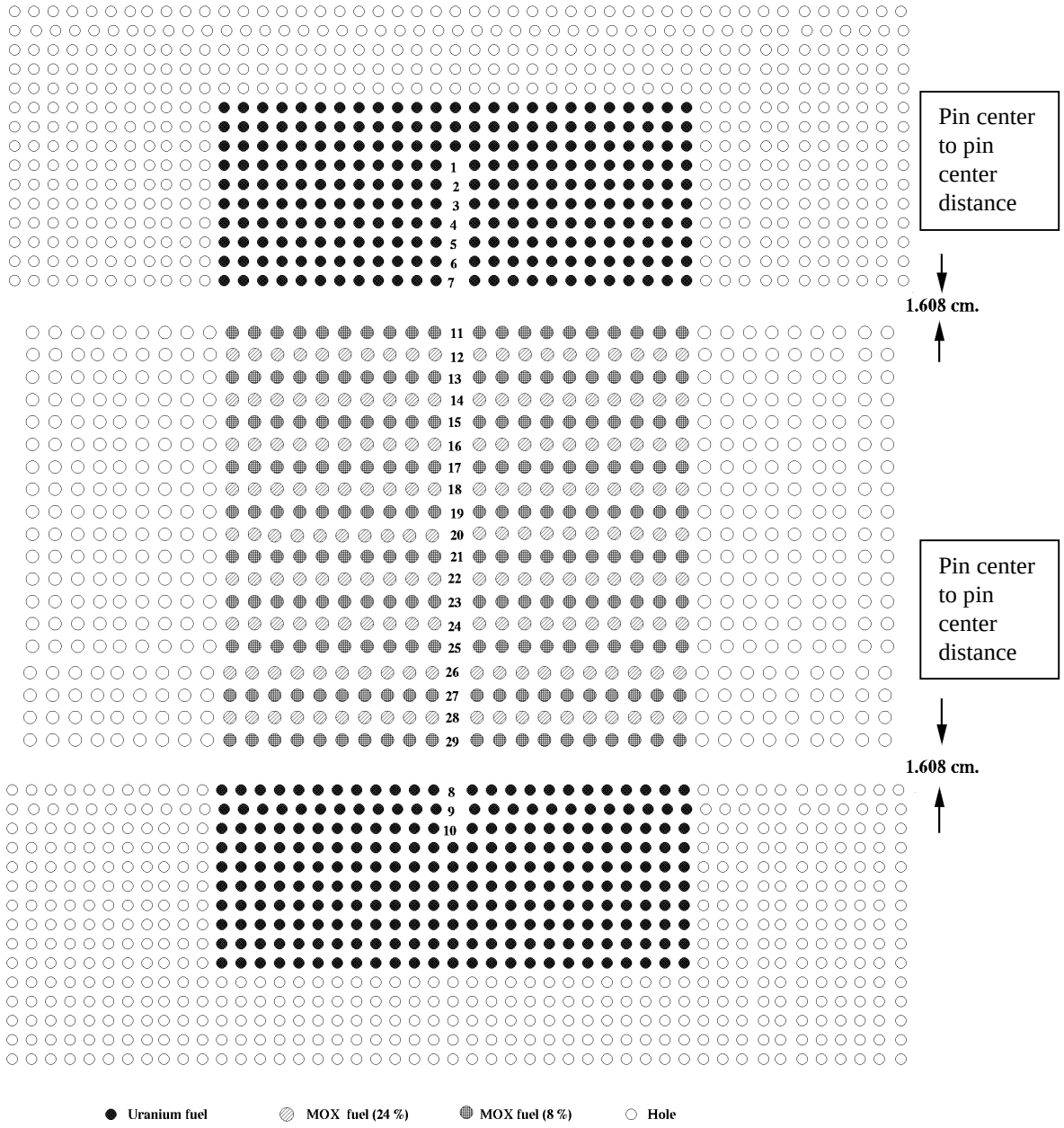

Fig. 29. A multiregion slab core configuration containing alternate rows of 8% ^{240}Pu and 24% ^{240}Pu in the central region (19 × 21) and UO_2 outer regions (10 × 25).

Table 23. Relative power data for the multiregion slab core configuration for the reference core

Fuel type	Rod No.	Relative power	Corrected, normalized, relative power[a]
UO_2	1	4.763	0.573
UO_2	2	3.626	0.436
UO_2	3	3.397	0.409
UO_2	4	3.618	0.435
UO_2	5	3.868	0.465
UO_2	6	4.295	0.517
UO_2	7	4.491	0.540
UO_2	8	4.790	0.576
UO_2	9	4.855	0.584
UO_2	10	4.750	0.571
8% ^{240}Pu	12	6.670	1.212
8% ^{240}Pu	13	6.505	1.182
8% ^{240}Pu	14	6.602	1.199
8% ^{240}Pu	15	6.755	1.227
8% ^{240}Pu	16	6.937	1.260
8% ^{240}Pu	17	7.047	1.280
8% ^{240}Pu	18	7.162	1.301
8% ^{240}Pu	19	7.161	1.301
8% ^{240}Pu	20	7.256	1.318
8% ^{240}Pu	21	7.218	1.311
8% ^{240}Pu	22	7.224	1.312
8% ^{240}Pu	23	6.937	1.260
8% ^{240}Pu	24	6.529	1.186
8% ^{240}Pu	25	7.210	1.310
8% ^{240}Pu	26	7.017	1.275
8% ^{240}Pu	27	6.917	1.256
8% ^{240}Pu	28	6.584	1.196
8% ^{240}Pu	30	5.666	1.029
8% ^{240}Pu	31	5.209	0.946
8% ^{240}Pu	32	5.469	0.993
8% ^{240}Pu	33	8.024	1.457
8% ^{240}Pu	35	5.956	1.082

[a]The relative power value for MOX fuel rods is multiplied by 1.51 to correct for the difference in thermal capacitance of the MOX and UO_2 fuel rods (see Sect. 1.3).

Table 24. Relative power data for the multiregion slab core configuration for a 4 × 4 central void pattern

Fuel type	Rod No.	Relative power	Corrected, normalized, relative power[a]
UO_2	1	4.813	0.599
UO_2	2	3.656	0.455
UO_2	3	3.433	0.427
UO_2	4	3.680	0.458
UO_2	5	3.898	0.485
UO_2	6	4.303	0.536
UO_2	7	4.551	0.566
UO_2	8	4.853	0.604
UO_2	9	4.930	0.614
UO_2	10	4.814	0.599
8% ^{240}Pu	12	6.705	1.260
8% ^{240}Pu	13	6.600	1.240
8% ^{240}Pu	14	6.646	1.249
8% ^{240}Pu	15	6.764	1.271
8% ^{240}Pu	16	6.939	1.304
8% ^{240}Pu	17	7.146	1.343
8% ^{240}Pu	18	7.105	1.335
8% ^{240}Pu	19	6.914	1.299
8% ^{240}Pu	20	6.691	1.257
8% ^{240}Pu	21	6.599	1.240
8% ^{240}Pu	22	6.558	1.233
8% ^{240}Pu	23	7.048	1.325
8% ^{240}Pu	24	6.664	1.252
8% ^{240}Pu	25	6.618	1.244
8% ^{240}Pu	26	6.743	1.267
8% ^{240}Pu	27	6.924	1.301
8% ^{240}Pu	28	6.697	1.259
8% ^{240}Pu	29	6.294	1.183
8% ^{240}Pu	30	5.898	1.109
8% ^{240}Pu	31	5.468	1.028
8% ^{240}Pu	32	5.539	1.041
8% ^{240}Pu	33	7.912	1.487
8% ^{240}Pu	35	6.000	1.128

[a]The relative power value for MOX fuel rods is multiplied by 1.51 to correct for the difference in thermal capacitance of the MOX and UO_2 fuel rods (see Sect. 1.3).

Table 25. Relative power data for the multiregion slab core configuration for a 10 × 10 central void pattern

Fuel type	Rod No.	Relative power	Corrected, normalized, relative power[a]
UO_2	1	1.328	0.620
UO_2	2	1.024	0.478
UO_2	3	0.971	0.454
UO_2	4	1.027	0.480
UO_2	5	1.091	0.510
UO_2	6	1.185	0.554
UO_2	7	1.243	0.581
UO_2	8	1.329	0.621
UO_2	9	1.348	0.630
UO_2	10	1.301	0.608
8% ^{240}Pu	12	1.847	1.303
8% ^{240}Pu	13	1.774	1.251
8% ^{240}Pu	14	1.811	1.278
8% ^{240}Pu	15	1.818	1.282
8% ^{240}Pu	16	1.746	1.232
8% ^{240}Pu	17	1.695	1.196
8% ^{240}Pu	18	1.664	1.173
8% ^{240}Pu	19	1.694	1.195
8% ^{240}Pu	20	1.679	1.184
8% ^{240}Pu	21	1.720	1.213
8% ^{240}Pu	22	1.691	1.193
8% ^{240}Pu	23	1.675	1.182
8% ^{240}Pu	24	1.768	1.247
8% ^{240}Pu	25	1.705	1.202
8% ^{240}Pu	26	1.648	1.163
8% ^{240}Pu	27	1.622	1.144
8% ^{240}Pu	28	1.564	1.103
8% ^{240}Pu	29	1.568	1.106
8% ^{240}Pu	30	1.526	1.077
8% ^{240}Pu	31	1.443	1.018
8% ^{240}Pu	32	1.492	1.052
8% ^{240}Pu	33	2.260	1.594
8% ^{240}Pu	35	1.530	1.079

[a]The relative power value for MOX fuel rods is multiplied by 1.51 to correct for the difference in thermal capacitance of the MOX and UO_2 fuel rods (see Sect. 1.3).

Table 26. Relative power data for the borated multiregion slab core configuration

Fuel type	Rod No.	Relative power	Corrected, normalized, relative power[a]
UO_2	1	0.629	0.455
UO_2	2	0.585	0.423
UO_2	3	0.538	0.389
UO_2	4	0.651	0.471
UO_2	5	0.652	0.472
UO_2	6	0.775	0.561
UO_2	7	0.789	0.571
UO_2	8	0.908	0.657
UO_2	9	0.911	0.659
UO_2	10	1.030	0.745
UO_2	11	1.018	0.737
UO_2	12	1.128	0.816
UO_2	13	1.122	0.812
UO_2	14	1.170	0.847
UO_2	15	1.091	0.790
8% ^{240}Pu	16	1.542	1.685
8% ^{240}Pu	17	1.455	1.590
8% ^{240}Pu	18	1.479	1.616
8% ^{240}Pu	19	1.495	1.634
8% ^{240}Pu	20	1.530	1.672
8% ^{240}Pu	21	1.547	1.691
8% ^{240}Pu	22	1.579	1.726
8% ^{240}Pu	23	1.582	1.729
8% ^{240}Pu	24	1.595	1.743
8% ^{240}Pu	25	1.591	1.739
8% ^{240}Pu	26	1.587	1.734
8% ^{240}Pu	27	1.567	1.713
8% ^{240}Pu	28	1.555	1.699
8% ^{240}Pu	29	1.572	1.718
8% ^{240}Pu	30	1.535	1.678
8% ^{240}Pu	31	1.492	1.631
8% ^{240}Pu	32	1.457	1.592
8% ^{240}Pu	33	1.481	1.619
8% ^{240}Pu	34	1.517	1.658
UO_2	36	1.079	0.781
UO_2	37	1.158	0.838
UO_2	40	1.040	0.753
UO_2	43	0.892	0.646
UO_2	46	0.679	0.491
UO_2	49	0.552	0.400
8% ^{240}Pu	50	0.623	0.451
8% ^{240}Pu	51	0.465	0.337
8% ^{240}Pu	52	0.484	0.350
8% ^{240}Pu	53	0.555	0.402

Table 26. (continued)

Fuel type	Rod No.	Relative power	Corrected, normalized, relative power[a]
8% ^{240}Pu	54	0.612	0.669
8% ^{240}Pu	55	0.649	0.709
8% ^{240}Pu	56	0.707	0.773
8% ^{240}Pu	57	0.722	0.789
8% ^{240}Pu	58	0.749	0.819
8% ^{240}Pu	59	0.784	0.857
8% ^{240}Pu	60	0.794	0.868
8% ^{240}Pu	61	0.775	0.847
8% ^{240}Pu	62	0.684	0.748
8% ^{240}Pu	63	0.607	0.663
8% ^{240}Pu	64	0.492	0.538

[a]The relative power value for MOX fuel rods is multiplied by 1.51 to correct for the difference in thermal capacitance of the MOX and UO_2 fuel rods (see Sect. 1.3).

Table 27. Relative power data for the borated multiregion core configuration with a 4 × 4 central void pattern

Fuel type	Rod No.	Relative power	Corrected, normalized, relative power[a]
UO_2	1	0.633	0.330
UO_2	2	0.683	0.356
UO_2	3	0.870	0.453
UO_2	4	0.982	0.511
UO_2	5	1.140	0.594
UO_2	6	1.221	0.636
UO_2	7	1.306	0.680
UO_2	8	1.241	0.646
8% ^{240}Pu	9	1.798	1.414
8% ^{240}Pu	10	1.726	1.358
8% ^{240}Pu	11	1.733	1.363
8% ^{240}Pu	12	1.765	1.388
8% ^{240}Pu	13	1.821	1.432
8% ^{240}Pu	14	1.854	1.458
8% ^{240}Pu	15	1.850	1.455
8% ^{240}Pu	16	1.766	1.389
8% ^{240}Pu	17	1.699	1.336
8% ^{240}Pu	18	1.684	1.324
8% ^{240}Pu	19	1.773	1.394
8% ^{240}Pu	20	1.704	1.340
8% ^{240}Pu	21	1.534	1.206
8% ^{240}Pu	22	1.302	1.024
8% ^{240}Pu	23	1.170	0.920
8% ^{240}Pu	24	1.120	0.881
8% ^{240}Pu	25	1.464	1.151

Table 27. (continued)

Fuel type	Rod No.	Relative power	Corrected, normalized, relative power[a]
UO_2	27	1.251	0.651
UO_2	28	1.285	0.669
UO_2	29	1.235	0.643

[a]The relative power value for MOX fuel rods is multiplied by 1.51 to correct for the difference in thermal capacitance of the MOX and UO_2 fuel rods (see Sect. 1.3).

Table 28. Relative power data for the borated multiregion core configuration with a 10 × 10 central void pattern

Fuel type	Rod No.	Relative power	Corrected, normalized, relative power[a]
UO_2	1	0.432	0.373
UO_2	2	0.486	0.419
UO_2	3	0.581	0.501
UO_2	4	0.687	0.593
UO_2	5	0.768	0.663
UO_2	6	0.853	0.736
UO_2	7	0.877	0.757
UO_2	8	0.889	0.767
UO_2	9	0.841	0.726
8% ^{240}Pu	10	1.108	1.444
8% ^{240}Pu	11	1.058	1.379
8% ^{240}Pu	12	1.061	1.382
8% ^{240}Pu	13	1.071	1.395
8% ^{240}Pu	14	1.044	1.360
8% ^{240}Pu	15	1.015	1.322
8% ^{240}Pu	16	0.994	1.295
8% ^{240}Pu	17	0.999	1.302
8% ^{240}Pu	18	1.000	1.303
8% ^{240}Pu	19	0.999	1.302
8% ^{240}Pu	20	0.997	1.299
8% ^{240}Pu	21	0.932	1.214
8% ^{240}Pu	22	0.924	1.204
8% ^{240}Pu	23	0.786	1.024
8% ^{240}Pu	24	0.708	0.922
8% ^{240}Pu	25	0.700	0.912
8% ^{240}Pu	26	0.918	1.196
UO_2	28	0.847	0.731
UO_2	29	0.865	0.746
UO_2	30	0.849	0.733

[a]The relative power value for MOX fuel rods is multiplied by 1.51 to correct for the difference in thermal capacitance of the MOX and UO_2 fuel rods (see Sect. 1.3).

Table 29. Relative power data for the multiregion slab core configuration containing central traverse slabs

Fuel type	Rod No.	Relative power	Corrected, normalized, relative power[a]
UO_2	1	1.582	0.569
UO_2	2	1.694	0.609
UO_2	3	1.785	0.642
UO_2	4	1.703	0.612
UO_2	5	1.925	0.692
UO_2	6	1.813	0.652
24% ^{240}Pu	7	2.004	1.088
24% ^{240}Pu	8	1.931	1.049
24% ^{240}Pu	9	1.940	1.053
24% ^{240}Pu	10	1.996	1.084
24% ^{240}Pu	11	2.026	1.100
24% ^{240}Pu	12	2.051	1.114
24% ^{240}Pu	13	2.077	1.128
24% ^{240}Pu	14	2.078	1.129
24% ^{240}Pu	15	2.096	1.138
24% ^{240}Pu	16	2.103	1.142
24% ^{240}Pu	17	2.127	1.155
24% ^{240}Pu	18	2.119	1.151
24% ^{240}Pu	19	2.101	1.141
24% ^{240}Pu	20	2.076	1.127
24% ^{240}Pu	21	2.011	1.092
24% ^{240}Pu	22	1.988	1.080
24% ^{240}Pu	23	1.967	1.068
24% ^{240}Pu	24	1.963	1.066
24% ^{240}Pu	25	2.046	1.111
UO_2	26	1.835	0.660
UO_2	27	1.904	0.685
UO_2	28	1.865	0.671
8% ^{240}Pu	29	1.740	0.945
8% ^{240}Pu	30	1.841	1.000
8% ^{240}Pu	31	1.939	1.053
8% ^{240}Pu	32	2.094	1.137
24% ^{240}Pu	33	1.968	1.069
24% ^{240}Pu	34	2.006	1.089
24% ^{240}Pu	35	2.065	1.122
24% ^{240}Pu	36	2.121	1.152
24% ^{240}Pu	37	2.119	1.151
24% ^{240}Pu	38	2.087	1.134
24% ^{240}Pu	39	2.042	1.109
24% ^{240}Pu	40	1.949	1.058
8% ^{240}Pu	41	2.104	1.143
8% ^{240}Pu	42	1.958	1.063
8% ^{240}Pu	43	1.873	1.017
8% ^{240}Pu	44	1.748	0.949

[a]The relative power value for MOX fuel rods is multiplied by 1.51 to correct for the difference in thermal capacitance of the MOX and UO_2 fuel rods (see Sect. 1.3).

Table 30. Relative power data for the multiregion slab core configuration containing a striped central slab region

Fuel type	Rod No.	Relative power	Corrected, normalized, relative power[a]
UO_2	1	1.000	0.511
UO_2	2	1.088	0.556
UO_2	3	1.141	0.583
UO_2	4	1.224	0.626
UO_2	5	1.283	0.656
UO_2	6	1.320	0.675
UO_2	7	1.228	0.628
UO_2	8	1.242	0.635
UO_2	9	1.284	0.656
UO_2	10	1.287	0.658
8% ^{240}Pu	11	1.634	1.261
24% ^{240}Pu	12	1.364	1.052
8% ^{240}Pu	13	1.583	1.222
24% ^{240}Pu	14	1.436	1.109
8% ^{240}Pu	15	1.652	1.275
24% ^{240}Pu	16	1.454	1.122
8% ^{240}Pu	17	1.685	1.301
24% ^{240}Pu	18	1.479	1.141
8% ^{240}Pu	19	1.722	1.329
24% ^{240}Pu	20	1.486	1.147
8% ^{240}Pu	21	1.715	1.323
24% ^{240}Pu	22	1.512	1.167
8% ^{240}Pu	23	1.710	1.320
24% ^{240}Pu	24	1.464	1.130
8% ^{240}Pu	25	1.632	1.259
24% ^{240}Pu	26	1.403	1.083
8% ^{240}Pu	27	1.595	1.231
24% ^{240}Pu	28	1.389	1.072
8% ^{240}Pu	29	1.650	1.274

[a]The relative power value for MOX fuel rods is multiplied by 1.51 to correct for the difference in thermal capacitance of the MOX and UO_2 fuel rods (see Sect. 1.3).

1.4.3 Description of Fuel Rods

The experiments were performed using the MOX fuel rods obtained from the Battelle–Pacific Northwest National Laboratory (PNNL).[1] The MOX fuels used in the ESADA program were also used in two different sets of experiments at PNNL.[6,7] One series of experiments at PNNL was conducted in 1965 using both types of MOX fuels,[8,9] and the 8% ^{240}Pu fuels were used in 1975–1976.[7]

The MOX fuel rod* length was 92.96 cm with a 91.44-cm active fuel length. The outer diameter of the fuel rod, including an 0.08-cm-thick Zircaloy-2 cladding, was 1.443 cm. Two plugs were welded on each side of the fuel rods. The total weight of the loaded fuel rod was 1340 g/rod with 1128 g of PuO_2–UO_2 per rod. The top end had 5 g of UO_2 powder. Dimensions of both types of MOX fuels were identical. A schematic representation of MOX fuel is given in Fig. 30.

The 2.72% (2.719%) enriched UO_2 fuel was the third type of fuel used in these experiments. The UO_2 fuel was obtained from the U.S. Atomic Energy Commission-sponsored Large Reactor Development Program for comparison with the plutonium data and also for later use in multiregion experiments.[1]

The total weight of UO_2 fuel was 1028.02 g/rod with 905.93-g/rod of uranium. The weight of the ^{235}U was 24.63 g/rod. The UO_2 fuel rod length was 140.18 cm with 121.92-cm active fuel length. The fuel pellet diameter was 1.016 cm. The outer diameter of the fuel rod was 1.196 cm. The fuel pellets were 1.52 cm in length. A schematic representation of the UO_2 fuel rod is given in Fig. 31. The MOX and UO_2 fuel rod specifications are summarized in Table 31.

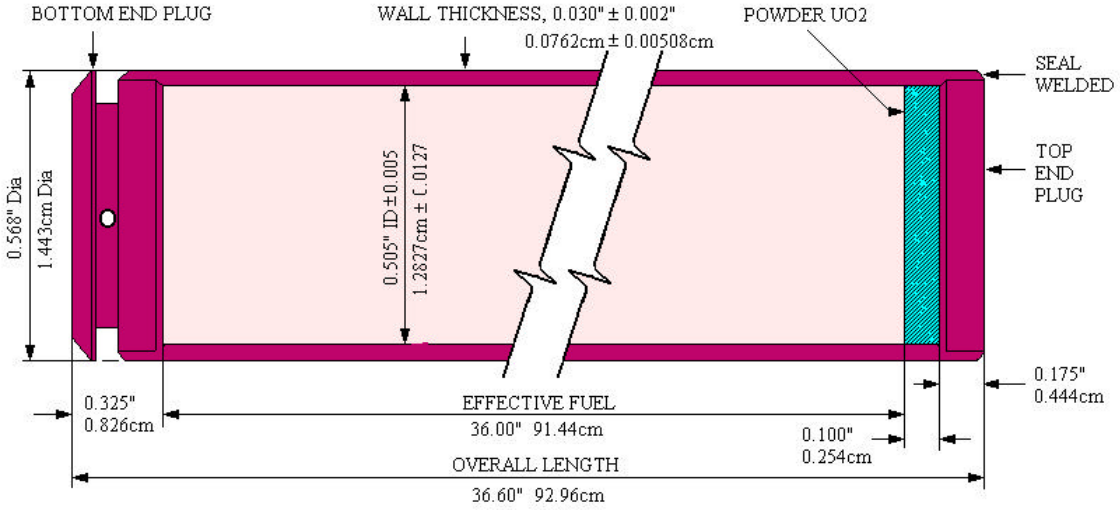

Fig. 30. MOX fuel rod.

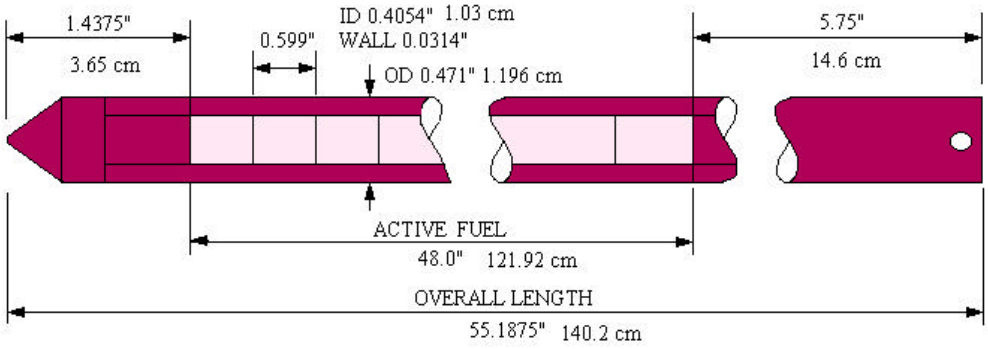

Fig. 31. Uranium fuel rod.

*See the footnote in Sect. 3.2 of this document.

Table 31. The MOX and UO_2 fuel rod specifications

Parameter	MOX	UO_2
Pellet diameter, cm (in.)	1.2827 (0.505)	1.0160 (0.400)
Clad inner diameter, cm (in.)	No gap[a]	1.0297 (0.4054)
Clad outer diameter, cm (in.)	1.4427[a] (0.568)	1.1963 (0.471)[b]
Fuel length, cm (in.)	92.9540 (36.6)	140.1762 (55.1875)
Active fuel length, cm (in.)	91.4400 (36.0)	121.9200 (48.0)
Weight, g/rod	1128 PuO_2-UO_2	1028.02 UO_2
	22.56 PuO_2	905.93 U
	19.85 Pu	24.63 ^{235}U
Clad material	Zircaloy-2	Zircaloy-4

[a]The clad outer diameter was reported as 1.4427 cm (0.568 in.) in Ref. 1, but it was reported as 1.435 cm (0.565 in.) in all the other sources.[7–9] This difference in clad outer diameter is within the reported uncertainty for wall thickness. When the reported dimensions of the fuel outer diameter, clad outer diameter, and clad thickness given in Ref. 1 (which are also given in Fig. 30 of this document) are considered, it appears that there was a gap between fuel and clad. However, these fuels were vibratory compacted, and there was no gap between fuel and clad.[1,7–9] The MCNP calculations for core configurations with the MOX fuel were performed assuming that there was a gap with a thickness of 0.004 cm between fuel and clad. Sensitivity calculations were performed for the gap that was considered as available before. The maximum uncertainty in the k_{eff} value due to the considered gap was calculated as 0.046% for the 8% ^{240}Pu and 0.011% for the 24% ^{240}Pu MOX fuels.[3]

[b]The clad outer diameter was reported as 1.196 cm (0.471 in.) and 1.1895 cm (0.4683 in.) of Ref. 1 (p. 125 and p. 123, respectively). Sensitivity calculations were performed for the difference in these reported clad outer diameters. The maximum uncertainty in the k_{eff} value due to this difference is calculated[3] as 0.229%.

1.4.4 Description of Test Configurations

Several test positions were formed by removing fuel rods at various locations. A uniformly distributed nine-rod pattern was arranged as a test configuration. These holes were filled either with control rods or left as empty water holes. Also, the reactivity worth of local voids was measured with voided aluminum tubes.

The isotopic composition of the control rod was 80% Ag, 15% In, and 5% Cd. For the reactivity worth measurement experiments with the salt-and-pepper core configuration, bare Ag-In-Cd control rods with an outer diameter of 1.0236 cm were used.

Also aluminum tubes were sealed to produce voids. The outer diameter of these aluminum tubes was 0.476 cm with 0.0559-cm thickness.

1.4.5 Description of Materials

Three different types of fuel rods were used during the experimental program. Two different MOX fuels and a low-enriched UO_2 fuel were used. The MOX fuels were distinguished by the distribution of plutonium isotopes. The distribution of plutonium isotopes used in MOX fuel for the 8% and 24% ^{240}Pu fuels is given in Table 32.

Both MOX fuels contained 2.0 wt % PuO_2 in natural (0.72 wt % ^{235}U) UO_2. The total weight of a MOX fuel rod was 1128 g with 22.56 g/rod of PuO_2. The fuel density was reported as 9.54 g/cm^3 (Ref. 1). The percentages of the elements in the MOX fuel rods are given in Table 33.

Table 32. Isotopic composition of the metal plutonium in the MOX fuel rods

Isotope[a]	Composition, 8% ^{240}Pu (wt %)	Composition, 24% ^{240}Pu (wt %)
^{239}Pu	91.615	71.762
^{240}Pu	7.654	23.503
^{241}Pu	0.701	4.080
^{242}Pu	0.030	0.656

[a]See the footnote in Sect. 3.3 of this document for ^{241}Am buildup.

Table 33. Percentages of the elements in the MOX fuel rods

Element	Composition (wt %)
PuO_2	2.0
UO_2	98.0
Plutonium metal	1.77
Uranium metal	86.39
Oxygen	11.84

Zircaloy-2 was used as the cladding material for the MOX fuel, but its composition is not reported in Ref. 1. During this work, the average values of weight fractions given in Ref. 10 are taken for the composition of Zircaloy-2. The density of Zircaloy-2 is taken as 6.56 g/cm^3. The isotopic composition of Zircaloy-2 clad is given in Table 34.

Table 34. Zircaloy-2 composition used for MOX fuel

Element	Composition (wt %)
Zr	98.27
Sn	1.45
Fe	0.13
Cr	0.10
Ni	0.05

A 2.72% (2.719%) enriched UO_2 fuel was used as a third type of fuel. The total weight of the UO_2 was 1028.02 g/rod with 905.93 g/rod of uranium, and the weight of the ^{235}U was 24.63 g/rod. The fuel density was 95% of the theoretical density. A detailed chemical analysis* of UO_2 fuel is given in Table 35. The clad material for the UO_2 fuel rod was Zircaloy-4. Chemical analysis† of Zircaloy-4 is given in Table 36.

*See Table 42 in Sect. 3.3 for the UO_2 composition used in this evaluation.
†See Table 43 in Sect. 3.3 for the Zircaloy-4 composition used in this evaluation.

Table 35. Chemical analysis of UO_2 fuel[1]

Isotope	2.72% ^{235}U
U (wt %)	88.15
C (ppm)	<10
F (ppm)	<10
Al (ppm)	40
B (ppm)	<0.5
Bi (ppm)	<1
Cd (ppm)	<0.3
Co (ppm)	<4
Ca (ppm)	9.5
Cr (ppm)	34
Cu (ppm)	2.0
Fe (ppm)	266
In (ppm)	<3
Mg (ppm)	4.4
Mn (ppm)	2.4
Mo (ppm)	6.2
Ni (ppm)	24.3
Pb (ppm)	<8
Si (ppm)	21
Sn (ppm)	<2
Ti (ppm)	3.9
V (ppm)	<1
W (ppm)	<50
N (ppm)	<18
Zn (ppm)	<8
O	Remainder

Table 36. Chemical analysis of Zircaloy-4 clad used for UO_2 fuel[1]

Composition	Zircaloy-4
Zr (wt %)	98.2
Sn (wt %)	1.4
Fe (wt %)	0.21
Cr (wt %)	0.10
Ni (wt %)	<0.004
C (ppm)	95
Hf (ppm)	<100
Al (ppm)	<20
B (ppm)	0.2
Cd (ppm)	0.2
Co (ppm)	10
Cu (ppm)	33
Mg (ppm)	<10

Table 36. (continued)

Composition	Zircaloy-4
Mn (ppm)	<20
Mo (ppm)	<20
Pb (ppm)	<20
Si (ppm)	58
Ti (ppm)	<20
V (ppm)	<20
W (ppm)	<50
N (ppm)	45

No information was given on the type of aluminum used in these experiments.[1] During this study Al-6061 was assumed for the grid structure material. The density of aluminum is taken to be 2.7 g/cm^3. The characteristics of this type of aluminum are given in Table 37.[10]

Table 37. Isotopic distribution of Al-6061

Element	Composition (wt %)
Al	96.95
Mg	1.00
Fe	0.70
Si	0.60
Cu	0.25
Cr	0.20
Ti	0.15
Mn	0.15

Control rods composed of Ag-In-Cd rods were used for the reactivity worth measurements. The isotopic composition of the control rod was provided in the report,[1] but the density was not provided. The isotopic composition of these rods is given in Table 38.[1] The density of the control rod is taken as 9.75 g/cm^3.

Table 38. Isotopic composition of Ag-In-Cd control rod

Element	Composition (wt %)
Ag	80
In	15
Cd	5

1.5 SUPPLEMENTAL EXPERIMENTAL MEASUREMENTS

Two standard lattice plates were used during the experimental program. By changing the loading pattern, standard lattice pitches were increased by a factor of $\sqrt{2}$ or 2.

The number of power distribution measurements in multiregion cores was increased by using a number of additional core configurations. Measurements in concentric-region cores using different fuels and cores with interspersed fuels in a salt-and-pepper distribution were examined as different methods for extending the scope of the experimental program.

In addition to buckling, reactivity, and power distribution, heat rate measurements were performed during the program. In the heat rate experiments, thermally insulated and instrumented fuel rods were irradiated, and the temperature response was measured. After shutdown, these same rods were counted in the fuel rod gamma counter. The resulting ratio of heating rate to gamma activity provides a time-dependent "calorimetric" correction factor.

Using both uranium and plutonium fuels, the heat rate experiments were conducted to correlate earlier power-to-gamma activity measurements made in the Saxton program.[5] Because fuel rods in this experiment were of different physical dimensions, new data were taken to reevaluate the time-dependent correction factors. Improved (over that used in Saxton) digital temperature measurements were taken by instrumenting the fuel rods during and after irradiation. The measurements of relative power distribution ratios of UO_2 vs 24 wt % ^{240}Pu, UO_2 vs 8 wt % ^{240}Pu, and 8 wt % ^{240}Pu vs 24 wt % ^{240}Pu are reported to have an accuracy of 1%.

2. EVALUATION OF THE EXPERIMENTAL DATA

The effects of some of the uncertainties in the measured data on the k_{eff} value for some selected single-region core configurations were calculated using the ONEDANT code[11] with ENDF/B-IV 27-group cross sections with the homogenized lattice-cell fuel region. The homogenized lattice-cell cross section sets for ONEDANT were prepared using the CSASIX[12] module of the SCALE code.

The sensitivity calculations for MOX fuels were performed only for some selected single-region core configurations. Calculations were performed for five cases with different lattice pitches for 8% ^{240}Pu fuel and for two cases with different lattice pitches for 24% ^{240}Pu MOX fuels. The calculations were also performed for UO_2 fuel with two different lattice pitches.

The sensitivity calculations were performed basically for the uncertainties in the fuel characteristics (including uncertainties in the fuel density, dimensions, and fuel content), aluminum type, the composition of Zircaloy-2, and the reference plane for critical water height measurements. For MOX fuels the particle self-shielding effect was also discussed. The parameters considered for the sensitivity calculations and the results of the sensitivity calculations are presented and discussed in detail in Ref. 3.

For 8% ^{240}Pu MOX fuel, the total uncertainties were calculated as 0.675%, 0.490%, 0.314%, 0.363%, 0.363%, and 0.556% for 1.7526-cm, 1.9050-cm, 2.4785-cm, 2.6942-cm, and 3.5052-cm lattice pitches, respectively. For 24% ^{240}Pu MOX fuel, total uncertainties were calculated as 0.371% and 0.413% for 2.4785-cm and 2.6942-cm lattice pitches, respectively. The fuel rod characterization parameters, especially uncertainty in clad thickness, were the parameters that yielded the largest uncertainty for 8% ^{240}Pu, whereas ^{241}Am content was the parameter that yielded the largest uncertainty for 24% ^{240}Pu MOX fuel.[3]

For UO_2 fuel, the total uncertainties were calculated as 0.281% and 0.162% for 1.7526-cm and 2.4785-cm lattice pitches, respectively. In this case, the fuel rod characterization parameters, especially uncertainty in clad thickness, were the parameters that yielded the largest uncertainty.[3]

Also, the sensitivity calculation results show that the missing information in the report,[1] the type of the aluminum used for grid materials, the Zircaloy-2 composition used as clad material, and reference plane for critical water height measurements do not have large impacts on the k_{eff} value. The total uncertainties[3] for these missing data are within ±0.07%.

3. BENCHMARK SPECIFICATIONS

3.1 DESCRIPTION OF MODEL

Three different types of fuel rods were used during the experimental program. Two MOX fuels with different plutonium contents and a low-enriched UO_2 fuel were used. Fuel rods were inserted in a square lattice pitch. Two standard lattice pitches were available. Additional lattice pitches were achieved by changing the fuel-loading pattern. The reactivity worth of different materials and power distribution measurements were performed for multiregion core configurations with all types of available fuels. The installations of MOX fuel for the multiregion core configurations composed of two different MOX fuels are given in Fig. 1. The installation of MOX and UO_2 fuels for salt-and-pepper and slab array core configurations are given in Figs. 2 and 3, respectively. The fuel rods were supported by bottom, middle, and top aluminum grid plates. The fuel rods rested on an aluminum plate.

3.2 DIMENSIONS

Schematic diagrams of the MOX and UO_2 fuel rods are shown in Figs. 30* and 31. Also, the specifications of the MOX and UO_2 fuel rods are given in Table 31.

3.3 MATERIAL DATA

The details of the atomic density calculations are given in Appendix A. Atomic densities for the 8% and 24% ^{240}Pu MOX fuels are calculated using the weight fractions given in Tables 32 and 33. The total weight of the PuO_2–UO_2 was reported as 1128 g/rod, and the fuel density was reported as 9.54 g/cm^3. The calculated atomic number densities are given in Table 39.

The top UO_2 powder density was not given in the original report.[1] The fuel density was reported as 9.54 g/cm^3, but it was not clear whether this density was for MOX only or for MOX plus UO_2 powder. It was reported that this layer is 5 g of UO_2 with a thickness of 0.254 cm. The UO_2 powder density is calculated as 15.23 g/cm^3 by using the reported weight and thickness, an unrealistic value.† Table 40 lists the atomic densities for the UO_2 powder using a density of 9.54 g/cm^3.

Cladding material for MOX fuel was reported as Zircaloy-2, but the composition of Zircaloy-2 was not provided. Atomic densities for Zircaloy-2 are calculated by taking the weight

---

*Although the fuel rods used in the ESADA and PNNL experiments were the same, the dimensions were reported slightly differently in different sources. During this study, the dimensions reported in the ESADA document[1] are used. One of the reasons for this difference is the length of the UO_2 powder region. References 1 and 9 give the fuel length as 36.0 in. excluding the powder; however, Refs. 7 and 8 give the fuel length as 36.0-in. including the powder region. Due to this difference in UO_2 powder length, the top plug was also reported differently in different sources. The top plug was reported as 0.444 cm (0.175 in.) in Refs. 1 and 9, whereas it was reported as 0.6985 cm (0.275 in.) in Refs. 7 and 8. Sensitivity calculations are performed to observe the sensitivity of the k_{eff} value to these differences in reported dimensions. Sensitivity calculations were performed using the dimensions given in Refs. 7 and 8. For this purpose, the dimensions shown in Fig. 30 are modified so that the MOX fuel, UO_2 powder, and top end plug lengths are assumed as 90.94 cm, 0.5 cm, and 0.6985 cm, respectively. Sensitivity calculations show that the maximum uncertainty in the k_{eff} value due to these inconsistent dimensions is 0.060% (for a 3.5052-cm lattice pitch) for 8% ^{240}Pu fuel and 0.042% (for a 2.4785-cm lattice pitch) for 24% ^{240}Pu fuel.[3]

†Sensitivity calculations showed that the UO_2 powder density has negligible effect on k_{eff} value. The maximum uncertainty is calculated[3] as 0.0009%.

Table 39. Atomic densities for the 8% and 24% ^{240}Pu MOX fuels

Element[a]	8% ^{240}Pu Atom density (atom/b-cm)	24% ^{240}Pu Atom density (atom/b-cm)
^{235}U	1.50490E-4	1.50490E-4
^{238}U	2.07511E-2	2.07511E-2
^{239}Pu	3.87455E-4	3.03494E-4
^{240}Pu	3.22350E-5	9.89834E-5
^{241}Pu	2.93999E-6	1.71115E-5
^{242}Pu	1.29476E-7	2.73988E-6
O	4.18019E-2	4.18019E-2

[a]The concentration of ^{241}Am in MOX fuels is not provided in Ref. 1 The ^{241}Am buildup is calculated as 0.0588 wt % (in 22 months) for the 8% ^{240}Pu fuel and 0.267 wt % (in 17 months) for the 24% ^{240}Pu MOX fuel. During the sensitivity calculations, ^{241}Pu contents for both MOX fuels, given in Table 5, are also reduced. The maximum uncertainty in the k_{eff} value due to ^{241}Am buildup was calculated as 0.054% for the 8% ^{240}Pu and 0.248% for the 24% ^{240}Pu MOX fuel.[3]

Table 40. Atomic densities for the UO_2 powder at the top of the MOX fuels

Element	Atom density (atom/b-cm)
^{235}U	1.55089E-4
^{238}U	2.11145E-2
O	4.25392E-4

fractions given in Table 34,* and density is taken as 6.56 g/cm^3. Calculated atomic number densities are given in Table 41.

The chemical composition of UO_2 fuel is given in Table 35. The fuel density was calculated as 10.40 g/cm^3 by using the 1.016-cm (0.400-in.) fuel rod diameter and the 121.92-cm (48.00-in.) fuel rod length with 1028.02 g/rod of UO_2. The atomic densities are calculated using the weights given in Ref. 1 rather than the given detailed chemical analysis. Although the uranium weight fraction is given as 88.15 wt % in Ref. 1 (p. 123), which was also given here in Table 35, different weight fractions are calculated with the given weights in Ref. 1. The uranium weight fraction was reported differently in two different places of Ref. 1. In Ref. 1, p. 123, the uranium weight fraction was given as 88.124%, while it was reported as 88.15% in the chemical analysis on the same page. Therefore, during this study, the weights reported in Ref. 1 are taken

*The effect of uncertainty in the Zircaloy-2 composition on the k_{eff} value was calculated by considering two extreme cases: (1) maximum zirconium content with an isotopic composition of 98.65 wt % Zr, 1.20 wt % Sn, 0.07 wt % Fe, 0.05 wt % Cr, 0.03 wt % Ni; and (2) minimum zirconium content with an isotopic composition of 97.89 wt % Zr, 1.70 wt % Sn, 0.20 wt % Fe, 0.15 wt % Cr, 0.06 wt % Ni. The composition yielding the maximum Δk_{eff} value is calculated as 0.016% (for 8% ^{240}Pu MOX fuel with 3.5052-cm lattice pitch), using the maximum zirconium content.[3]

Table 41. Atomic densities for the Zircaloy-2 clad used for MOX fuel

Element	Atom density (atom/b-cm)
Zr	4.25563E-2
Sn	4.82539E-4
Fe	9.19592E-5
Cr	7.59770E-5
Ni	3.36556E-5

as the basis instead of the given weight fractions. The weights and weight fractions along with the calculated atomic densities using 10.40-g/cm^3 fuel density for the UO_2 fuel are given in Table 42.

Zircaloy-4 was used as the clad material for the UO_2 fuel. The chemical analysis of Zircaloy-4 is given in Table 36. Atom densities for the impurities listed in Table 36 are not calculated. The density is taken as 6.56 g/cm^3, and the calculated atomic number densities are presented in Table 43.

The type of aluminum was not reported in Ref. 1; Al-6061 is used in the benchmark calculations.* The density of aluminum is taken to be 2.7 g/cm^3. The isotopic composition of Al-6061 is given in Table 37. Calculated atomic densities for Al-6061 are given in Table 44.

Table 42. Atomic densities for the UO_2 fuel

Element	Weight (g)	Weight fraction (wt %)	Atom density (atom/b-cm)
^{235}U	24.63	2.39587	6.38404E-4
^{238}U	881.30	85.7279	2.25545E-2
O	122.09	11.8762	4.64896E-2

Table 43. Atomic densities for the Zircaloy-4 clad

Element	Weight fraction (wt %)	Atom density (atom/b-cm)
Zr	98.286	4.25632E-2
Sn	1.400	4.65900E-4
Fe	0.210	1.48550E-4
Cr	0.100	7.59770E-5
Ni	0.004	2.69245E-6

*Sensitivity calculations are performed using 100% Al instead of Al-6061, and the maximum uncertainty is calculated as 0.062% for the 8% ^{240}Pu fuel with a 3.5052-cm lattice pitch and 0.018% for the UO_2 fuel with a 2.4785-cm lattice pitch.[3]

Table 44. Atomic densities for the Al-6061

Element	Atom density (atom/b-cm)
Al	5.84243E-2
Mg	6.68985E-4
Fe	2.03803E-4
Si	3.47361E-4
Cu	6.39681E-5
Cr	6.25420E-5
Ti	5.09388E-5
Mn	4.43946E-5

The density of water at 23ºC is taken as 0.997518 g/cm^3. Atomic densities for water are given in Table 45.

The power distribution measurements were performed using two boron concentrations: 315 ppm for single-region measurements and 526 ppm for multiregion slab array measurements. The details of the atomic density calculations for borated water are given in Appendix A. The calculated atomic densities for 315- and 526-ppm boron concentrations are presented in Table 46.

The density of air is taken as 1.20E-4. The nitrogen and oxygen weight fractions are taken as 0.78 wt % and 0.22 wt %, respectively. The calculated atomic densities for air are given in Table 47.

Table 45. Atomic densities for water

Element	Atom density (atom/b-cm)
H	6.66898E-02
O	3.33449E-02

Table 46. Atomic densities for 315- and 526-ppm borated water

Boron concentration (ppm)	Density[a] (g/cm^3)	Element	Atom density (atom/b-cm)
315	0.998382	H	6.66799E-02
		O	3.33662E-02
		^{10}B	3.46828E-06
		^{11}B	1.43636E-05
526	0.998962	H	6.66733E-02
		O	3.33805E-02
		^{10}B	5.79484E-06
		^{11}B	2.39988E-05

[a]Borated water density (see Appendix A).

Table 47. Atomic densities for air

Element	Atom density (atom/b-cm)
N	4.02428E-6
O	9.93684E-7

Table 48 gives the atomic densities for the Ag-In-Cd control rod using the weight fractions given in Table 38 and a density of 9.75 g/cm^3.

Table 48. Atomic densities for the control rod

Element	Atom density (atom/b-cm)
Ag	4.35461E-2
In	7.67055E-3
Cd	2.61167E-3

3.4 TEMPERATURE DATA

No temperature data were specified in the original report.[1] But another report[13] indicated that these experiments were performed at 23°C.

4. RESULTS OF CALCULATIONS

All experimental configurations were modeled in detail using the MCNP-4B[14] Monte Carlo code with ENDF/B-V cross section libraries. During the calculations, the S(α,β) thermal neutron scattering treatment was used for hydrogen in water. The calculations for relative pin power distribution have been accomplished by tallying the fission reaction rates. The power distribution calculations were performed with 1150 generations of 10,000 neutrons each, and the first 150 generations were skipped. Therefore, the computed results are based on 10 million active histories. The average CPU time for each power distribution calculation was ~60 h.

Reference 1 does not indicate which rod is taken as the reference rod for power distribution measurements. During this study, to compare the measured and calculated data, an arithmetic average normalization method is used. The experimental and calculational values for each pin are divided by the arithmetic average value of the experimental and calculational values, respectively.

The arithmetic average normalized MCNP calculational and experimental results are given in Tables 49–74. The uncertainties for the measurements were not reported. Uncertainties (1 σ) for the MCNP calculations are within ±1.5%. These tables also provide the relative error in percentage, (C/E-1) × 100 where C stands for calculational and E stands for experimental.

Table 49. Normalized values of experimental and calculational power data for a 23 × 25 single-region core configuration with a center water hole in a 1.7526-cm lattice (Fig. 4)

Rod No.	Experiment	Calculation	(C/E-1) × 100
1	0.8074	0.8000	–0.92
2	0.8473	0.8675	2.38
3	0.8983	0.8999	0.18
4	0.9492	0.9478	–0.16
5	0.9722	0.9771	0.50
6	1.0242	1.0377	1.32
7	1.2390	1.2310	–0.64
8	1.1081	1.1083	0.02
9	1.2520	1.2548	0.23
10	0.7744	0.7861	1.51
11	0.7894	0.7853	–0.51
12	0.8963	0.8955	–0.09
13	0.9932	0.9887	–0.45
14	1.2650	1.2437	–1.68
15	1.1241	1.0948	–2.61
16	1.2545	1.2675	1.04
17	0.8054	0.8142	1.10

Table 50. Normalized values of experimental and calculational power data for a 23 × 25 single-region core configuration with a five-rod water slot pattern in a 1.7526-cm lattice (Fig. 5)

Rod No.	Experiment	Calculation	(C/E-1) × 100
1	0.6733	0.6682	–0.77
2	0.7369	0.7265	–1.41
3	0.7833	0.7851	0.23
4	0.8405	0.8321	–1.00
5	0.9187	0.9128	–0.63
6	1.1804	1.1812	0.07
7	1.0186	1.0230	0.43
8	1.5529	1.5343	–1.20
9	0.6988	0.7011	0.33
10	0.7124	0.7097	–0.38
11	0.8087	0.8105	0.22
12	0.8651	0.8520	–1.51
13	0.9259	0.9128	–1.42
14	1.0731	1.0533	–1.85
15	1.5529	1.5552	0.15
16	1.4139	1.4888	5.30
17	1.2994	1.3275	2.16
18	1.0413	1.0293	–1.15
19	1.1686	1.1762	0.65
20	0.7351	0.7203	–2.01

Table 51. Normalized values of experimental and calculational power data for a 27 × 27 single-region core configuration with a center water hole in a 1.7526-cm lattice (Fig. 6)

Rod No.	Experiment	Calculation	(C/E-1) × 100
1	0.8041	0.8185	1.79
2	0.8487	0.8632	1.71
3	0.9013	0.9086	0.81
4	0.9449	0.9463	0.15
5	0.9682	0.9838	1.61
6	1.0371	1.0391	0.20
7	1.2295	1.2384	0.72
8	1.1049	1.0915	–1.21
9	1.2052	1.2317	2.20
10	1.2264	1.2346	0.66
11	1.1566	1.0771	–6.87
12	1.2457	1.2432	–0.20
13	0.9672	0.9701	0.30
14	0.9115	0.9120	0.06
15	0.8163	0.8029	–1.64
16	0.8163	0.8223	0.73
17	0.8163	0.8168	0.06

Table 52. Normalized values of experimental and calculational power data for a 27 × 27 single-region core configuration with a five-rod water slot pattern in a 1.7526-cm lattice (Fig. 7)

Rod No.	Experiment	Calculation	(C/E-1) × 100
1	0.6820	0.6992	–2.52
2	0.7388	0.7459	–0.95
3	0.7779	0.7777	0.03
4	0.8338	0.8363	–0.29
5	0.9018	0.9243	–2.49
6	1.1562	1.1796	–2.02
7	0.9959	1.0212	–2.54
8	1.4925	1.4947	–0.14
9	0.7435	0.7396	0.52
10	0.7537	0.7405	1.76
11	0.8301	0.8415	–1.37
12	0.8767	0.8629	1.58
13	0.9205	0.9320	–1.25
14	1.0593	1.0330	2.48
15	1.4776	1.4893	–0.79
16	1.4758	1.4629	0.87
17	1.3127	1.2880	1.88
18	1.0425	1.0362	0.61
19	1.1720	1.1505	1.84
20	0.7565	0.7448	1.54

Table 53. Normalized values of experimental and calculational power data for a 21 × 21 single-region core configuration with a center water hole in a 1.9050-cm lattice (Fig. 8)

Rod No.	Experiment	Calculation	(C/E-1) × 100
1	0.7542	0.7521	–0.27
2	0.8365	0.8370	0.06
3	0.8879	0.9045	1.87
4	0.9614	0.9579	–0.36
5	0.9984	1.0072	0.89
6	1.0708	1.0642	–0.61
7	1.2503	1.2578	0.60
8	1.1293	1.1298	0.04
9	1.2542	1.2748	1.65
10	0.7553	0.7642	1.18
11	0.7497	0.7549	0.69
12	0.8928	0.9026	1.09
13	1.0409	0.9977	–4.15
14	1.2581	1.2545	–0.28
15	1.1371	1.1248	–1.08
16	1.2619	1.2631	0.09
17	0.7614	0.7528	–1.12

Table 54. Normalized values of experimental and calculational power data for a cylindrical single-region core configuration with a center water hole in a 2.6942-cm lattice (Fig. 9)

Rod No.	Experiment	Calculation	(C/E-1) × 100
1	0.6078	0.6019	–0.97
2	0.7413	0.7362	–0.69
3	0.8684	0.8667	–0.19
4	0.9721	0.9668	–0.55
5	1.0684	1.0745	0.58
6	1.1502	1.1371	–1.14
7	1.2217	1.2144	–0.60
8	1.3934	1.3870	–0.46
9	1.3764	1.3962	1.44
10	1.2255	1.2209	–0.37
11	1.1471	1.1546	0.66
12	1.0627	1.0801	1.64
13	0.9754	0.9770	0.16
14	0.8613	0.8565	–0.55
15	0.7213	0.7259	0.63
16	0.6070	0.6040	–0.49

Table 55. Normalized values of experimental and calculational power data for a 25 × 25 concentric-region core configuration containing a 15 × 15 8% ^{240}Pu inner region and UO_2 outer region (Fig. 10)

Rod No.	Fuel type	Experiment	Calculation	(C/E-1) × 100
1	8% ^{240}Pu	1.1792	1.1470	–2.73
2	8% ^{240}Pu	0.9724	0.9428	–3.04
3	8% ^{240}Pu	0.9484	0.9417	–0.70
4	8% ^{240}Pu	0.9998	0.9737	–2.61
5	8% ^{240}Pu	1.0523	1.0165	–3.41
6	8% ^{240}Pu	1.0843	1.0533	–2.86
7	8% ^{240}Pu	1.1197	1.0767	–3.84
8	8% ^{240}Pu	1.1038	1.0746	–2.64
9	8% ^{240}Pu	1.1106	1.0825	–2.53
10	8% ^{240}Pu	1.1232	1.0790	–3.93
11	8% ^{240}Pu	1.1277	1.0636	–5.69
12	8% ^{240}Pu	1.1060	1.0622	–3.97
13	8% ^{240}Pu	1.0546	1.0383	–1.55
14	8% ^{240}Pu	1.0318	1.0111	–2.01
15	8% ^{240}Pu	1.0421	1.0272	–1.42
16	8% ^{240}Pu	1.2214	1.1705	–4.17
17	UO_2	0.7212	0.7854	8.90
18	UO_2	0.6426	0.7027	9.35
19	UO_2	0.8079	0.8692	7.59
20	UO_2	0.8890	0.9534	7.24
21	UO_2	0.8614	0.9466	9.89
22	UO_2	0.8444	0.9163	8.51
23	UO_2	0.9562	1.0657	11.45

Table 56. Normalized values of experimental and calculational power data for a 25 × 25 concentric-region core configuration containing a 15 × 15 UO_2 inner region and a 24% ^{240}Pu outer region (Fig. 11)

Rod No.	Fuel type	Experiment	Calculation	(C/E-1) × 100
1	24% ^{240}Pu	0.5195	0.5220	–0.24
2	24% ^{240}Pu	0.3230	0.3362	–1.32
3	24% ^{240}Pu	0.3355	0.3322	0.32
4	24% ^{240}Pu	0.4056	0.4099	–0.43
5	24% ^{240}Pu	0.5610	0.5403	2.07
6	UO_2	0.5681	0.5738	–0.57
7	UO_2	0.9026	0.9013	0.13
8	UO_2	1.1009	1.1166	–1.57
9	UO_2	1.2906	1.2853	0.52
10	UO_2	1.3695	1.3982	–2.86
11	UO_2	1.5004	1.4792	2.12
12	UO_2	1.5193	1.5450	–2.57
13	UO_2	1.5812	1.5429	3.83
14	UO_2	1.5350	1.5457	–1.07
15	UO_2	1.5113	1.5056	0.56
16	UO_2	1.4286	1.4682	–3.95
17	UO_2	1.4244	1.4077	1.67
18	UO_2	1.3166	1.3130	0.36
19	UO_2	1.1967	1.1718	2.50
20	UO_2	0.9304	0.9293	0.12
21	24% ^{240}Pu	0.9974	0.9779	1.95
22	24% ^{240}Pu	0.7154	0.7076	0.78
23	24% ^{240}Pu	0.5847	0.5967	–1.20
24	24% ^{240}Pu	0.5666	0.5826	–1.60
25	24% ^{240}Pu	0.8157	0.8112	0.45

Table 57. Normalized values of experimental and calculational power data for a 25 × 25 concentric-region core configuration containing a 15 × 15 24% ^{240}Pu inner region and a UO_2 outer region (Fig. 12)

Rod No.	Fuel type	Experiment	Calculation	(C/E-1) × 100
1	24% ^{240}Pu	1.1681	1.1508	–1.48
2	24% ^{240}Pu	0.9408	0.9301	–1.14
3	24% ^{240}Pu	0.9066	0.8990	–0.84
4	24% ^{240}Pu	0.9469	0.9202	–2.83
5	24% ^{240}Pu	0.9836	0.9657	–1.81
6	24% ^{240}Pu	1.0117	0.9773	–3.40
7	24% ^{240}Pu	1.0483	1.0156	–3.13
8	24% ^{240}Pu	1.0459	0.9878	–5.55
9	24% ^{240}Pu	1.0337	1.0113	–2.16
10	24% ^{240}Pu	1.0496	1.0064	–4.12
11	24% ^{240}Pu	1.0361	0.9967	–3.81
12	24% ^{240}Pu	0.9958	0.9737	–2.22

Table 57. (continued)

Rod No.	Fuel type	Experiment	Calculation	(C/E-1) × 100
13	24% ^{240}Pu	0.9726	0.9694	–0.32
14	24% ^{240}Pu	0.9763	0.9583	–1.84
15	24% ^{240}Pu	0.9848	0.9707	–1.43
16	24% ^{240}Pu	1.1644	1.1540	–0.90
17	UO_2	0.8232	0.8997	9.29
18	UO_2	0.9116	0.9863	8.19
19	UO_2	1.0139	1.0895	7.46
20	UO_2	0.9939	1.0771	8.37
21	UO_2	0.9922	1.0605	6.88

Table 58. Normalized values of experimental and calculational power data for a 27 × 27 concentric-region core configuration containing a 15 × 15 24% ^{240}Pu inner region and 8% ^{240}Pu outer region (Fig. 13)

Rod No.	Fuel type	Experiment	Calculation	(C/E-1) × 100
1	8% ^{240}Pu	1.315	1.2661	–3.72
2	8% ^{240}Pu	0.851	0.8434	–0.89
3	8% ^{240}Pu	0.698	0.8434	20.83
4	8% ^{240}Pu	0.929	0.8975	–3.39
5	8% ^{240}Pu	1.033	0.9587	–7.19
6	8% ^{240}Pu	1.064	1.0465	–1.64
7	24% ^{240}Pu	0.995	1.0018	0.68
8	24% ^{240}Pu	1.036	1.0515	1.50
9	24% ^{240}Pu	1.079	1.1004	1.98
10	24% ^{240}Pu	1.119	1.1120	–0.63
11	24% ^{240}Pu	1.146	1.1390	–0.61
12	24% ^{240}Pu	1.139	1.1410	0.18
13	24% ^{240}Pu	1.162	1.1682	0.53
14	24% ^{240}Pu	1.161	1.1764	1.33
15	24% ^{240}Pu	1.156	1.1652	0.80
16	24% ^{240}Pu	1.133	1.1508	1.57
17	24% ^{240}Pu	1.049	1.0655	1.57
18	24% ^{240}Pu	0.933	0.9224	–1.14
19	24% ^{240}Pu	0.839	0.8406	0.19
20	8% ^{240}Pu	0.814	0.8028	–1.38
21	8% ^{240}Pu	0.768	0.7043	–8.29
22	8% ^{240}Pu	0.579	0.6026	4.08

Table 59. Normalized values of experimental and calculational power data for a cylindrical concentric-region core configuration containing a 24% ^{240}Pu inner region and an 8% ^{240}Pu outer region in a 1.7526-cm lattice (Fig. 14)

Rod No.	Fuel type	Experiment	Calculation	(C/E-1) × 100
1	8% ^{240}Pu	1.153	1.1416	–0.99
2	8% ^{240}Pu	0.786	0.7869	0.11
3	8% ^{240}Pu	0.782	0.7704	–1.48
4	8% ^{240}Pu	0.845	0.8254	–2.32
5	8% ^{240}Pu	0.938	0.9048	–3.54
6	8% ^{240}Pu	1.003	0.9871	–1.59
7	8% ^{240}Pu	0.842	0.8406	–0.17
8	8% ^{240}Pu	0.778	0.7860	1.03
9	8% ^{240}Pu	0.866	0.8311	–4.03
10	8% ^{240}Pu	0.847	0.8311	–1.88
11	24% ^{240}Pu	0.951	0.9526	0.17
12	24% ^{240}Pu	1.001	1.0124	1.14
13	24% ^{240}Pu	1.065	1.0659	0.08
14	24% ^{240}Pu	1.096	1.0921	–0.36
15	24% ^{240}Pu	1.116	1.1288	1.15
16	24% ^{240}Pu	1.124	1.1645	3.60
17	24% ^{240}Pu	1.159	1.1765	1.51
18	24% ^{240}Pu	1.176	1.1801	0.35
19	24% ^{240}Pu	1.197	1.1955	–0.13
20	24% ^{240}Pu	1.157	1.1707	1.18
21	24% ^{240}Pu	1.109	1.1559	4.23

Table 60. Normalized values of experimental and calculational power data for a cylindrical concentric-region core configuration containing a 24% ^{240}Pu inner region and an 8% ^{240}Pu outer region in a 1.9050-cm lattice (Fig. 15)

Rod No.	Fuel type	Experiment	Calculation	(C/E-1) × 100
1	24% ^{240}Pu	1.221	1.2368	1.29
2	24% ^{240}Pu	1.227	1.2219	–0.42
3	24% ^{240}Pu	1.226	1.2129	–1.07
4	24% ^{240}Pu	1.164	1.1870	1.98
5	24% ^{240}Pu	1.117	1.1485	2.82
6	24% ^{240}Pu	1.062	1.0878	2.43
7	24% ^{240}Pu	1.017	1.0343	1.70
8	24% ^{240}Pu	0.935	0.9435	0.91
9	8% ^{240}Pu	0.961	0.9364	–2.56
10	8% ^{240}Pu	0.859	0.8393	–2.29
11	8% ^{240}Pu	0.808	0.7934	–1.81
12	8% ^{240}Pu	1.069	1.0397	–2.74
13	8% ^{240}Pu	0.864	0.8511	–1.49
14	8% ^{240}Pu	0.812	0.8141	0.26
15	8% ^{240}Pu	0.851	0.8455	–0.65
16	8% ^{240}Pu	0.808	0.8077	–0.04

Table 61. Normalized values of experimental and calculational power data for a cylindrical concentric-region core configuration containing a 24% ^{240}Pu inner region and an 8% ^{240}Pu outer region with a regional variation in lattice pitch (Fig. 16)

Rod No.	Fuel type	Experiment	Calculation	(C/E-1) × 100
1	8% ^{240}Pu	1.1572	1.1714	1.23
2	8% ^{240}Pu	1.2262	1.2314	0.42
3	8% ^{240}Pu	1.3821	1.4012	1.38
4	8% ^{240}Pu	1.1476	1.1477	0.02
5	24% ^{240}Pu	0.7772	0.7793	0.27
6	24% ^{240}Pu	0.7653	0.7606	–0.61
7	24% ^{240}Pu	0.7660	0.7751	1.18
8	24% ^{240}Pu	0.7809	0.7792	–0.22
9	24% ^{240}Pu	0.7749	0.7651	–1.27
10	24% ^{240}Pu	0.7683	0.7586	–1.26
11	24% ^{240}Pu	0.7957	0.7964	0.09
12	8% ^{240}Pu	1.1639	1.1567	–0.61
13	8% ^{240}Pu	1.3903	1.3920	0.12
14	8% ^{240}Pu	1.2403	1.2377	–0.21
15	8% ^{240}Pu	1.1639	1.1662	0.20
16	24% ^{240}Pu	0.7816	0.7595	–2.82
17	24% ^{240}Pu	0.7601	0.7531	–0.92
18	24% ^{240}Pu	0.7638	0.7679	0.54
19	24% ^{240}Pu	0.7972	0.7994	0.28
20	24% ^{240}Pu	0.8959	0.9099	1.56
21	8% ^{240}Pu	1.3376	1.3342	–0.25
22	8% ^{240}Pu	1.3205	1.3170	–0.27
23	8% ^{240}Pu	1.0436	1.0404	–0.31

Table 62. Normalized values of experimental and calculational power data for a 27 × 27 salt-and-pepper core configuration composed of the 8% ^{240}Pu and 24% ^{240}Pu fuels (Fig. 17)

Rod No.	Fuel type	Experiment	Calculation	(C/E-1) × 100
1	24% ^{240}Pu	0.9638	1.0111	4.91
2	8% ^{240}Pu	0.8018	0.7852	–2.07
3	24% ^{240}Pu	0.6727	0.6782	0.82
4	8% ^{240}Pu	0.8557	0.8413	–1.68
5	24% ^{240}Pu	0.7800	0.8094	3.78
6	8% ^{240}Pu	0.9941	0.9781	–1.62
7	24% ^{240}Pu	0.8895	0.9312	4.69
8	8% ^{240}Pu	1.1473	1.0830	–5.60
9	24% ^{240}Pu	0.9897	1.0180	2.86
10	8% ^{240}Pu	1.2132	1.1854	–2.29
11	24% ^{240}Pu	1.0551	1.0832	2.66
12	8% ^{240}Pu	1.2826	1.2110	–5.58
13	24% ^{240}Pu	1.0685	1.1229	5.09
14	8% ^{240}Pu	1.2862	1.2619	–1.89

Table 63. Normalized values of experimental and calculational power data for a 23 × 23 salt-and-pepper core configuration composed of the 8% ^{240}Pu and UO_2 fuels (Fig. 18)

Rod No.	Fuel type	Experiment	Calculation	(C/E-1) × 100
1	8% ^{240}Pu	0.778588	0.770	–1.10
2	8% ^{240}Pu	0.597293	0.591	–1.05
3	8% ^{240}Pu	0.64548	0.639	–1.00
4	8% ^{240}Pu	0.765946	0.758	–1.04
5	8% ^{240}Pu	0.910506	0.901	–1.04
6	8% ^{240}Pu	1.040866	1.030	–1.04
7	8% ^{240}Pu	1.191289	1.179	–1.03
8	8% ^{240}Pu	1.340154	1.326	–1.06
9	8% ^{240}Pu	1.447154	1.432	–1.05
10	8% ^{240}Pu	1.502669	1.487	–1.04
11	8% ^{240}Pu	1.524747	1.509	–1.03
12	8% ^{240}Pu	1.555619	1.540	–1.00
13	UO_2	0.664168	0.704	6.00
14	8% ^{240}Pu	1.533725	1.518	–1.03
15	UO_2	0.650702	0.690	6.04
16	8% ^{240}Pu	1.442665	1.428	–1.02
17	UO_2	0.584468	0.619	5.91
18	8% ^{240}Pu	1.264943	1.252	–1.02
19	UO_2	0.511272	0.542	6.01
20	8% ^{240}Pu	1.096198	1.085	–1.02
21	UO_2	0.426533	0.452	5.97
22	8% ^{240}Pu	0.963548	0.954	–0.99
23	UO_2	0.561474	0.595	5.97

Table 64. Normalized values of experimental and calculational power data for a 23 × 23 salt-and-pepper core configuration composed of the 24% ^{240}Pu and UO_2 fuels (Fig. 19)

Rod No.	Fuel type	Experiment	Calculation	(C/E-1) × 100
1	24% ^{240}Pu	1.151	1.1448	–0.54
2	UO_2	0.697	0.7010	0.57
3	24% ^{240}Pu	1.272	1.2711	–0.07
4	UO_2	0.741	0.7672	3.54
5	24% ^{240}Pu	1.357	1.3405	–1.22
6	UO_2	0.780	0.7894	1.21
7	UO_2	0.771	0.7977	3.46
8	24% ^{240}Pu	1.378	1.3350	–3.12
9	UO_2	0.755	0.7574	0.32
10	24% ^{240}Pu	1.287	1.2561	–2.40
11	UO_2	0.688	0.7030	2.18
12	24% ^{240}Pu	1.124	1.1367	1.13

Table 65. Normalized values of experimental and calculational power data for a 24 × 24 salt-and-pepper core configuration composed of the 24% ^{240}Pu and UO_2 fuels (Fig. 20)

Rod No.	Fuel type	Experiment	Calculation	(C/E-1) × 100
1	24% ^{240}Pu	1.131	1.1040	–2.39
2	UO_2	0.631	0.6856	8.65
3	24% ^{240}Pu	1.278	1.2562	–1.71
4	UO_2	0.721	0.7518	4.27
5	24% ^{240}Pu	1.349	1.3527	0.27
6	UO_2	0.751	0.7798	3.83
7	24% ^{240}Pu	1.388	1.3802	–0.56
8	UO_2	0.749	0.7899	5.46
9	24% ^{240}Pu	1.389	1.3484	–2.92
10	UO_2	0.753	0.7574	0.58
11	24% ^{240}Pu	1.322	1.2933	–2.17
12	UO_2	0.702	0.7062	0.60
13	24% ^{240}Pu	1.210	1.1656	–3.67
14	UO_2	0.625	0.6290	0.64

Table 66. Normalized values of experimental and calculational power data for a 25 × 25 salt-and-pepper core configuration composed of the 24% ^{240}Pu and UO_2 fuels (Fig. 21)

Rod No.	Fuel type	Experiment	Calculation	(C/E-1) × 100
1	24% ^{240}Pu	0.685	0.6892	0.61
2	24% ^{240}Pu	0.525	0.5192	–1.10
3	24% ^{240}Pu	0.561	0.5494	–2.07
4	24% ^{240}Pu	0.677	0.6660	–1.62
5	24% ^{240}Pu	0.806	0.7967	–1.15
6	24% ^{240}Pu	0.960	0.9254	–3.60
7	24% ^{240}Pu	1.090	1.0623	–2.54
8	24% ^{240}Pu	1.191	1.1712	–1.66
9	24% ^{240}Pu	1.294	1.2926	–0.11
10	24% ^{240}Pu	1.381	1.3800	–0.07
11	24% ^{240}Pu	1.462	1.4301	–2.18
12	24% ^{240}Pu	1.490	1.4579	–2.15
13	24% ^{240}Pu	1.490	1.4884	–0.11
14	UO_2	0.808	0.8749	8.28
15	24% ^{240}Pu	1.461	1.4652	0.29
16	UO_2	0.802	0.8377	4.45
17	24% ^{240}Pu	1.408	1.4037	–0.31
18	UO_2	0.741	0.7856	6.02
19	24% ^{240}Pu	1.278	1.2545	–1.84
20	UO_2	0.672	0.6911	2.84
21	24% ^{240}Pu	1.099	1.0773	–1.97
22	UO_2	0.551	0.5843	6.04
23	24% ^{240}Pu	0.921	0.9315	1.14
24	UO_2	0.500	0.5389	7.78
25	24% ^{240}Pu	1.147	1.1271	–1.73

Table 67. Normalized values of experimental and calculational power data for a multiregion slab core configuration containing an 8% ^{240}Pu central region and UO_2 outer regions (Fig. 22)

Rod No.	Fuel type	Experiment	Calculation	(C/E-1) × 100
1	UO_2	0.573	0.7255	26.62
2	UO_2	0.436	0.5394	23.71
3	UO_2	0.409	0.5211	27.41
4	UO_2	0.435	0.5502	26.48
5	UO_2	0.465	0.5870	26.25
6	UO_2	0.517	0.6308	22.01
7	UO_2	0.540	0.6655	23.24
8	UO_2	0.576	0.7045	22.30
9	UO_2	0.584	0.7173	22.82
10	UO_2	0.571	0.6922	21.22
12	8% ^{240}Pu	1.212	1.2235	0.95
13	8% ^{240}Pu	1.182	1.1714	–0.90
14	8% ^{240}Pu	1.199	1.1795	–1.63
15	8% ^{240}Pu	1.227	1.2026	–1.99
16	8% ^{240}Pu	1.260	1.2208	–3.11
17	8% ^{240}Pu	1.280	1.2647	–1.20
18	8% ^{240}Pu	1.301	1.2738	–2.09
19	8% ^{240}Pu	1.301	1.2741	–2.06
20	8% ^{240}Pu	1.318	1.2947	–1.77
21	8% ^{240}Pu	1.311	1.3097	–0.10
22	8% ^{240}Pu	1.312	1.2975	–1.10
23	8% ^{240}Pu	1.260	1.2651	0.41
24	8% ^{240}Pu	1.186	1.1912	0.44
25	8% ^{240}Pu	1.310	1.2978	–0.93
26	8% ^{240}Pu	1.275	1.2750	0.00
27	8% ^{240}Pu	1.256	1.2236	–2.58
28	8% ^{240}Pu	1.196	1.1675	–2.38
30	8% ^{240}Pu	1.029	1.0206	–0.81
31	8% ^{240}Pu	0.946	0.9743	2.99
32	8% ^{240}Pu	0.993	0.9800	–1.31
33	8% ^{240}Pu	1.457	1.4594	0.17
35	8% ^{240}Pu	1.082	1.0997	1.64

Table 68. Normalized values of experimental and calculational power data for a multiregion slab core configuration containing an 8% ^{240}Pu central region and UO_2 outer regions with a 4 × 4 central void pattern (Fig. 23)

Rod No.	Fuel type	Experiment	Calculation	(C/E-1) × 100
1	UO_2	0.599	0.7198	20.17
2	UO_2	0.455	0.5373	18.08
3	UO_2	0.427	0.5101	19.45
4	UO_2	0.458	0.5324	16.24
5	UO_2	0.485	0.5814	19.88
6	UO_2	0.536	0.6325	18.00
7	UO_2	0.566	0.6564	15.97
8	UO_2	0.604	0.6935	14.82
9	UO_2	0.614	0.7054	14.88
10	UO_2	0.599	0.6823	13.91
12	8% ^{240}Pu	1.260	1.1860	–5.87
13	8% ^{240}Pu	1.240	1.1435	–7.78
14	8% ^{240}Pu	1.249	1.1510	–7.84
15	8% ^{240}Pu	1.271	1.1860	–6.69
16	8% ^{240}Pu	1.304	1.2246	–6.09
17	8% ^{240}Pu	1.343	1.2138	–9.62
18	8% ^{240}Pu	1.335	1.2350	–7.49
19	8% ^{240}Pu	1.299	1.2297	–5.34
20	8% ^{240}Pu	1.257	1.2273	–2.36
21	8% ^{240}Pu	1.240	1.1643	–6.11
22	8% ^{240}Pu	1.233	1.1856	–3.85
23	8% ^{240}Pu	1.325	1.1368	–14.21
24	8% ^{240}Pu	1.252	1.0832	–13.48
25	8% ^{240}Pu	1.244	1.0016	–19.49
26	8% ^{240}Pu	1.267	0.9249	–27.00
27	8% ^{240}Pu	1.301	0.9683	–25.57
28	8% ^{240}Pu	1.259	1.4404	14.41
29	8% ^{240}Pu	1.183	1.0780	–8.87
30	8% ^{240}Pu	1.109	1.1936	7.63
31	8% ^{240}Pu	1.028	1.1916	15.91
32	8% ^{240}Pu	1.041	1.2047	15.73
33	8% ^{240}Pu	1.487	1.1954	–19.61
35	8% ^{240}Pu	1.128	1.1836	4.93

Table 69. Normalized values of experimental and calculational power data for a multiregion slab core configuration containing an 8% ^{240}Pu central region and UO_2 outer regions with a 10 × 10 central void pattern (Fig. 24)

Rod No.	Fuel type	Experiment	Calculation	(C/E-1) × 100
1	UO_2	0.620	0.7255	17.01
2	UO_2	0.478	0.5407	13.12
3	UO_2	0.454	0.5161	13.67
4	UO_2	0.480	0.5286	10.13
5	UO_2	0.510	0.5713	12.02
6	UO_2	0.554	0.6218	12.25
7	UO_2	0.581	0.6556	12.84
8	UO_2	0.621	0.6926	11.52
9	UO_2	0.630	0.7071	12.24
10	UO_2	0.608	0.6930	13.98
12	8% ^{240}Pu	1.303	1.1837	–9.16
13	8% ^{240}Pu	1.251	1.1497	–8.09
14	8% ^{240}Pu	1.278	1.1559	–9.55
15	8% ^{240}Pu	1.282	1.1775	–8.15
16	8% ^{240}Pu	1.232	1.2276	–0.36
17	8% ^{240}Pu	1.196	1.2530	4.77
18	8% ^{240}Pu	1.173	1.2805	9.16
19	8% ^{240}Pu	1.195	1.2714	6.39
20	8% ^{240}Pu	1.184	1.2544	5.95
21	8% ^{240}Pu	1.213	1.1542	–4.85
22	8% ^{240}Pu	1.193	1.2646	6.00
23	8% ^{240}Pu	1.182	1.2480	5.58
24	8% ^{240}Pu	1.247	1.1894	–4.62
25	8% ^{240}Pu	1.202	0.9884	–17.77
26	8% ^{240}Pu	1.163	0.9499	–18.33
27	8% ^{240}Pu	1.144	0.9735	–14.90
28	8% ^{240}Pu	1.103	1.4295	29.60
29	8% ^{240}Pu	1.106	1.1424	3.29
30	8% ^{240}Pu	1.077	1.1610	7.80
31	8% ^{240}Pu	1.018	1.1677	14.70
32	8% ^{240}Pu	1.052	1.0934	3.94
33	8% ^{240}Pu	1.594	1.0181	–36.13
35	8% ^{240}Pu	1.079	1.0140	–6.03

Table 70. Normalized values of experimental and calculational power data for a multiregion slab core configuration containing an 8% ^{240}Pu central region and UO_2 outer regions (Fig. 25)

Rod No.	Fuel type	Experiment	Calculation	(C/E-1) × 100
1	UO_2	0.455	0.3469	–23.75
2	UO_2	0.423	0.2856	–32.47
3	UO_2	0.389	0.2950	–24.18
4	UO_2	0.471	0.3206	–31.94
5	UO_2	0.472	0.3568	–24.40
6	UO_2	0.561	0.3859	–31.21
7	UO_2	0.571	0.4222	–26.05
8	UO_2	0.657	0.4635	–29.45
9	UO_2	0.659	0.4837	–26.61
10	UO_2	0.745	0.5210	–30.07
11	UO_2	0.737	0.5446	–26.11
12	UO_2	0.816	0.5620	–31.12
13	UO_2	0.812	0.5725	–29.50
14	UO_2	0.847	0.5790	–31.64
15	UO_2	0.790	0.5552	–29.72
16	8% ^{240}Pu	1.685	0.9697	–42.45
17	8% ^{240}Pu	1.590	0.9167	–42.35
18	8% ^{240}Pu	1.616	0.9342	–42.19
19	8% ^{240}Pu	1.634	0.9604	–41.22
20	8% ^{240}Pu	1.672	0.9591	–42.64
21	8% ^{240}Pu	1.691	0.9756	–42.30
22	8% ^{240}Pu	1.726	0.9829	–43.05
23	8% ^{240}Pu	1.729	0.9966	–42.36
24	8% ^{240}Pu	1.743	1.0044	–42.38
25	8% ^{240}Pu	1.739	0.9950	–42.78
26	8% ^{240}Pu	1.734	1.0072	–41.92
27	8% ^{240}Pu	1.713	1.0076	–41.18
28	8% ^{240}Pu	1.699	1.0022	–41.01
29	8% ^{240}Pu	1.718	0.9987	–41.87
30	8% ^{240}Pu	1.678	0.9591	–42.85
31	8% ^{240}Pu	1.631	0.9496	–41.78
32	8% ^{240}Pu	1.592	0.9301	–41.57
33	8% ^{240}Pu	1.619	0.9189	–43.24
34	8% ^{240}Pu	1.658	0.9719	–41.38
36	UO_2	0.781	0.3450	–55.82
37	UO_2	0.838	0.2870	–65.75
40	UO_2	0.753	0.3540	–52.98
43	UO_2	0.646	0.4468	–30.84
46	UO_2	0.491	0.5389	9.75
49	UO_2	0.400	0.5833	45.83
50	8% ^{240}Pu	0.451	0.7865	74.38
51	8% ^{240}Pu	0.337	0.6034	79.06

Table 70. (continued)

Rod No.	Fuel type	Experiment	Calculation	(C/E-1) × 100
52	8% ^{240}Pu	0.350	0.6292	79.78
53	8% ^{240}Pu	0.402	0.7055	75.49
54	8% ^{240}Pu	0.669	0.7647	14.30
55	8% ^{240}Pu	0.709	0.8084	14.01
56	8% ^{240}Pu	0.773	0.8703	12.59
57	8% ^{240}Pu	0.789	0.9178	16.33
58	8% ^{240}Pu	0.819	0.9537	16.44
59	8% ^{240}Pu	0.857	1.0021	16.93
60	8% ^{240}Pu	0.868	1.0166	17.12
61	8% ^{240}Pu	0.847	0.9914	17.05
62	8% ^{240}Pu	0.748	0.8689	16.16
63	8% ^{240}Pu	0.663	0.7585	14.41
64	8% ^{240}Pu	0.538	0.6336	17.77

Table 71. Normalized values of experimental and calculational power data for a multiregion slab core configuration containing an 8% ^{240}Pu in the central region and UO_2 outer regions with a 4 × 4 central void pattern (Fig. 26)

Rod No.	Fuel type	Experiment	Calculation	(C/E-1) × 100
1	UO_2	0.330	0.3977	20.53
2	UO_2	0.356	0.4370	22.76
3	UO_2	0.453	0.5256	16.02
4	UO_2	0.511	0.6174	20.82
5	UO_2	0.594	0.7180	20.88
6	UO_2	0.636	0.7832	23.15
7	UO_2	0.680	0.8185	20.37
8	UO_2	0.646	0.7715	19.42
9	UO_2	1.414	1.3325	–5.76
10	8% ^{240}Pu	1.358	1.2697	–6.50
11	8% ^{240}Pu	1.363	1.2631	–7.33
12	8% ^{240}Pu	1.388	1.2822	–7.62
13	8% ^{240}Pu	1.432	1.3092	–8.58
14	8% ^{240}Pu	1.458	1.3073	–10.34
15	8% ^{240}Pu	1.455	1.3634	–6.30
16	8% ^{240}Pu	1.389	1.3137	–5.42
17	8% ^{240}Pu	1.336	1.2920	–3.29
18	8% ^{240}Pu	1.324	1.3140	–0.76
19	8% ^{240}Pu	1.394	1.2895	–7.49
20	8% ^{240}Pu	1.340	1.2785	–4.59
21	8% ^{240}Pu	1.206	1.1125	–7.76
22	8% ^{240}Pu	1.024	0.9527	–6.96
23	8% ^{240}Pu	0.920	0.8685	–5.60
24	8% ^{240}Pu	0.881	0.8246	–6.40
25	8% ^{240}Pu	1.151	1.0895	–5.34
27	UO_2	0.651	0.8347	28.22
28	UO_2	0.669	0.8161	21.99
29	UO_2	0.643	0.8174	27.12

Table 72. Normalized values of experimental and calculational power data for a multiregion slab core configuration containing an 8% ^{240}Pu in the central region and UO_2 outer regions with a 10 × 10 central void pattern (Fig. 27)

Rod No.	Fuel type	Experiment	Calculation	(C/E-1) × 100
1	UO_2	0.373	0.4267	14.39
2	UO_2	0.419	0.4694	12.03
3	UO_2	0.501	0.5628	12.34
4	UO_2	0.593	0.6726	13.42
5	UO_2	0.663	0.7498	13.09
6	UO_2	0.736	0.8257	12.19
7	UO_2	0.757	0.8473	11.93
8	UO_2	0.767	0.8618	12.37
9	UO_2	0.726	0.8146	12.21
10	8% ^{240}Pu	1.444	1.4185	–1.77
11	8% ^{240}Pu	1.379	1.3363	–3.09
12	8% ^{240}Pu	1.382	1.3193	–4.54
13	8% ^{240}Pu	1.395	1.3223	–5.21
14	8% ^{240}Pu	1.360	1.1462	–15.72
15	8% ^{240}Pu	1.322	0.9848	–25.51
16	8% ^{240}Pu	1.295	0.9082	–29.87
17	8% ^{240}Pu	1.302	0.8790	–32.49
18	8% ^{240}Pu	1.303	1.1341	–12.96
19	8% ^{240}Pu	1.302	1.2538	–3.70
20	8% ^{240}Pu	1.299	1.2422	–4.37
21	8% ^{240}Pu	1.214	1.2327	1.54
22	8% ^{240}Pu	1.204	1.2243	1.69
23	8% ^{240}Pu	1.024	1.2306	20.17
24	8% ^{240}Pu	0.922	1.2041	30.60
25	8% ^{240}Pu	0.912	1.1617	27.38
26	8% ^{240}Pu	1.196	1.2838	7.34
28	UO_2	0.731	0.8490	16.14
29	UO_2	0.746	0.8143	9.16
30	UO_2	0.733	0.8239	12.40

Table 73. Normalized values of experimental and calculated power data for a multiregion slab core configuration containing central traverse slabs of 8% ^{240}Pu and 24% ^{240}Pu in the central region and UO_2 outer regions (Fig. 28)

Rod No.	Fuel type	Experiment	Calculation	(C/E-1) × 100
1	UO_2	0.569	0.5957	4.69
2	UO_2	0.609	0.6293	3.33
3	UO_2	0.642	0.6808	6.04
4	UO_2	0.612	0.7066	15.46
5	UO_2	0.692	0.7129	3.03
6	UO_2	0.652	0.6910	5.98
7	24% ^{240}Pu	1.088	1.0818	–0.57
8	24% ^{240}Pu	1.049	1.0380	–1.05
9	24% ^{240}Pu	1.053	1.0429	–0.96
10	24% ^{240}Pu	1.084	1.0553	–2.64
11	24% ^{240}Pu	1.100	1.0551	–4.08
12	24% ^{240}Pu	1.114	1.0764	–3.38
13	24% ^{240}Pu	1.128	1.0959	–2.85
14	24% ^{240}Pu	1.129	1.1133	–1.39
15	24% ^{240}Pu	1.138	1.1205	–1.53
16	24% ^{240}Pu	1.142	1.0991	–3.76
17	24% ^{240}Pu	1.155	1.0985	–4.89
18	24% ^{240}Pu	1.151	1.0941	–4.94
19	24% ^{240}Pu	1.141	1.0938	–4.14
20	24% ^{240}Pu	1.127	1.0730	–4.79
21	24% ^{240}Pu	1.092	1.0765	–1.42
22	24% ^{240}Pu	1.080	1.0532	–2.48
23	24% ^{240}Pu	1.068	1.0259	–3.94
24	24% ^{240}Pu	1.066	1.0328	–3.12
25	24% ^{240}Pu	1.111	1.0883	–2.04
26	UO_2	0.660	0.6981	5.77
27	UO_2	0.685	0.7072	3.24
28	UO_2	0.671	0.7080	5.52
29	8% ^{240}Pu	0.945	1.0582	11.98
30	8% ^{240}Pu	1.000	1.0828	8.28
31	8% ^{240}Pu	1.053	1.1212	6.47
32	8% ^{240}Pu	1.137	1.1301	–0.61
33	24% ^{240}Pu	1.069	0.8882	–16.91
34	24% ^{240}Pu	1.089	0.9365	–14.01
35	24% ^{240}Pu	1.122	1.0052	–10.41
36	24% ^{240}Pu	1.152	1.0766	–6.54
37	24% ^{240}Pu	1.151	1.0853	–5.70
38	24% ^{240}Pu	1.134	1.0102	–10.91
39	24% ^{240}Pu	1.109	0.9560	–13.80
40	24% ^{240}Pu	1.058	0.9029	–14.66
41	8% ^{240}Pu	1.143	1.1032	–3.48
42	8% ^{240}Pu	1.063	1.0929	2.81
43	8% ^{240}Pu	1.017	1.0742	5.63
44	8% ^{240}Pu	0.949	1.0446	10.08

Table 74. Normalized values of experimental and calculational power data for a multiregion slab core configuration containing alternate rows of 8% ^{240}Pu and 24% ^{240}Pu in the central region and UO_2 outer regions (Fig. 29)

Rod No.	Fuel type	Experiment	Calculation	(C/E-1) × 100
1	UO_2	0.511	0.5772	12.95
2	UO_2	0.556	0.6249	12.39
3	UO_2	0.583	0.6635	13.81
4	UO_2	0.626	0.6958	11.16
5	UO_2	0.656	0.7327	11.69
6	UO_2	0.675	0.7400	9.63
7	UO_2	0.628	0.7119	13.36
8	UO_2	0.635	0.7019	10.53
9	UO_2	0.656	0.7325	11.66
10	UO_2	0.658	0.7286	10.73
11	8 ^{240}Pu	1.261	1.1033	–12.50
12	24% ^{240}Pu	1.052	1.1707	11.28
13	8 ^{240}Pu	1.222	1.0579	–13.43
14	24% ^{240}Pu	1.109	1.2037	8.54
15	8 ^{240}Pu	1.275	1.1030	–13.49
16	24% ^{240}Pu	1.122	1.2415	10.65
17	8 ^{240}Pu	1.301	1.1184	–14.03
18	24% ^{240}Pu	1.141	1.2656	10.92
19	8 ^{240}Pu	1.329	1.1439	–13.93
20	24% ^{240}Pu	1.147	1.2665	10.42
21	8 ^{240}Pu	1.323	1.1293	–14.64
22	24% ^{240}Pu	1.167	1.2648	8.38
23	8 ^{240}Pu	1.320	1.1400	–13.64
24	24% ^{240}Pu	1.130	1.2292	8.78
25	8 ^{240}Pu	1.259	1.1162	–11.34
26	24% ^{240}Pu	1.083	1.2000	10.81
27	8 ^{240}Pu	1.231	1.0644	–13.53
28	24% ^{240}Pu	1.072	1.1603	8.24
29	8 ^{240}Pu	1.274	1.1122	–12.70

REFERENCES

1. R. D. Leamer et al., *PuO_2-UO_2 Fueled Critical Experiments*, Westinghouse Electric Corporation, WCAP-3726-1, July 1967.
2. W. L. Orr, "Westinghouse Pu Recycle Experience and Design," *Proceedings of the Topical Meeting on The Plutonium Fuel Cycle, May 1977*.
3. H. Akkurt and N. M. Abdurrahman, *ESADA Plutonium Program Critical Experiments: Single-Region Core Configurations*, Lockheed Martin Energy Research Corp., Oak Ridge National Laboratory, ORNL/SUB/99-XSZ175V-1, May 1999.
4. H. Akkurt and N. M. Abdurrahman, *ESADA Plutonium Program Critical Experiments: Multiregion Core Configurations*, Lockheed Martin Energy Research Corp., Oak Ridge National Laboratory, ORNL/SUB/00-XSZ175V-1, February 2000.
5. E. G. Taylor et al., *Saxton Plutonium Program—Critical Experiments for the Saxton Partial Plutonium Core*, Westinghouse Electric Corporation, EURAEC-1493 (WCAP-3385-54), December 1965.
6. V. O. Uotinen, B. R. Leonard, Jr., and R. C. Liikala, "The Neutronics of Plutonium Recycling," *Nuc. Tech.*, **18**, 115 (1973).
7. H.-K. Joo, *Rectangular Arrays of Water-Moderated UO_2–2 wt % PuO_2 (8% ^{240}Pu) Fuel Rods*, NEA/NSC/DOC/95(03)/VI, Revision: 0, OECD Nuclear Energy Agency, 1997.
8. V. O. Uotinen, J. H. Lauby, L. C. Schmid, and W. P. Stinson, "Lattices of Plutonium-Enriched Rods in Light Water-Part I: Experimental Results," *Nuc. Tech.*, **15**, 257 (1972).
9. D. F. Newman, "Measurement of k_∞ and Relative Reaction Rates in an H_2O Moderated UO_2-PuO_2 Particulate Fueled Lattice," *Nuc. Tech.*, **15**, 192 (1972).
10. Harold Etherington, *Nuclear Engineering Handbook*, 1st ed., McGraw-Hill Book Company, New York, 1958.
11. R. E. Alcouffe, R. S. Baker, F. W. Brinkley, D. R. Marr, R. D. O'Dell, and W. F. Walters, *DANTSYS: A Diffusion Accelerated Neutral Particle Transport Code System*, LA-12965-M, Los Alamos National Laboratory, 1995.
12. N. F. Landers and L. M. Petrie, *CSAS: Control Module for Enhanced Criticality Safety Analysis Sequences*, NUREG/CR-0200, Vol. 1 Sect. C4, ORNL/NUREG/CSD/-2/V2/R6, Lockheed Martin Energy Research Corp., Oak Ridge National Laboratory, 1998.
13. L. C. Schmid et al., *Reactor Physics Data for the Utilization of Plutonium in Thermal Power Reactors*, BNWL-801, May 1968.
14. J. F. Briesmeister, *MCNP-A General Monte Carlo N-Particle Transport Code*, LA-12625-M, Los Alamos National Laboratory, 1994.

Appendix A
ATOMIC NUMBER DENSITY CALCULATIONS

Appendix A

ATOMIC NUMBER DENSITY CALCULATIONS

Atomic densities of the fuels are calculated using Avogadro's number and atomic weights from* using the following formula:

$$N_i = \frac{\rho\, w_e\, w_i\, N_A}{A_i} \quad ,$$

where

N_I = atom density of *i*th isotope,
ρ = density of mixture,
w_e = weight fraction of the element in the mixture,
w_i = weight fraction of the *i*th isotope in the element,
N_A = Avogadro's number,
A_I = atomic weight of the *i*th isotope.

The density of MOX fuel[1] is taken as 9.54 g/cm^3.

The H, O, ^{10}B, and ^{11}B number densities are calculated by using the borated water density formula:†

$$\rho_{bwat} = \frac{0.997518 + C_B / 1000}{1 + C_B / 1920} \quad ,$$

where 0.997518 g/cm^3 is the density of water at 23ºC temperature, and ρ_{bwat} is the density (g/cm^3) of borated water by adding C_B grams of H_3BO_3 crystals to 1 L of water at 23°C temperature.

The H_3BO_3 density in the borated water is calculated using the formula:†

$$\rho_{H_3BO_3} = \frac{C_B}{1000 \leftrightarrow (1 + C_B / 1920)} \quad .$$

The H_2O density in borated water is calculated using the formula:†

$$\rho_{H_2O} = \frac{997.518}{1000 \leftrightarrow (1 + C_B / 1920)} \quad .$$

The ^{10}B and ^{11}B atomic fractions in boron are 19.8% and 80.2%, respectively. Then, the fraction of boron in H_3BO_3 is calculated as:

$$f_B = \frac{(0.198 \leftrightarrow 10.0129 + 0.802 \leftrightarrow 11.0093)}{3 \leftrightarrow 1.0079 + (0.198 \leftrightarrow 10.0129 + 0.802 \leftrightarrow 11.0093) + 3 \leftrightarrow 15.9994} = 0.17485571 \quad .$$

---

*F. W. Walker, J. R. Parrington, and F. Feiner, *Nuclides and Isotopes*, 14th ed., General Electric Nuclear Energy Operations, 1989.

†H.-K. Joo, *Rectangular Arrays of Water-Moderated UO_2–2 wt % PuO_2 (8% ^{240}Pu) Fuel Rods*, NEA/NSC/DOC/95(03)/VI, Revision: 0, OECD Nuclear Energy Agency, 1997.

C_B can be determined using the reported boron concentration p (in ppm) and the formula:

$$C_B = \frac{997.518 \leftrightarrow p}{(f_B \leftrightarrow 10^6 - p)} \quad .$$

The H_3BO_3 and H_2O densities are calculated by substituting the calculated C_B value into the equations given above. Then, the boron number density is calculated with H_3BO_3 density, ^{10}B and ^{11}B atomic fractions, and Avogadro's number. The H and O number densities are calculated by summing the atomic number densities from H_2O and H_3BO_3.

Power distribution measurements were performed using 315- and 526-ppm boron concentrations. The calculated values of C_B, ρ_{bwat}, $\rho_{H_3BO_3}$, and ρ_{H_2O} for these boron concentrations are summarized in Table A.1. The calculated number densities using these values were given in Table 46 in Sect. 3.3.

Table A.1. The calculated values of C_B and densities for the specified boron concentrations

Parameter	Boron concentration	
	315 ppm	526 ppm
C_B, g	1.80026	3.00978
ρ_{bwat}, g/cm^3	9.98382E-1	9.98962E-1
$\rho_{H_3BO_3}$, g/cm^3	1.79857E-3	3.00507E-3
ρ_{H_2O}, g/cm^3	9.96584E-1	9.95957E-1

Commentary from R. T. Primm III and M. W. Yambert, Oak Ridge National Laboratory

As a part of the review of this document, the value of the correction factor, described in Sect. 1.3, for modifying the measured powers for the MOX pins in mixed UO_2/MOX cores was reevaluated with current values for physical properties (Tables 1–3). Based on these values, a correction factor value of 1.51 was calculated (as compared to 1.41 in Sect. 1.3). Application of this factor acts to increase the reported, experimentally measured pin powers.

Table 1. ESADA fuel rod specifications

Parameter	UO_2	MOX
Pellet diameter, cm	1.0160	1.2827
Cladding inner diameter, cm	1.0297	No gap
Cladding outer diameter, cm	1.1963	1.4427
Gap material	Helium at 20 atm	N/A
Active fuel length, cm	121.92	91.44
Cladding material	Zircaloy-4	Zircaloy-2

Table 2. Density

Zircaloy (g/cm^3)	UO_2 (g/cm^3)	MOX (g/cm^3)
6.55	10.43	10.44

Table 3. Specific heat

Temperature (°C)	Zircaloy cal/(g °C)	UO_2 cal/(g °C)	2% MOX cal/(g °C)
20	0.0668	0.0558	0.0559
30	0.0673	0.0568	0.0569
40	0.0678	0.0577	0.0578
50	0.0683	0.0585	0.0587
60	0.0688	0.0593	0.0595
70	0.0693	0.0601	0.0602
80	0.0698	0.0608	0.0609
90	0.0703	0.0614	0.0616
100	0.0708	0.0620	0.0622
110	0.0713	0.0626	0.0627
120	0.0718	0.0631	0.0633
130	0.0722	0.0637	0.0638

Table 4. Thermal conductivity

Temperature (°C)	Zircaloy W/(cm °C)	UO_2 W/(cm °C)	MOX cal/(g cm s °C)
0	0.02937	0.02053	0.02027
100	0.03270	0.01769	0.01745
200	0.03576	0.01513	0.01495

For the computational results, Akkurt reported values from the F7 tally option in the MCNP. This tally is for fission rates. The parameter measured in the experiments was related to the power in a UO_2 rod. Because the energy per fission from ^{235}U is different from the value for ^{239}Pu, a correction for differing fission energies must be made. The recoverable energy from ^{239}Pu is approximately 4% greater than the recoverable energy from ^{235}U. Akkurt normalized the F7 tallies by the arithmetic average of the tallies. To account for the differences in recoverable fission energies, the F7 tallies for the MOX pins were multiplied by 1.04 prior to computing the arithmetic average. This correction acts to increase the calculated relative powers in the MOX rods.

The correction factor for the F7 tally was made for cases reported in Tables 67–74. These cases were rerun by J. M. Barnes, ORNL, to correct a modeling error related to the gap thickness between the MOX and LEU regions.

A possible explanation for the poorer comparison for mixed lattices is the fact that the experimenters did not note the location of the reference or monitor pin as was done in the SAXTON measurements. Thus, the reader does not know the manner in which the pin powers in Ref. 1 were normalized.

Akkurt, in consultation with Primm, renormalized the reported relative pin power values against the arithmetic average of all the pins for which measurements were provided. This methodology is as defensible as any other, given the lack of information provided by the experimenters. It seems to work well for single-region, cylindrical multiregion, and salt-and-pepper experiments yielding calculation-to-experiment ratios that are comparable to those observed for the same computational methodology (MCNP) applied to the SAXTON experiments.

Noteworthy though is the location of the maximum deviation between measured and calculated pin powers over all of the experimental measurements. For every multiregion slab experiment, the pin powers for the LEU pins adjacent to the MOX region show the greatest discrepancy between calculation and experiment. In all cases, the experimental measurements are much higher than the calculated values. These experimental measurements would not have been modified by the application of a power correction factor as was done for the MOX pins. The phenomenon does not appear in multiregion cylindrical configurations (Figs. 10–12; discrepancies in the uranium region in Figs. 10 and 12, while higher than expected, are not position dependent). The results lead one to question if the descriptions of the experimental configurations for the multiregion slab experiments are accurate.

INTERNAL DISTRIBUTION

1–5. B. B. Bevard
6. J. M. Barnes
7. M. E. Dunn
8. M. D. DeHart
9. F. C. Difilippo
10. R. J. Ellis
11–15. J. C. Gehin
16. S. Golguoglu
17. S. R. Greene
18. D. Hollenbach
19. D. T. Ingersoll
20. M. A. Kuliasha
21. S. B. Ludwig
22. G. E. Michaels
23. M. P. McGinnis
24. C. V. Parks
25. W. P. Poore III
26–30. R. T. Primm III
31. B. T. Rearden
32. J. P. Renier
33. C. C. Southmayd
34. M. W. Yambert
35. Central Research Library
36. ORNL Laboratory Records–RC

EXTERNAL DISTRIBUTION

37. N. Abdurrahman, College of Engineering, Dept. of Mechanical Engineering, University of Texas, Austin, TX 78712
38. M. L. Adams, Department of Nuclear Engineering, Texas A&M University, Zachry 129, College Station, TX 77843
39. H. Akkurt, 2919 Cooley Building, 2355 Bonisteel Boulevard, Ann Arbor, MI, 48109-2104
40. D. Alberstein, Los Alamos National Laboratory, P.O. Box 1663, MS-K551, Los Alamos, NM 87545
41. J. B. Briggs, Idaho National Environmental and Engineering Laboratory, P.O. Box 1625-3855, Idaho Falls, ID 83415-3855
42. N. Fletcher, Office of Fissile Materials Disposition, U. S. Department of Energy, NN-63, 1000 Independence Avenue SW, Washington, DC 20585
43. K. Chidester, Los Alamos National Laboratory, P.O. Box 1663, MS-E502, Los Alamos, NM 87545
44. W. Danker, U. S. Department of Energy, NN-62, 1000 Independence Avenue SW, Washington, DC 20585
45. T. Gould, Lawrence Livermore National Laboratory, P.O. Box 808, MS-L186, Livermore, CA 94551
46. L. Jardine, Lawrence Livermore National Laboratory, P.O. Box 808, MS-L166, Livermore, CA 94551
47. Dr. Alexander Kalashnikov, Institute of Physics and Power Engineering, 1 Bondarenko Square, Obninsk, Kaluga Region, Russia 249020
48. S. L. Passman, Booz-Allen & Hamilton, 555 13th Street, NW, No. 480E, Washington, DC 20004

49–53. Dr. Alexander Pavlovitchev, Russian Research Center “Kurchatov Institute,” Institute of Nuclear Reactors, VVER Division, VVER Physics Department, 123182, Kurchatov Square, 1, Moscow, Russia

54. K. L. Peddicord, Associate Vice Chancellor, Texas A&M University, 120 Zachry, College Station, TX 77843-3133
55. G. Radulescu, Framatom Cogema Fuels, 1261 Town Center Drive, MS-423, Las Vegas, NV 89143
56. P. T. Rhoads, Office of Fissile Materials Disposition, U.S. Department of Energy, 1000 Independence Avenue SW, NN-61, Washington, DC 20585
57. J. Thompson, Office of Fissile Materials Disposition, U.S. Department of Energy, 1000 Independence Avenue SW, NN-61, Washington, DC 20585
58. Fitz Trumble, Westinghouse Savannah River Company, Building 730R, Room 3402, WSRC, Aiken, SC 29808
59. R. H. Clark, Duke/Cogema/Stone & Webster, 400 South Tryon Street, WC-32G, P.O. Box 1004, Charlotte, NC 28202
60. S. Nesbit, Duke/Cogema/Stone & Webster, 400 South Tryon Street, WC-32G, P.O. Box 1004, Charlotte, NC 28202
61. M. S. Chatterton, Office of Nuclear Reactor Regulation, MS O10B3, U.S. Nuclear Regulatory Commission, Washington, DC 20555-0001
62. R. W. Lee, Office of Nuclear Reactor Regulation, MS O10B3, U.S. Nuclear Regulatory Commission, Washington, DC 20555-0001
63. U. Shoop, Office of Nuclear Reactor Regulation, MS O10B3, U.S. Nuclear Regulatory Commission, Washington, DC 20555-0001
64. J. P. Halloway, 2919 Cooley Building, 2355 Bonisteel Boulevard, Ann Arbor, MI 48109-2104
65. Nagao Ogawa; Director and General Manager; Plant Engineering Department; Nuclear Power Engineering Corporation; Shuwa-Kamiyacho Building, 2F; 3-13, 4-Chome Toranomon; Minato-Ku, Tokyo 105-0001, Japan
66. Dr. Kiyonori Aratani; Surplus Weapons Plutonium Disposition Group; International Cooperation and Nuclear Material Control Division; Japan Nuclear Cycle Development Institute; 4-49 Muramatsu, Tokai-mura, Naka-gun, Ibaraki-ken, Japan
67. Boris E. Volkov; Head of Division; EDO Gidropress; 21 Ordzhonikidze Street; Podolsk, Moscow district, Russia 142103
68. Dr. Alexandre Ermolaev; Balakovo Nuclear Power Plant, Saratov Region, Balakovo-26, Russia, 413866